MARTIN MARIETTA ENERGY SYSTEMS LIBRARIES

3 4456 0315370 8

ORNL/TM-11161

ornl

OAK RIDGE NATIONAL LABORATORY

MARTIN MARIETTA

Low-Order Dynamic Modeling of the Experimental Breeder Reactor II

R. C. Berkan
B. R. Upadhyaya
R. A. Kisner

OAK RIDGE NATIONAL LABORATORY
CENTRAL RESEARCH LIBRARY
CIRCULATION SECTION
4500N ROOM 175
LIBRARY LOAN COPY
DO NOT TRANSFER TO ANOTHER PERSON
If you wish someone else to see this report, send in name with report and the library will arrange a loan.

OPERATED BY
MARTIN MARIETTA ENERGY SYSTEMS, INC.
FOR THE UNITED STATES
DEPARTMENT OF ENERGY

This report has been reproduced directly from the best available copy.

Available to DOE and DOE contractors from the Office of Scientific and Technical Information, P.O. Box 62, Oak Ridge, TN 37831; prices available from (615) 576-8401, FTS 626-8401.

Available to the public from the National Technical Information Service, U.S. Department of Commerce, 5285 Port Royal Rd., Springfield, VA 22161.
NTIS price codes—Printed Copy: A07 Microfiche A01

This report was prepared as an account of work sponsored by an agency of the United States Government. Neither the United States Government nor any agency thereof, nor any of their employees, makes any warranty, express or implied, or assumes any legal liability or responsibility for the accuracy, completeness, or usefulness of any information, apparatus, product, or process disclosed, or represents that its use would not infringe privately owned rights. Reference herein to any specific commercial product, process, or service by trade name, trademark, manufacturer, or otherwise, does not necessarily constitute or imply its endorsement, recommendation, or favoring by the United States Government or any agency thereof. The views and opinions of authors expressed herein do not necessarily state or reflect those of the United States Government or any agency thereof.

ORNL/TM-11161
Dist. Category UC-530
Liquid Metal Fast Breeder Reactors

Instrumentation and Controls Division

LOW-ORDER DYNAMIC MODELING OF THE EXPERIMENTAL BREEDER REACTOR II

R. C. Berkan*
B. R. Upadhyaya
R. A. Kisner

Date Published: July 1990

*Department of Nuclear Engineering, The University of Tennessee, Knoxville.

Prepared for the
Office of Technology Support Programs
Budget Activity No. AF 20 10 20 2

Prepared by the
OAK RIDGE NATIONAL LABORATORY
Oak Ridge, Tennessee 37831-6010
operated by
MARTIN MARIETTA ENERGY SYSTEMS, INC.
for the
U.S. DEPARTMENT OF ENERGY
under Contract No. DE-AC05-84OR21400

MARTIN MARIETTA ENERGY SYSTEMS LIBRARIES

3 4456 0315370 8

TABLE OF CONTENTS

	Page
LIST OF FIGURES	v
LIST OF TABLES	xi
LIST OF ABBREVIATIONS	xiii
ABSTRACT	xv
1. INTRODUCTION	1
1.1 PURPOSE OF RESEARCH	1
1.2 RECOGNITION OF SIMILAR WORK	2
1.3 SCOPE OF THIS REPORT	2
1.4 DEVELOPMENT AND APPLICATION	3
2. BRIEF DESCRIPTION OF THE EBR-II	5
2.1 GENERAL FEATURES	5
2.2 PRIMARY SYSTEM	6
2.2.1 Reactor Core	6
2.2.2 Inner and Outer Blankets	13
2.2.3 Control Rods	13
2.3 PRIMARY COOLING SYSTEM	13
2.4 SECONDARY SYSTEM	13
2.5 EBR-II CONTROL SYSTEMS	23
3. EBR-II PRIMARY SYSTEM MODEL DEVELOPMENT	24
3.1 INTRODUCTION	24
3.2 REACTOR CORE	24
3.2.1 Reactor Kinetics	24
3.2.2 Core Heat Transfer	28
3.2.3 Reflector and Blanket Models	30
3.2.4 Piping and Plenum Models	31
3.2.5 Intermediate Heat Exchanger (IHX) Model	33
4. EBR-II STEAM GENERATOR MODEL DEVELOPMENT	38
4.1 INTRODUCTION	38
4.2 EVAPORATOR AND DRUM BALANCE EQUATIONS	38
4.2.1 Drum Liquid	44
4.2.2 Drum Steam	47
4.2.3 Primary Coolant Lumps	48
4.2.4 Tube Wall Lumps	50
4.2.5 Subcooled Region	52
4.2.6 Boiling Region	54
4.2.7 Downcomer Region	56
4.2.8 Momentum Equations	56

TABLE OF CONTENTS (continued)

Page

4.3 SUPERHEATER STATE EQUATIONS 59
4.4 THREE-ELEMENT CONTROLLER 59

5. TRANSIENT SIMULATIONS USING OPEN-LOOP MODELS 62

5.1 CALCULATION PROCEDURE 62
5.2 PRIMARY SYSTEM DYNAMIC SIMULATION 63
5.2.1 Reactivity Perturbation Results 63
5.2.2 Sodium Inlet Temperature Perturbation Results 70
5.3 ISOLATED STEAM GENERATOR DYNAMIC SIMULATION 70
5.3.1 Feedwater Temperature Perturbation Results . . . 70
5.3.2 Sodium Inlet Temperature Perturbation Results . . 74
5.3.3 Feedwater Flow Perturbation Results 74
5.3.4 Steam Valve Opening Perturbation Results 74
5.3.5 Comparison of the Results with a PWR U-Tube Steam Generator Model 78
5.4 SIMULATION OF THE COMBINED SYSTEM 80
5.4.1 Combining Subsystem Models 80
5.4.2 Combined Model Simulations 80
5.4.3 Predictions of the ANL Safety Tests 85

6. CONCLUSIONS 89

6.1 SUMMARY 89
6.2 RECOMMENDATIONS 90

REFERENCES 93

BIBLIOGRAPHY 95

APPENDIX A. AUXILIARY CALCULATIONS 97

A.1 BOUNDARY FLOW APPROXIMATION 97
A.2 HEAT TRANSFER 98
APPENDIX A REFERENCES 101

APPENDIX B. SUMMARY OF TRANSIENT RESPONSES 103

APPENDIX C. CAPABILITIES OF $MATRIX_X$ 115

C.1 REPRESENTATION OF DYNAMIC SYSTEMS 115
C.2 SIMULATION COMMANDS 116
C.3 SYSTEM-BUILD OPTION 116
APPENDIX C REFERENCE 120

LIST OF FIGURES

Figure		Page
2.1	EBR-II primary and secondary sodium systems	7
2.2	EBR-II primary cooling system	8
2.3	Diagram of EBR-II plant flow	10
2.4	EBR-II core cross section	11
2.5	EBR-II core subassembly	12
2.6	EBR-II reactor vessel assembly	14
2.7	EBR-II control subassembly	15
2.8	EBR-II intermediate heat exchanger	16
2.9	EBR-II steam generator components	17
2.10	EBR-II evaporator details and sensor locations	19
2.11	EBR-II superheater details and sensor locations	20
2.12	EBR-II evaporator assembly	21
2.13	EBR-II superheater assembly	22
3.1	Nodal representation of the EBR-II primary system model	25
3.2	Measured and calculated feedback reactivity in EBR-II for SHRT Group IV	28
3.3	Mann's core heat transfer model	29
3.4	Lumped-parameter approximation of a counterflow heat exchanger	34
4.1	Nodal representation of the EBR-II steam generator model	39
5.1	Step response of fractional reactor power to a −5-cent reactivity perturbation	66

LIST OF FIGURES (continued)

Figure		Page
5.2	Step response of fractional power to a −5-cent reactivity perturbation	66
5.3	Temperature responses of the IHX coolant lumps to a −5-cent step reactivity perturbation (Greene's model)	67
5.4	Temperature responses (deviations from steady state) of the IHX coolant lumps to a −5-cent step reactivity perturbation (open-loop primary model)	68
5.5	Temperature response of tank sodium to a sudden flow reduction test	69
5.6	Step response of tank sodium temperature to a −5-cent reactivity perturbation	69
5.7	Step response of fractional reactor power to a −5-cent reactivity perturbation	69
5.8	Step response of IHX secondary inlet temperature to a +10°F (+5.5°C) IHX secondary inlet temperature perturbation	71
5.9	Step response of IHX secondary outlet temperature to a +10°F (+5.5°C) IHX secondary inlet temperature perturbation	71
5.10	Step response of IHX primary inlet temperature to a +10°F (+5.5°C) IHX secondary inlet temperature perturbation	71
5.11	Step response of IHX primary outlet temperature to a +10°F (+5.5°C) IHX secondary inlet temperature perturbation	71
5.12	Step response of fractional reactor power to a +10°F (+5.5°C) IHX secondary inlet temperature perturbation	72
5.13	Step response of sodium tank temperature to a +10°F (+5.5°C) IHX secondary inlet temperature perturbation	72
5.14	Step response of core outlet temperature to a +10°F (+5.5°C) IHX secondary inlet temperature perturbation.	72

LIST OF FIGURES (continued)

Figure		Page
5.15	Step response of drum water temperature to a +10°F (+5.5°C) feedwater temperature perturbation	73
5.16	Step response of downcomer temperature to a +10°F (+5.5°C) feedwater temperature perturbation	73
5.17	Step response of subcooled height to a +10°F (+5.5°C) feedwater temperature perturbation	75
5.18	Step response of steam exit quality to a +10°F (+5.5°C) feedwater temperature perturbation	75
5.19	Step response of drum pressure to a +10°F (+5.5°C) feedwater temperature perturbation	75
5.20	Step response of superheated steam outlet temperature to a +10°F (+5.5°C) inlet sodium temperature perturbation.	75
5.21	Step response of steam exit quality to a +10°F inlet sodium temperature perturbation	76
5.22	Step response of subcooled height to a +10°F (+5.5°C) inlet sodium temperature perturbation	76
5.23	Step response of evaporator sodium outlet temperature to a +10°F (+5.5°C) inlet sodium temperature perturbation	76
5.24	Step response of drum water temperature to a +10-lb_m/s feedwater flow perturbation	76
5.25	Step response of downcomer flow to a +10-lb_m/s feedwater flow perturbation	77
5.26	Step response of evaporator flow to a +10-lb_m/s feedwater flow perturbation	77
5.27	Step response of subcooled height to a +10-lb_m/s feedwater flow perturbation	77
5.28	Step response of steam outlet quality to a +10-lb_m/s feedwater flow perturbation	77

LIST OF FIGURES (continued)

Figure		Page
5.29	Step response of drum pressure to a +10-lb_m/s feedwater flow perturbation	78
5.30	Step response of drum pressure to a +10% steam valve opening perturbation	78
5.31	Step response of downcomer flow to a +10% steam valve opening perturbation	79
5.32	Step response of evaporator flow to a +10% steam valve opening perturbation	79
5.33	Step response of subcooled height to a +10% steam valve opening perturbation	79
5.34	Step responses of steam exit quality to a +10% steam valve opening perturbation	79
5.35	Step responses to a 10% change in steam valve opening	81
5.36	Step responses to a 10°F change in feedwater temperature	82
5.37	Step response of fractional reactor power to a −5-cent reactivity perturbation	83
5.38	Step response of IHX outlet sodium temperature to a −5-cent reactivity perturbation	83
5.39	Step response of superheated steam temperature to a −5-cent reactivity perturbation	84
5.40	Step response of drum pressure to a −5-cent reactivity perturbation	84
5.41	Step response of drum pressure to a +10% steam valve opening perturbation	84
5.42	Step response of fractional power response to a +10% steam valve opening perturbation	84
5.43	Drum pressure response to a large steam reduction test (B402)	86

LIST OF FIGURES (continued)

Figure		Page
5.44	Drum level response to a large steam reduction test (B402)	86
5.45	Relative flow response to a large steam reduction test (B402)	86
5.46	Neutron power response to the SHRT-39 test	88
5.47	IHX secondary outlet temperature response to the SHRT-39 test	88
5.48	High-pressure plenum inlet temperature response to the SHRT-26 test	88
5.49	Neutron power response to the SHRT-26 test	88
A.1	Heat transfer	99
B.1	Step responses of primary model to a −5-cent reactivity perturbation	104
B.2	Step responses of primary model to a +10°F IHX inlet sodium temperature perturbation	107
B.3	Step responses of steam generator model to a +10°F feedwater temperature perturbation	108
B.4	Step responses of steam generator model to a +10°F inlet sodium temperature perturbation	109
B.5	Step responses of steam generator model to a +10% steam valve opening perturbation	110
B.6	Step responses of steam generator model to a +10-lb_m/s feedwater flow perturbation	111
B.7	Step responses of combined model to a −5-cent reactivity perturbation	112
B.8	Step responses of combined model to a +10% steam valve opening perturbation	113
C.1	Coupling the primary and steam generator models using SYSTEM-BUILD	119

LIST OF TABLES

Table		Page
2.1	Summary of EBR-II design and operating data	9
3.1	EBR-II neutronic data	27
3.2	EBR-II reactivity feedback coefficients	27
3.3	Core heat transfer parameters	29
3.4	Reflector and blanket region data	31
3.5	Primary piping and plenum data	33
3.6	IHX design data	36
3.7	Nonzero elements of system matrix *A* of the EBR-II primary system model	36
4.1	List of assumptions used in the EBR-II steam generator model	40
4.2	Evaporator design data	41
4.3	Superheater design data	43
4.4	Steam drum design data	44
4.5	Nonzero elements of system matrix *A* of the EBR-II steam generator model	45
5.1	List of state variables	64
5.2	Forcing functions used in the EBR-II subsystem model simulation studies	73
B.1	Organization of the results	103
C.1	Steps describing model buildings using SYSTEM-BUILD	117

LIST OF ABBREVIATIONS

ANL	Argonne National Laboratory
CAD	Computer-aided design
EBR-II	Experimental Breeder Reactor II
FFTF	Fast Flux Test Facility
IHX	Intermediate heat exchanger
LMR	Liquid metal reactor
LOFWS	Loss-of-flow-without-scram (test)
MIMO	Multiple-input, multiple-output
PI	Proportional-integral (controller)
PWR	Pressurized water reactor
SHRT	Shutdown heat removal test

ABSTRACT

This report describes the development of a low-order, linear model of the Experimental Breeder Reactor II (EBR-II), including the primary system, intermediate heat exchanger, and steam generator subsystems. The linear model is developed to represent full-power steady state dynamics for low-level perturbations. Transient simulations are performed using model building and simulation capabilities of the computer software $Matrix_X$.* The inherently safe characteristics of the EBR-II are verified through the simulation studies. The results presented in this report also indicate an agreement between the linear model and the actual dynamics of the plant for several transients. Such models play a major role in the learning and in the improvement of nuclear reactor dynamics for control and signal validation studies.

This research and development is sponsored by the Advanced Controls Program in the Instrumentation and Controls Division of the Oak Ridge National Laboratory.

*$Matrix_X$, Version 5.0, ©1985 by Integrated Systems, Inc., Santa Clara, California.

1. INTRODUCTION

1.1 PURPOSE OF RESEARCH

The development of advanced liquid metal reactor technology involves research activities in various fields such as safety, controls, signal processing, and reliability, in which dynamic modeling plays a major role and is a useful tool for system engineers. New design ideas can be developed and simulated using dynamic models which are most likely to represent a certain mode of operation of interest. The focus in this study has been on developing a low-order, linear model of the Experimental Breeder Reactor II (EBR-II) representing the full-power steady state operation of the plant.

The EBR-II is a liquid metal fast breeder reactor built during the early 1960s as an engineering test facility in which the inherent capability of sodium-cooled fast reactors to sustain unprotected loss-of-coolant accidents was demonstrated successfully. The EBR-II tests and demonstrations, which are highly important in the development of future advanced reactors, have been studied extensively in the past using nonlinear large-scale models of the plant. Besides studying the safety aspects, recent research projects have included advanced controls and signal validation issues in which most of the known methods use linear modeling. Thus, an important motivation for developing a low-order, linear EBR-II model has been to provide the necessary mathematical testing environment for applications in which linear techniques are widely used.

Although the linear models cannot represent the entire physics of a plant, they can provide efficient predictions of certain transients. It is well known that large-scale systems such as nuclear power plants tend to behave in a linear fashion for low-level perturbations around steady state operation; therefore, the linear models are expected to provide close predictions of such transients. Another important point is that linear modeling enables us to classify the subsystems of a plant in terms of the degree of their linearity with respect to other subsystems. Using such information, large-scale nonlinear models can be simplified within some reasonable limits of computational accuracy. We assume that a low-order, linear EBR-II model will be adequate in simplifying some models, including the entire nonlinear representation of actual plant dynamics.

The general trend towards low-order modeling, at the developmental stage or through model reduction techniques, is in order to reduce computation costs and provide efficient real-time applications. Commercial software aims at satisfying the criteria stated above. One of the latest developments is the simulation and control software, Matrix_X, which includes several integration algorithms as well as some model reduction techniques. It also provides model building structure for handling large-scale system models. The EBR-II model described in this report is simulated and partially constructed using Matrix_X.

Evaluation of this software through the applications of this work was one of the goals.

1.2 RECOGNITION OF SIMILAR WORK

The concept of advanced LMR design based upon the expected fuel cycle economy and the inherently safe features has been investigated based on the pioneering prototypes such as the Fast Flux Test Facility (FFTF) and EBR-II. There have been many studies since then, mainly including the safety tests and their predictions using generic computer codes. EBR-II data from several instrumented assemblies were used in the validation of codes NATDEMO, DSNP, COBRA-WC, FORE-2M, COMMIX-1A, SASSYS, SSC, MINET, and CORA.[1] These successful efforts include detailed transient analyses of large perturbations as in the Shutdown Heat Removal Test (SHRT) program at EBR-II.

One of the first examples of low-order modeling of nuclear plants was developed by Kerlin[2] entitled, *Pressurized Water Reactor Modeling for Long-Term Power System Dynamics Simulation.* This work verified the adequacy of low-order modeling for low-level perturbations. It also demonstrated the effectiveness of linear models in comparison with nonlinear versions. An early study by Madell[3] is entitled *Analysis of the Linear Components of the PRD in EBR-II.* Linear modeling of the EBR-II primary system was developed by Green[4] in a cost-benefit analysis study. A similar development was completed by Marshall[5] associated with a numerical Fourier transform technique in dynamic system analysis.

1.3 SCOPE OF THIS REPORT

This report is intended to provide a simple low-order, linear model of the EBR-II primary and steam generator systems that can be considered as the reference point for future extensions and improvements. The purpose of this study is not to develop a linear model for the prediction of test transients, but rather to create a test bed for the applications of linear methods of classical and modern control theories. The validation of the linear model is incomplete, but the comparison with the available test data is encouraging. The linear model is also adequate for representing the steady state dynamic behavior, which may be used for modern control theory applications.[6] The future of linear modeling of EBR-II is strongly dependent on the direction of the needs in advanced LMR development. Since the recent interests are related to issues such as automation and advanced reactor control, the linear modeling may find more applications.

1.4 DEVELOPMENT AND APPLICATION

The EBR-II plant consists of three subsystems: the primary system, the steam generator system, and the balance of plant system. In this study, the dynamic modeling of the EBR-II includes the primary and steam generator subsystems (the primary system includes the reactor core, sodium tank, and the intermediate heat exchanger). A previously developed primary system model[4] is modified and updated with the most recent available data. The modified primary model is a linear, lumped-parameter model with 37 state variables. The formulation is made using the point reactor kinetics equation, Mann's heat transfer model, and the first-order transport-lag approximation.[4] The six-group precursor equations of the Greene model are replaced with one "averaged" precursor equation, which is a well-known physical model reduction technique.[2] Another modification is made in the intermediate heat exchanger (IHX) side of the Greene model. The five-lump configuration is converted to a ten-lump model. Mann's five-lump model is valid only if the ratio of total heat capacity to overall heat transfer coefficient is smaller than about 2 s.[7] The IHX data of the EBR-II are such that the ratios for the primary and the secondary sides both exceed the 2-s limit when the IHX is divided into five lumps. Using the ten-lump model, the 2-s limit is not exceeded. The open-loop simulation results verify that the physical consistency and the computational accuracy are retained with these modifications. Important reactivity feedback mechanisms, namely, the Doppler, steel expansion, core sodium expansion, inner and outer reflector expansion, and fuel expansion effects, are included in the model. The core bowing and control rod reactivity feedback effects are not taken into consideration because their contribution to steady state operation is not significant.

The development of the steam generator model is accomplished using the energy and mass balance equations for 13 different regions. The system includes seven shell-and-tube type evaporators, two shell-and-tube type superheaters, and a steam drum. Evaporator dynamics is represented using a moving boundary approach.[8] This technique has been used in several previous studies and gives accurate results. The moving boundary approach uses the height of the subcooled region as a state variable, which is a function of the saturation pressure and temperature. In the boiling region, a homogeneous flow model is considered.[9] This is the assumption of the homogeneous steam-water mixture with average enthalpy, quality, and density. The downcomer and the evaporator flows are represented by the momentum equations. The friction multiplier for the boiling region is an integral average taken over the boiling region.[10] The lumped-parameter steam generator model uses 20 state variables including the three-element controller dynamics. A proportional-integral (PI) controller is designed for drum level control using three signals, namely feedwater flow, steam flow, and drum water level. The actuator is the feedwater flow valve which is represented as a first-order system in the model. The design objective of the three-element controller is to maintain the drum level at its steady-state value of 8 in. (~20 cm) below the centerline at 100% power level.

The responses of the open-loop models to standard perturbations are obtained through simulations using the special features of $Matrix_X$. The combined model is also tested for the same perturbations. The inherent stability characteristics of the EBR-II subsystems are verified.

2. BRIEF DESCRIPTION OF THE EBR-II*

2.1 GENERAL FEATURES

The Experimental Breeder Reactor II (EBR-II) is a liquid metal fast breeder reactor located at the National Reactor Testing Station in Idaho. The plant consists of a heterogeneous, unmoderated, sodium-cooled reactor (62.5 MWt); an intermediate sodium coolant loop; a steam plant which produces 20 MW of electrical power through a conventional turbine generator; and a fuel processing system consisting of systems for disassembly, decontamination, fabrication, and assembly of fuel elements and subassemblies. Both the reactor and the associated fuel recycle facilities were designed with the philosophy of providing a highly flexible installation that would permit the investigation and evaluation of various core configurations, types of fuel, fuel element designs, and processing techniques. The reactor, primary coolant system, and the fuel-handling system components are submerged in a large primary sodium tank. This concept is also sometimes referred to as the pool-type design (such as the Phoenix and Super-Phoenix liquid metal reactors in France).

> The original purpose of the EBR-II facility was to demonstrate the feasibility of fast reactors for central station power plant applications. It was also intended to prove that a breeding ratio greater than unity could be obtained in a power-producing reactor. When the purpose of the facility was redirected to provide irradiation services for the development of fuels and structural materials, the transition required changes in several original concepts of operation, including an increase in overall core size to compensate for reactivity losses to the system caused by additional irradiation experiments. Other changes made were in fuel enrichment, in blanket composition, and in operating philosophy from that of an engineering test facility to that of a high-priority neutron producer.
>
> A simple functional description of the plant can be stated as follows. Heat generated by nuclear fission in the core is absorbed by liquid sodium that circulates through the reactor. The absorbed heat is transferred in a shell-tube type intermediate heat exchanger to nonradioactive secondary sodium. The secondary sodium transfers the heat to the steam system in the steam generator which includes sodium-to-water/steam shell-and-tube type heat exchangers. The resulting superheated steam drives a turbine generator to produce electricity and is condensed to water in the condenser. The heat transferred to the condenser is dissipated to the atmosphere by cooling towers.[11]

---

*For a similar description of the EBR-II system, see I. K. Madni, *Modeling Considerations for the Primary System of the EBR-II*, BNL/NUREG/51797, June 1984. Further information is available from ref. 11.

Figure 2.1 is a schematic of the primary and sodium systems, and Fig. 2.2 shows the detailed primary cooling system. A summary of the EBR-II design and operating data is reproduced in Table 2.1 (from ref. 12).

The secondary sodium system, an intermediate closed loop between the primary system and the steam system, absorbs heat produced in the primary system and transfers the heat to the steam system. The flow of secondary sodium is regulated manually to absorb all heat in excess of that required to maintain the primary bulk sodium at a constant temperature of 700°F (~371°C).

Heat transfer between the primary and secondary sodium occurs in the intermediate heat exchanger submerged in the primary tank bulk sodium. The heated secondary sodium then flows from the reactor building through yard piping to the sodium boiler building where it enters the steam generator. Heat transfer between the secondary system and the steam system is effected at this interface to produce superheated steam used to drive the turbine generator.

2.2 PRIMARY SYSTEM

The primary system is housed in the reactor plant (see Fig. 2.3) and contains reactor, primary, and shutdown cooling systems; a neutron shield; instrumentation, control, and safety drive systems; a fuel-handling system; a primary tank and biological shield; and fuel unloading and interbuilding transfer, primary sodium purification, and argon blanket gas systems.

The reactor contains a central core of fissionable fuel material that is completely surrounded by radial and axial blankets. The fuel and blanket materials are contained within a cylindrical reactor vessel. In the radial and upper axial direction, a neutron shield surrounds the vessel. Fuel bearing subassemblies contain upper and lower axial blanket regions in addition to the fuel material. Blanket subassemblies contain only blanket material.

2.2.1 Reactor Core

The reactor core consists of 53 fuel subassemblies, 12 control rod subassemblies, and 2 safety rod assemblies. The active core height is 14.22 in. (~35.5 cm) and has an equivalent diameter of 19.94 in. (~49.85 cm). Each fuel assembly consists of 91 fuel elements. The subassemblies are hexagonal in shape. Figure 2.4 shows the typical core cross section. The fuel alloy composition contains 95% by weight uranium (48.4% enrichment) and other elements. As shown in Fig. 2.5, the core assembly consists of the upper blanket, core, and lower blanket. The upper and lower blanket subassemblies consist of 19 pins each, each 18 in. (~45 cm) long. The core fuel elements have sodium thermal bonding between the fuel and the cladding. The total number of fissions/cm^3-s is 4.4×10^{13} (average).

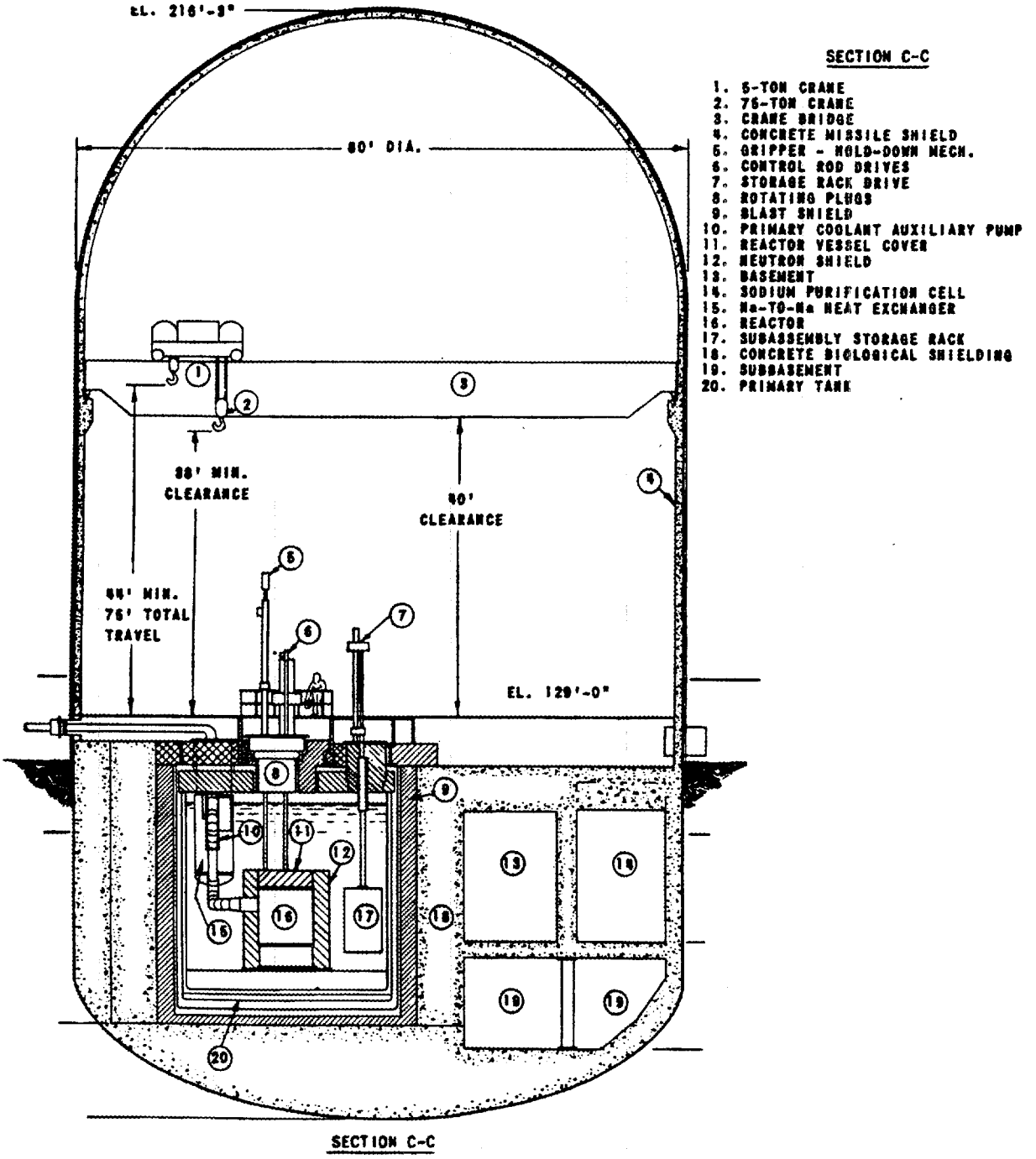

Fig. 2.1. EBR-II primary and secondary sodium systems. *Source: EBR-II System Design Descriptions*, Vols. 1 through 5, Argonne National Laboratory, Argonne, Ill., June 1972.

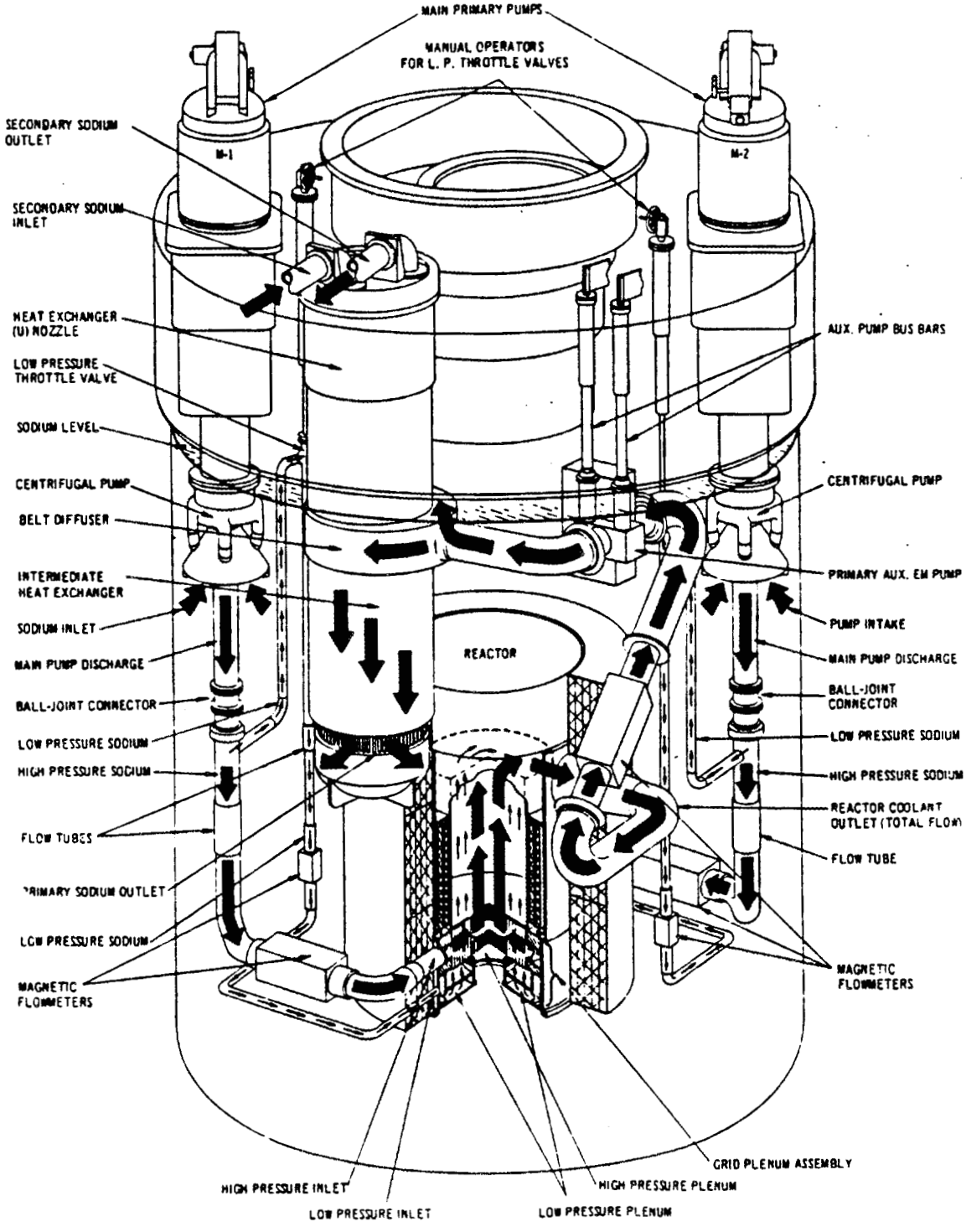

Fig. 2.2. EBR-II primary cooling system. *Source: EBR-II System Design Descriptions*, Vols. 1 through 5, Argonne National Laboratory, Argonne, Ill., June 1972.

Table 2.1. Summary of EBR-II design and operating data

Operational 100% power	From ref. a
Heat output, MW	62.5
Gross electrical output, MW	20
Primary sodium temperature to reactor, °F (°C)	700 (~371)
Primary sodium temperature from reactor, °F (°C)	883 (~472.7)
Sodium flow rate through reactor, gpm	9,000
Sodium maximum velocity in core, ft/s (m/s)	23.8 (~7.25)
Secondary sodium flow rate, gal/min (ℓ/min)	5,890 (22,382)
Secondary sodium temperature to IHX, °F (°C)	588 (~308.8)
Secondary sodium temperature from IHX, °F (°C)	866 (~463.3)
Core equivalent diameter, in. (cm)	19.94 (49.85)
Core composition, fuel alloy %	31.8
Stainless steel %	19.5
Sodium volume %	48.7
Subassemblies	
Core	53
Control (rod and thimble)	12
Safety (rod and thimble)	2
Inner blanket	60
Outer blanket	510
Total	637
Configuration	Hexagonal
Fuel pin diameter, in. (cm)	0.144 (~0.36)
Fuel pin length, in. (cm)	14.22 (~35.5)
Fuel tube OD, in. (cm)	0.174 (~0.43)
Fuel tube wall thickness, in. (cm)	0.009 (~0.22)
Fuel elements/subassembly	91
Total fission cm^3/s at center	3.7×10^{13}
Power density average, MW/ℓ	0.735
Power density maximum, MW/ℓ	1.23
Specific power, MW/kg	0.311
Maximum heat flux, Btu/h-ft^2	929,000
Average heat flux, Btu/h-ft^2	619,000

[a]Adapted from *Addendum to Hazard Summary Report on EBR-II*, L. J. Koch, W. B. Lowenstein, and H. O. Monson, Argonne National Laboratory, ANL-5719, January 1964.

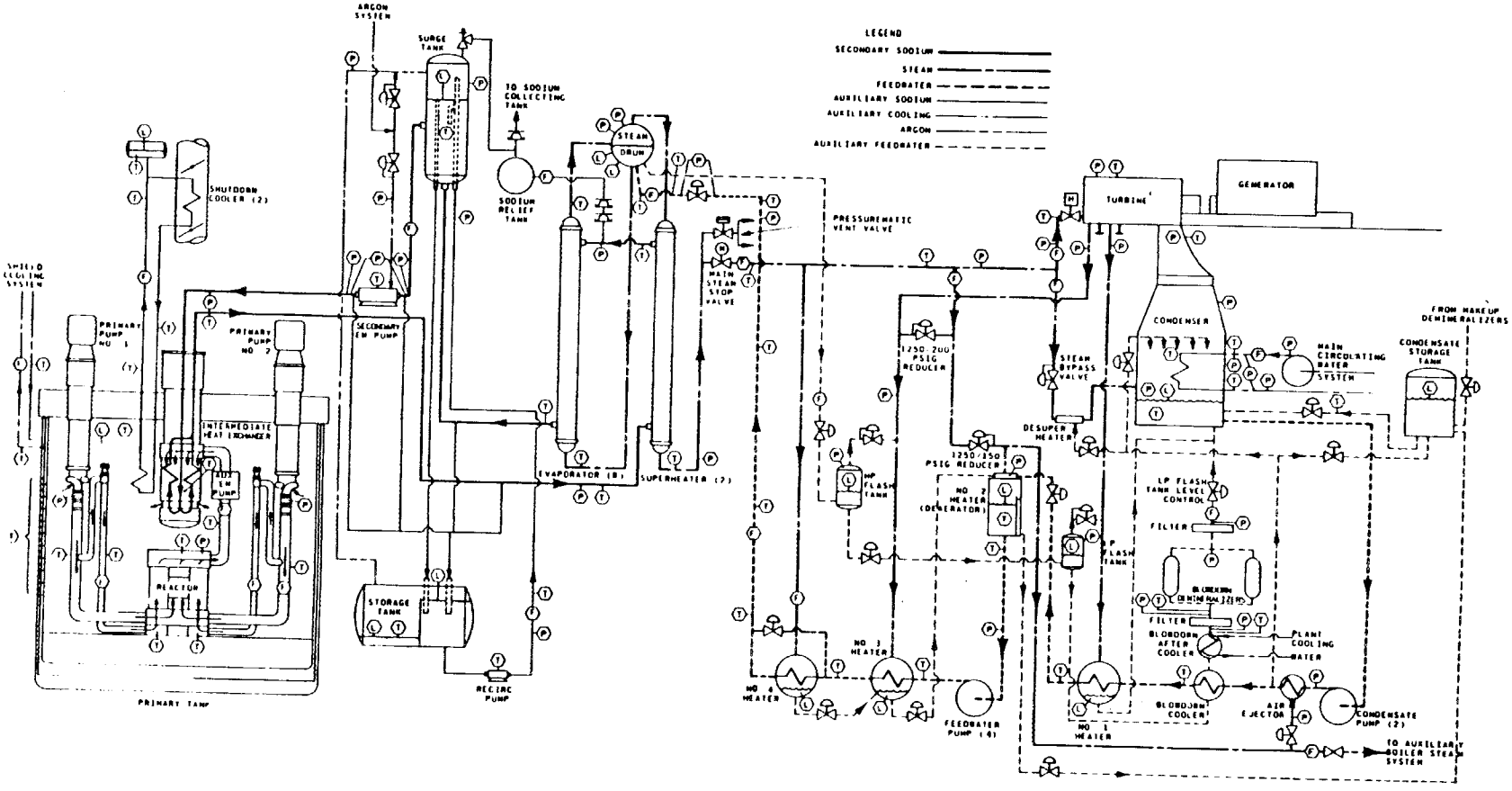

Fig. 2.3. Diagram of EBR-II plant flow. *Source: EBR-II System Design Descriptions*, Vols. 1 through 5, Argonne National Laboratory, Argonne, Ill., June 1972.

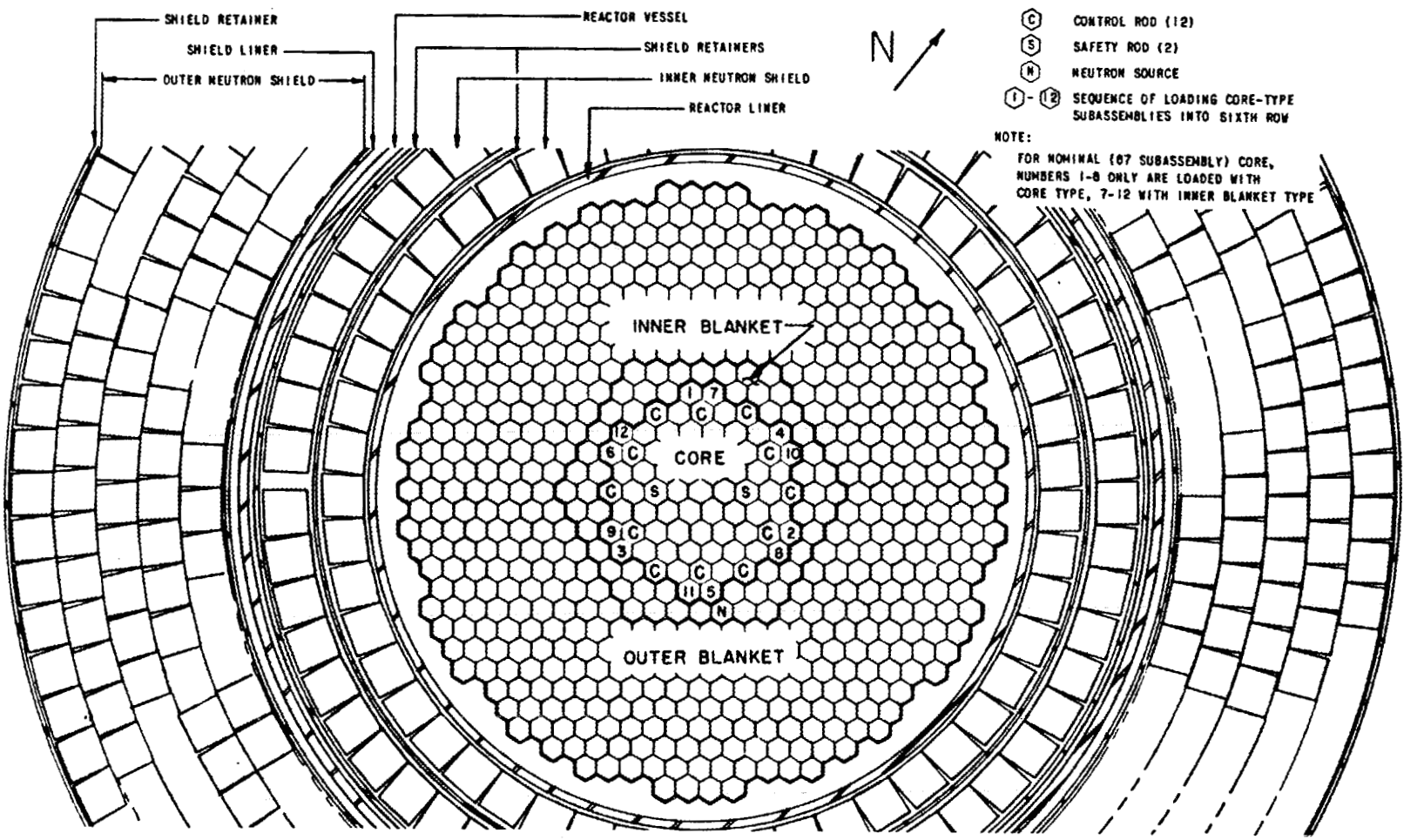

Fig. 2.4. EBR-II core cross section. *Source: EBR-II System Design Descriptions*, Vols. 1 through 5, Argonne National Laboratory, Argonne, Ill., June 1972.

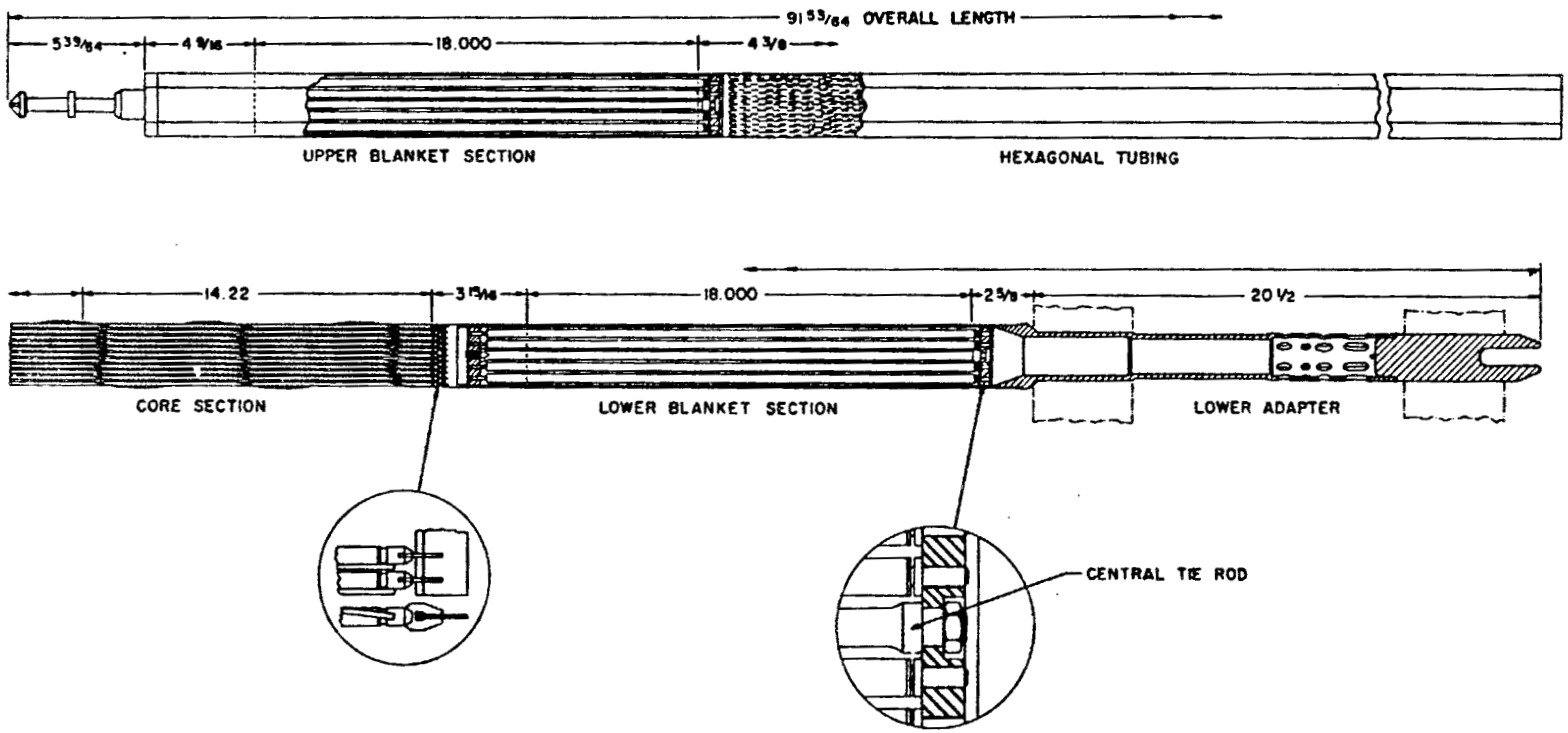

Fig. 2.5. EBR-II core subassembly. *Source: EBR-II System Design Descriptions*, Vols. 1 through 5, Argonne National Laboratory, Argonne, Ill., June 1972.

2.2.2 Inner and Outer Blankets

The reactor vessel assembly also consists of inner and outer blanket subassemblies. There are 66 inner and 510 outer blanket subassemblies. Each of these consists of 19 cylindrical elements, containing 60% uranium, with sodium bonding. The total pin length for the blanket subassemblies is 50 in. (~125 cm). Figure 2.6 shows the reactor vessel assembly with upper and lower blanket sections and inner and outer blanket sections.

2.2.3 Control Rods

EBR-II contains 12 control subassemblies with a fuel pin section identical to the active core subassemblies. Figure 2.7 shows the cross section of a control rod subassembly with an axial void section above the core (normally filled with sodium). Two safety rods provide shutdown reactivity during reactor loading operation, and these are driven from below the core.

About 85.3% of the heat is generated in the active core region, 1.9% in the upper and lower blankets, 9.8% in the inner blanket, 2.2% in the outer blanket, and the remaining (0.8%) in the neutron shield.

2.3 PRIMARY COOLING SYSTEM

Figure 2.2 shows a detailed flow path of sodium through the core, the intermediate heat exchanger, the primary pumps, and the connecting piping. The total sodium coolant flow rate through the core is 3.81×10^6 lb_m/h (1.725×10^6kg/h). The secondary sodium flow rate is 2.5×10^6 lb_m/h (1.132×10^6 kg/h). The inlet temperature of secondary sodium to the intermediate heat exchanger is about 588°F (~309°C), and the outlet temperature is 866°F (~463°C). This is also the inlet temperature to the steam generator.

Figure 2.8 is a detailed schematic of the intermediate heat exchanger (IHX). This equipment is at an elevation above the reactor vessel. The coolant from the primary sodium tank is pumped through the core and the blanket assemblies. From the reactor vessel the primary coolant enters the shell side of IHX, then flows down and discharges into the bulk sodium in the primary tank. The secondary sodium enters and leaves the IHX at the top, flowing through tubes in the IHX.

2.4 SECONDARY SYSTEM

The steam generator and distribution system uses the heat delivered by the primary cooling system to produce superheated steam at 820°F (~437.7°C), 1250 psig, and delivers at a rate of 240,000 lb_m/h (108,862 kg/h) (when the reactor is operating at full power of 62.5 MW) to a conventionally designed turbine generator to produce 20 MWe. Figure 2.9 shows the basic steam generator components: a steam drum with moisture-separating components, two shell-and-tube type once-

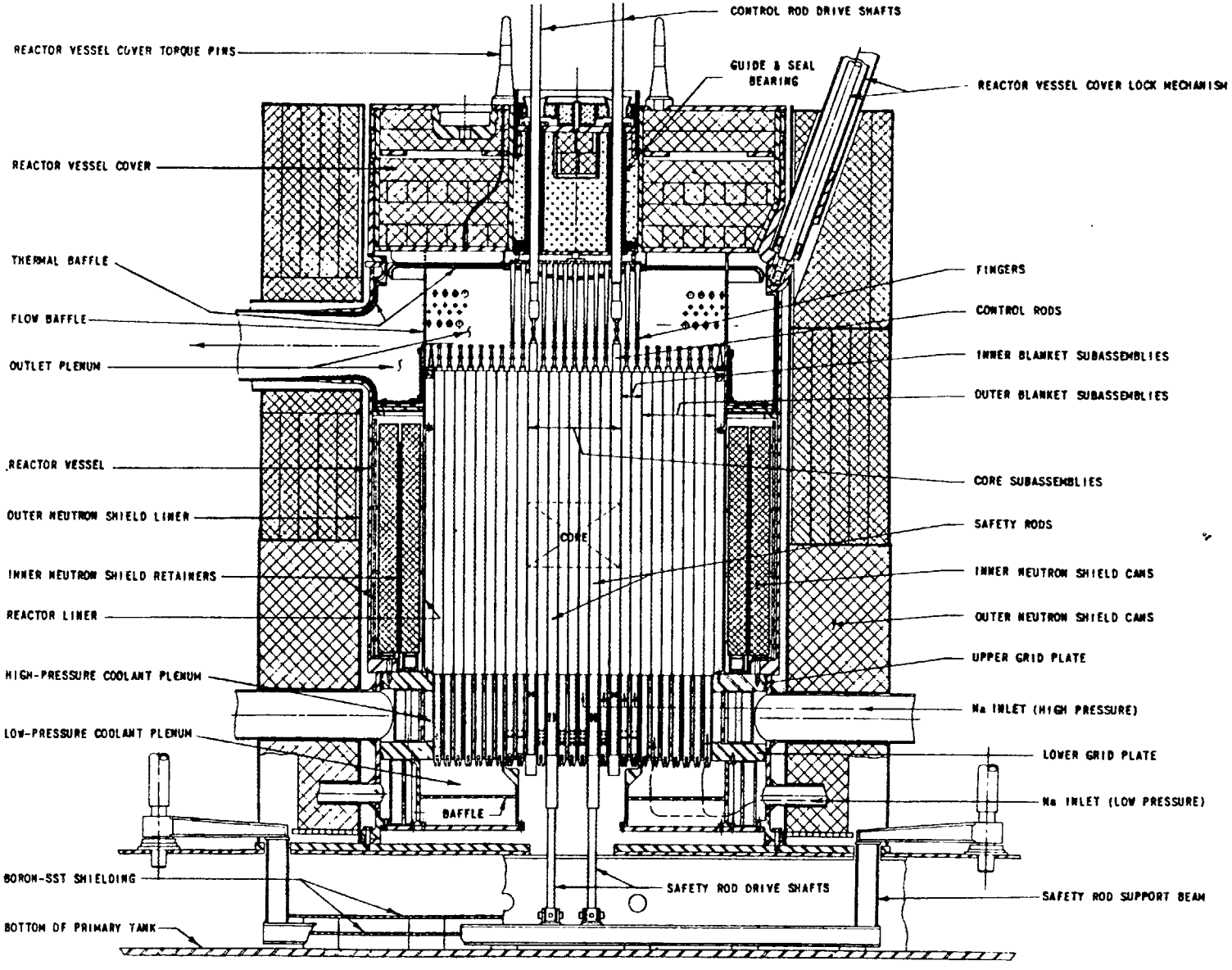

Fig. 2.6. EBR-II reactor vessel assembly. *Source: EBR-II System Design Descriptions*, Vols. 1 through 5, Argonne National Laboratory, Argonne, Ill., June 1972.

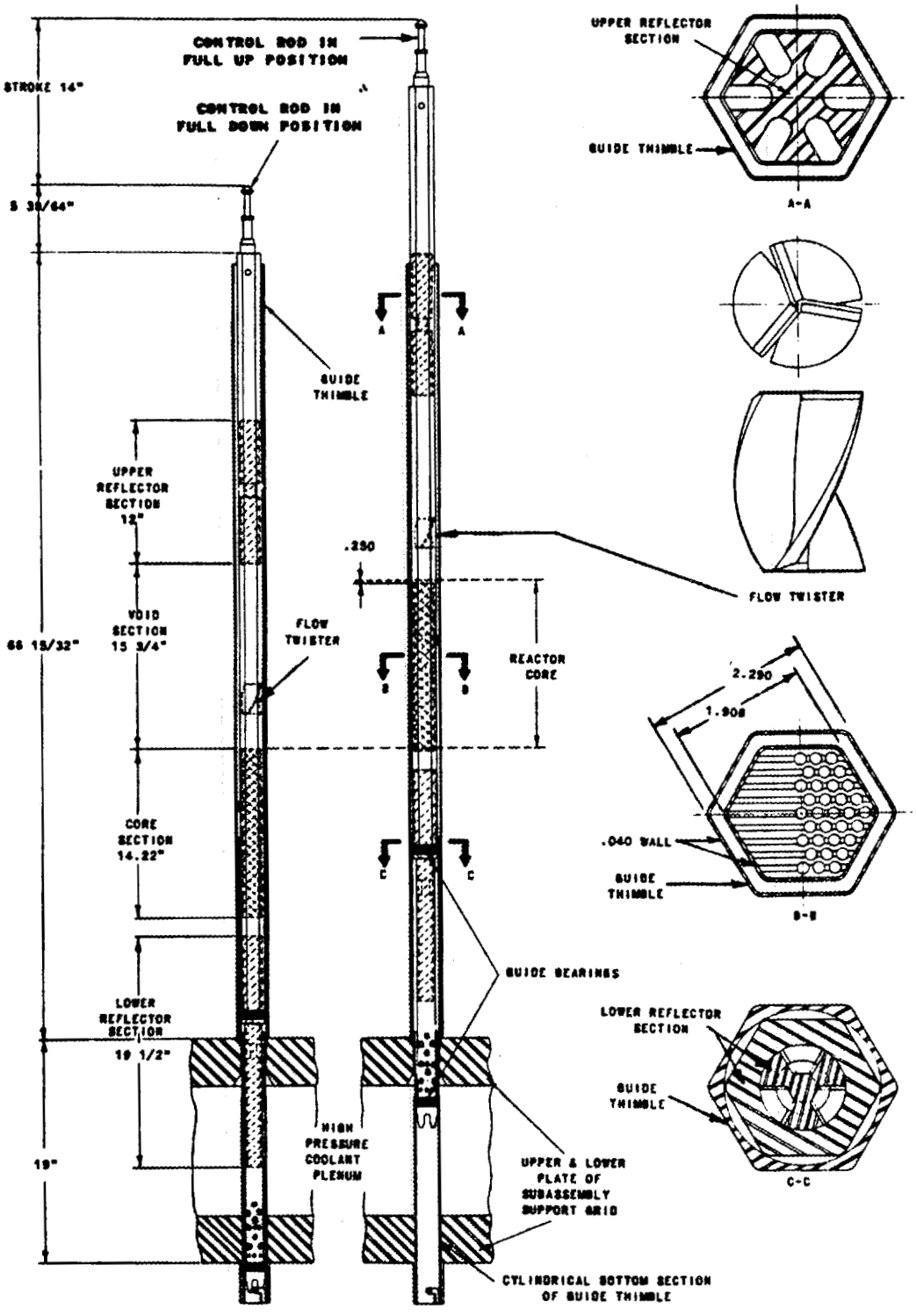

Fig. 2.7. EBR-II control subassembly. *Source: EBR-II System Design Descriptions*, Vols. 1 through 5, Argonne National Laboratory, Argonne, Ill., June 1972.

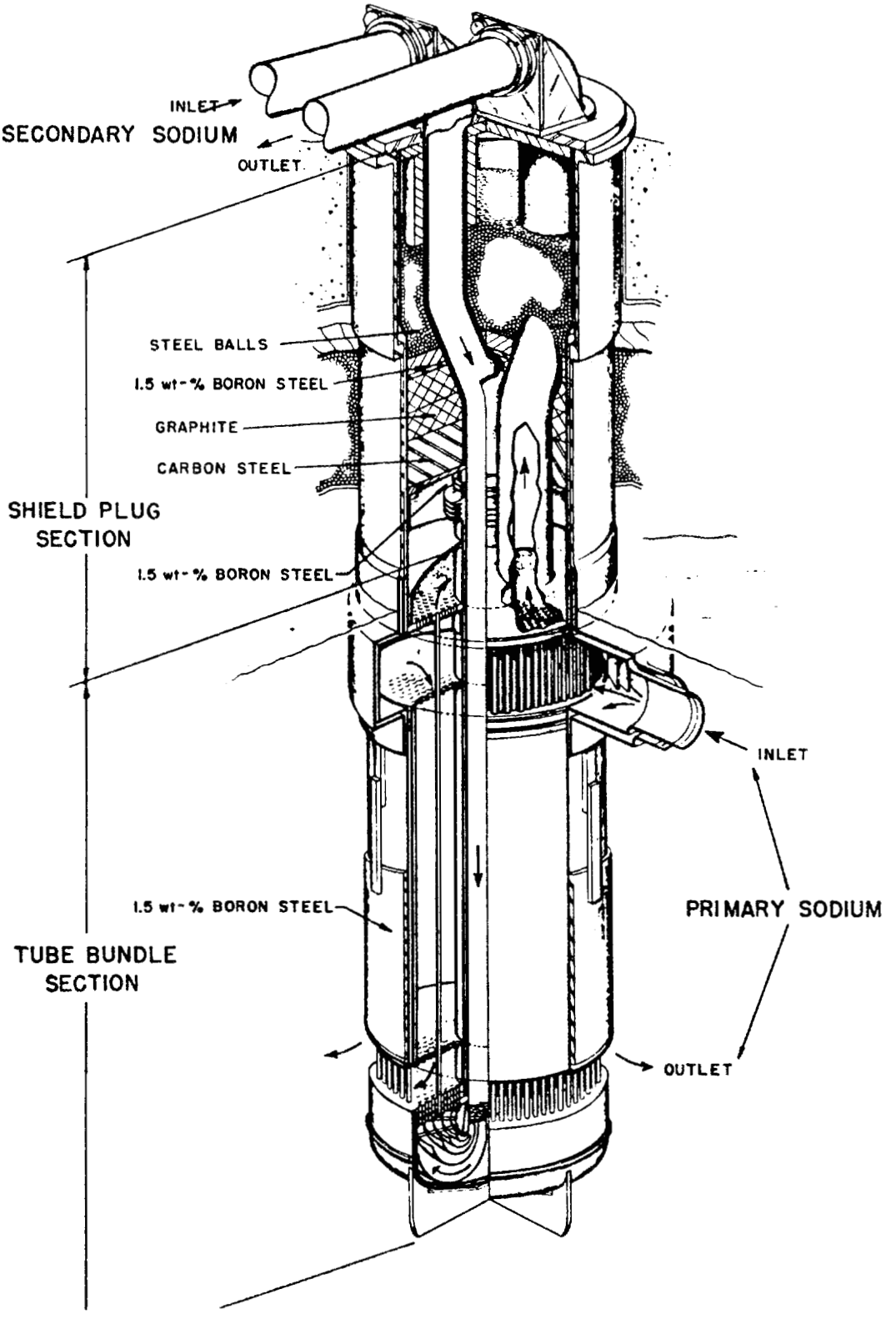

Fig. 2.8. EBR-II intermediate heat exchanger. *Source: EBR-II System Design Descriptions*, Vols. 1 through 5, Argonne National Laboratory, Argonne, Ill., June 1972.

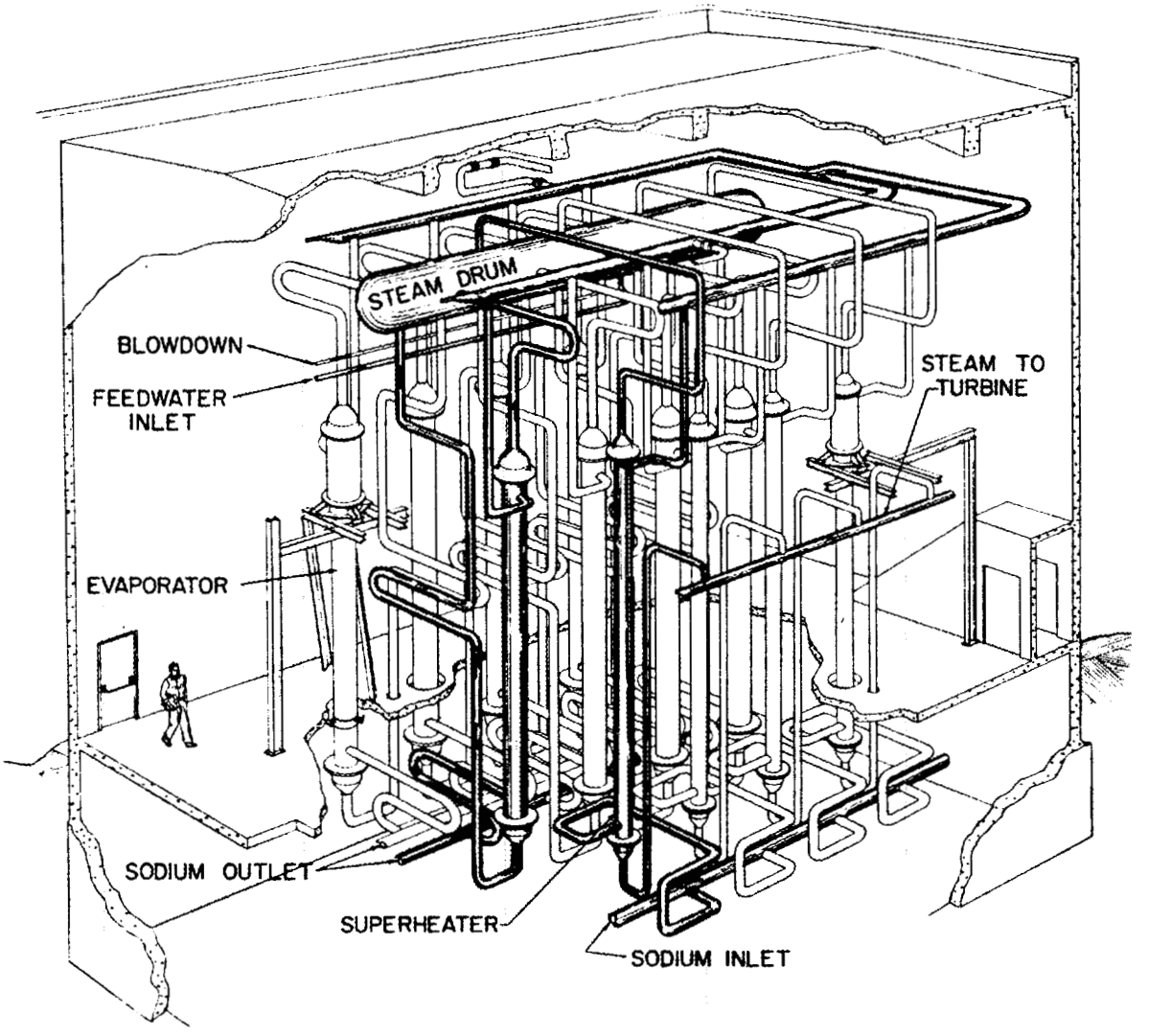

Fig. 2.9. EBR-II steam generator components. *Source: EBR-II System Design Descriptions*, Vols. 1 through 5, Argonne National Laboratory, Argonne, Ill., June 1972.

through superheaters, and seven shell-and-tube type recirculating evaporators. The feedwater flows out of the drum through the downcomer pipes to the bottom of seven parallel-connected evaporators, as shown in Fig. 2.10. The feedwater rises through the duplex tubes, absorbing heat from the sodium flowing in the shell, and is returned to the steam drum through the riser nozzles. The saturated steam-water mixture [six parts water and one part steam at 579°F (~303.8°C) at full power] hits the moisture-separating components, the condensed water recirculates through the downcomer, and the dry steam flows into the superheater section. The superheater details are shown in Fig. 2.11.

The evaporator assembly has an overall length of 30 ft 2 in. (~9 m 5 cm) and a maximum diameter of 56 in. (~140 cm). It consists of a shell assembly through which the sodium flows and a tube assembly through which the water flows (Fig. 2.12). The shell assembly consists of a schedule 20 pipe, two tee headers, a baffle nest assembly, and two sodium sheets with thermal plates.

Two parallel-connected once-through superheaters are shell-and-tube type heat exchangers (Fig. 2.13). The superheaters convert saturated steam at 578°F (~303°C) to superheated steam at 820°F (~438°C) by absorbing heat from the secondary sodium. The superheater assembly has exactly the same dimensions as the evaporators because it is an inverted and modified evaporator assembly. The modification is made by inserting core tubes in the duplex tubes. The core tubes decrease the cross-sectional area of the duplex tubes to cause the steam velocity to be increased.

The steam drum is mounted above the evaporators with its centerline at the 154-ft (~46-m) elevation, and it is 48 ft (~14 m) long with a 4-ft (120-cm) ID. The water/steam mixture that enters the drum through the riser nozzles at the centerline is deflected downward by diffuser plates anchored across each side of the drum above the riser nozzles. The diffuser plates prevent the water/steam mixture from impacting directly on the deflector and screen assembly; they also cause diffusion of the saturated steam to the side and bottom of the drum to cause initial fallout of the heaviest moisture particles. The steam passes through the primary and final screen dryer assemblies located on each side of the drum near the top and extending along the entire length of the drum.

In the EBR-II, the natural recirculation-type steam generator is selected over the once-through type because of its proven operation and inherent stability. Other design specifications especially characteristic of the EBR-II are the location of evaporators and superheaters with sodium on the shell side with water/steam flowing through the tubes to minimize stress corrosion and the use of bonded duplex tubes and double tube sheets to minimize the possibility of interaction between sodium and water/steam.[11]

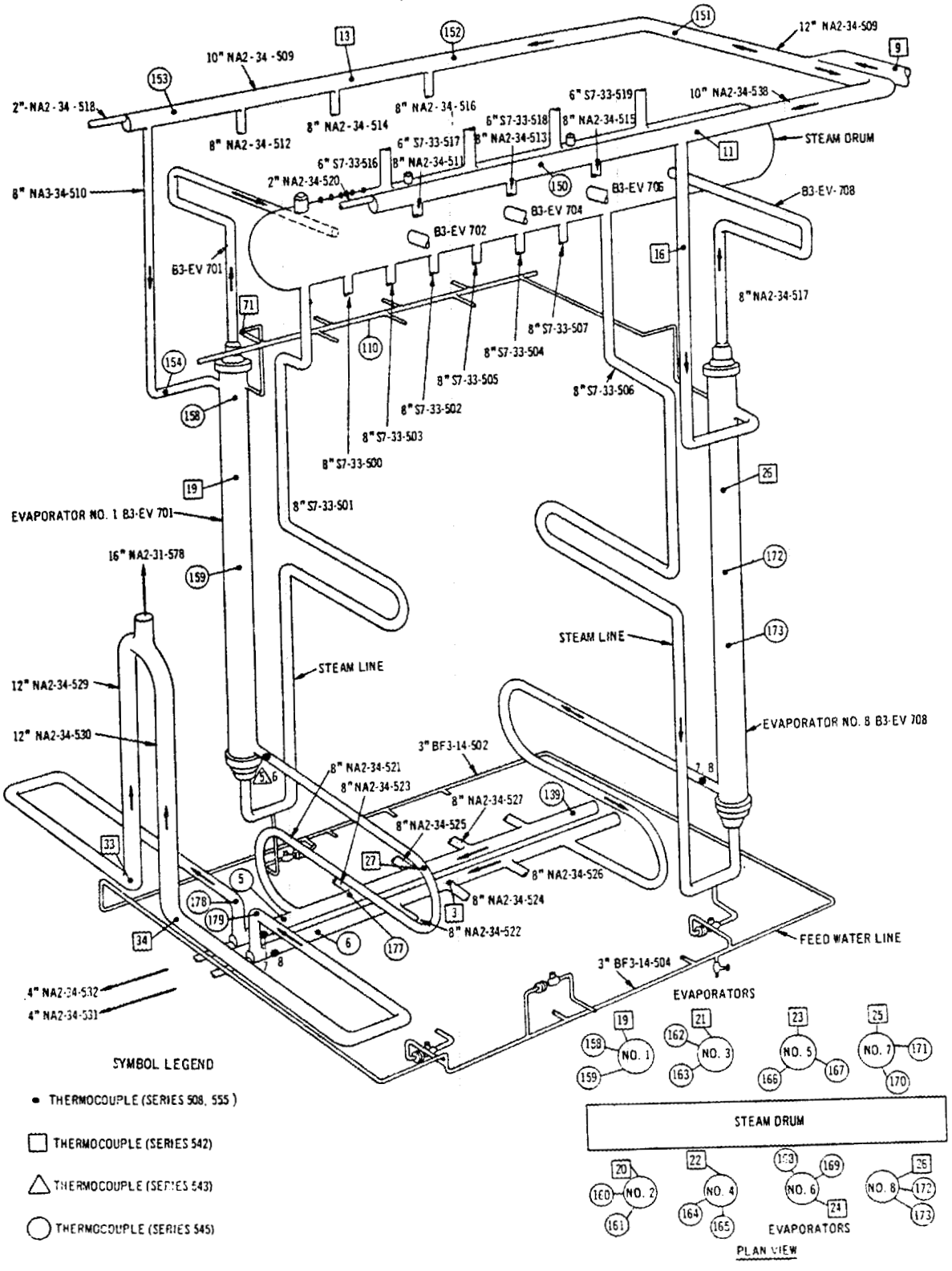

Fig. 2.10. EBR-II evaporator details and sensor locations. *Source: EBR-II System Design Descriptions*, Vols. 1 through 5, Argonne National Laboratory, Argonne, Ill., June 1972.

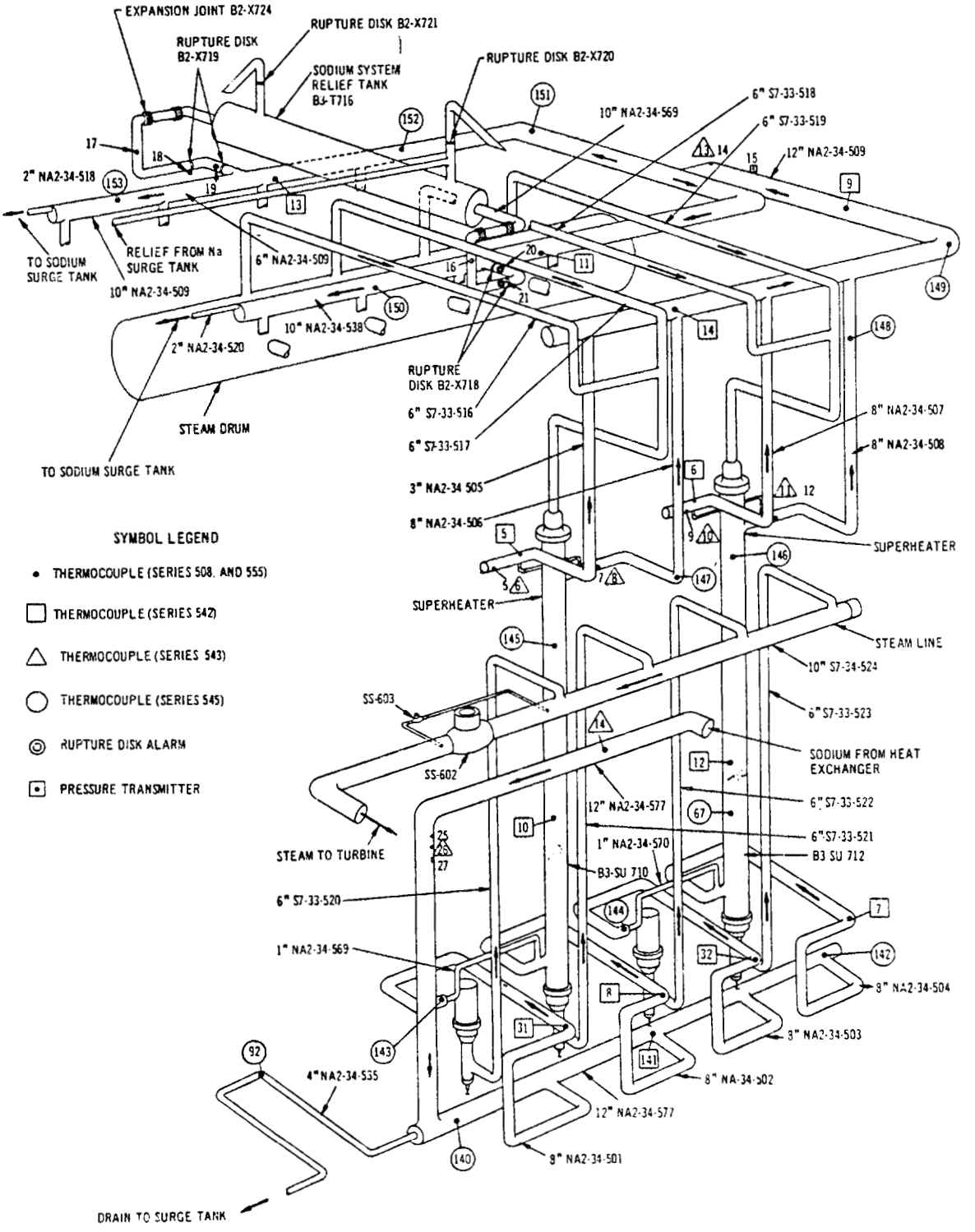

Fig. 2.11. EBR-II superheater details and sensor locations. *Source: EBR-II System Design Descriptions*, Vols. 1 through 5, Argonne National Laboratory, Argonne, Ill., June 1972.

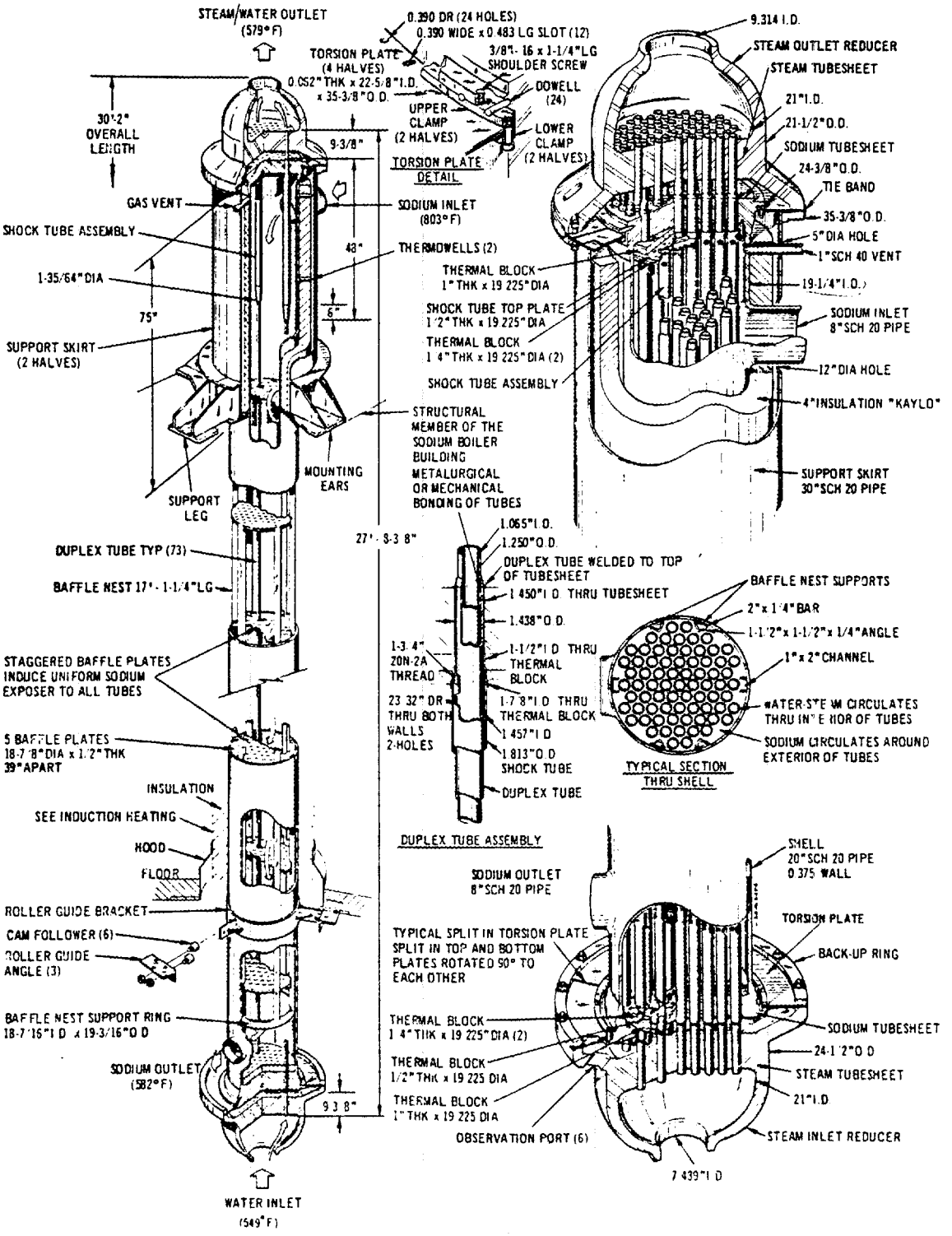

Fig. 2.12. EBR-II evaporator assembly. *Source: EBR-II System Design Descriptions*, Vols. 1 through 5, Argonne National Laboratory, Argonne, Ill., June 1972.

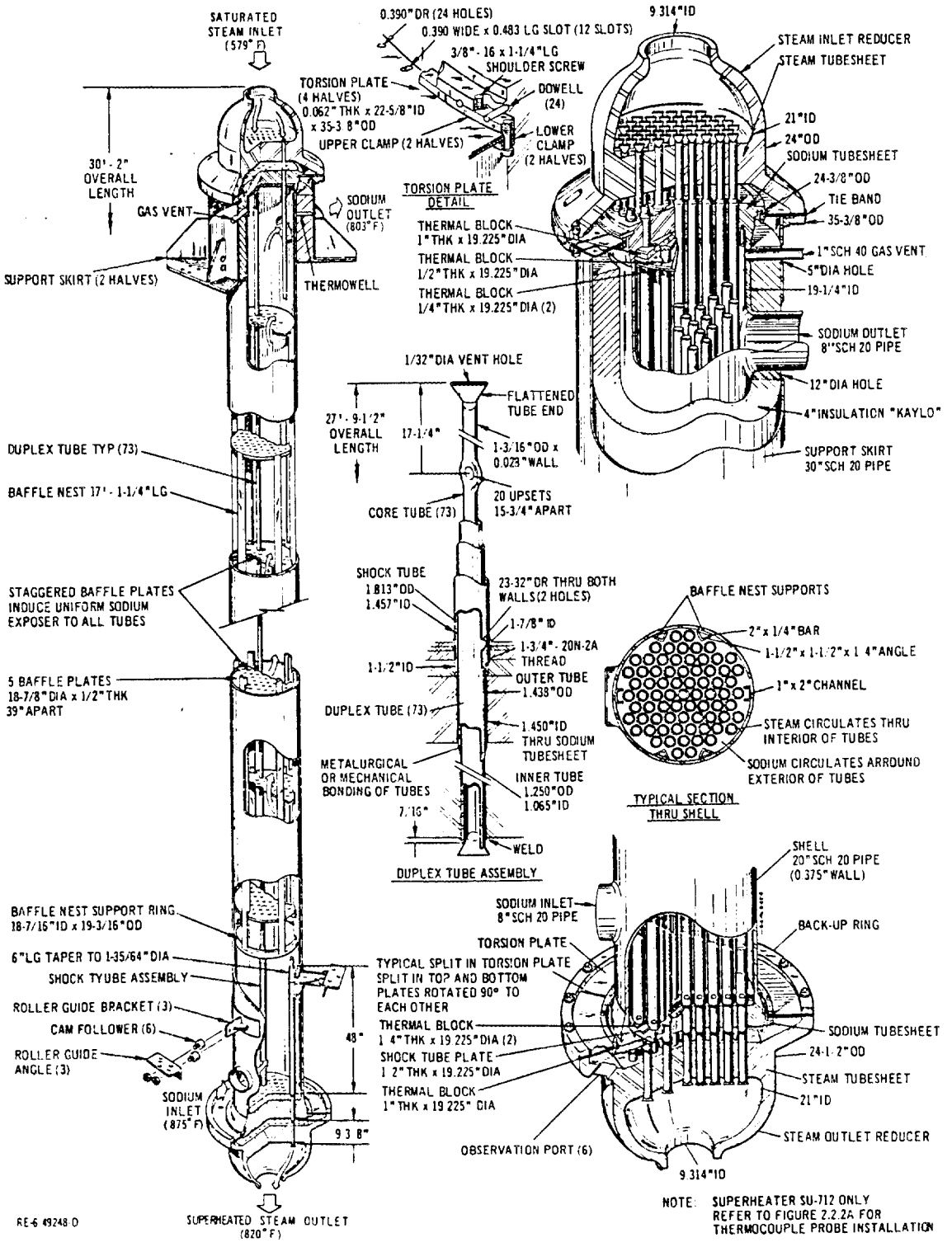

Fig. 2.13. EBR-II superheater assembly. *Source: EBR-II System Design Descriptions*, Vols. 1 through 5, Argonne National Laboratory, Argonne, Ill., June 1972.

2.5 EBR-II CONTROL SYSTEMS

EBR-II reactivity control is maintained by using 12 control rods and 2 safety rod subassemblies as described in Sect. 2.2.3. A computer-controlled rod drive system controls reactor power during steady state and also changes reactor power. An error signal from the reactor power reading is the input to the digital computer. The permanent automatic control rod drive system (ACRDS) provides a fast-speed automatic mode plus two slow-speed modes, manual and automatic. The technical specification limit of reactivity insertion is 0.01 $/s (safety related). The reactor is subcritical when the control rods are fully withdrawn. The control rod contains fuel elements in the approximate center and provides positive reactivity as it is inserted into the active core region. The two safety rods are always fully inserted for normal operations. They are automatically ejected from the core when hazardous incidents are detected.[11]

The primary sodium flow (loop between core and IHX) is controlled by motor-driven impeller-type primary pumps and the pumping rate is variable from 0 to 100% in a continuous stepless manner. There are no valves or other control devices in the main sodium loop. During normal operation the pump is operated at a flow rate sufficient to maintain bulk sodium temperature at 700°F (~371°C) at all power levels.

Secondary sodium flow is controlled by an electromagnetic pump. Flow is adjustable from 0 to 100% of full flow capacity by varying the voltage applied to the pump windings. The control signal is adjusted manually from the sodium recirculating pump panel.

The feedwater temperature is controlled by bypassing some feedwater around the last heater, mixing a portion of the 480°F (~248.8°C) feedwater with the 568°F (~298°C) water to maintain 550°F (~288°C) input. The bypass valve is manually controlled from the steam panel in the main control room.

The turbine generator is controlled by two circuits. The primary circuit controls the speed and load of the turbine while the secondary circuit controls the turbine stop valve to trip the turbine when an abnormal condition occurs.

The main control of the steam generator is by the steam drum level control. This control system is capable of single-element, four-element, or manual control. The controller accepts four analog signals: steam-drum level, feedwater flow, steam flow, and blowdown flow. The actuator is the feedwater valve.

3. EBR-II PRIMARY SYSTEM MODEL DEVELOPMENT

3.1 INTRODUCTION

A nodal formulation of the reactor core and the intermediate heat exchanger is presented. The core model includes the active core, inner and outer blankets, lower and upper reflectors, and piping. The 25-node model is shown in Fig. 3.1. The formulation of the core model is partially adapted from earlier work by S. R. Greene.[4] All the system parameters are recalculated and updated using ref. 11. Two changes made in the Greene model include an application of a physical model reduction method[2] and a modification in the IHX model formulation. Physical and numerical reasons for these modifications are explained in the following sections. Core bowing and control rod expansion reactivity effects have not been taken into account in the present model.

The intermediate heat exchanger (IHX) is modeled using 12 state variables and includes the primary sodium tank, as shown in Fig. 3.1. The core and IHX models are coupled into one module for the purpose of simulation studies. The governing equations for each subsystem, the definition of variables, and the table of parameters are presented in the following sections.

3.2 REACTOR CORE

The active core dynamics are described by the point reactor kinetics equations.[4]

3.2.1 Reactor Kinetics

$$\frac{d}{dt}\frac{\delta P}{P_o} = \frac{-\beta_T}{\Lambda}\frac{\delta P}{P_o} + \bar{\lambda}\frac{\delta C}{P_o} + \sum_i \frac{\alpha_i}{\Lambda}\delta T_i + \frac{\delta\rho_{ext}}{\Lambda} , \tag{3.1}$$

$$\frac{d}{dt}\frac{\delta C}{P_o} = \frac{\beta_T}{\Lambda}\frac{\delta P}{P_o} - \bar{\lambda}\frac{\delta C}{P_o} , \tag{3.2}$$

where

δ = denotes variation from the steady state value,

P = power,

P_o = steady state power,

β_T = total delayed neutron fraction,

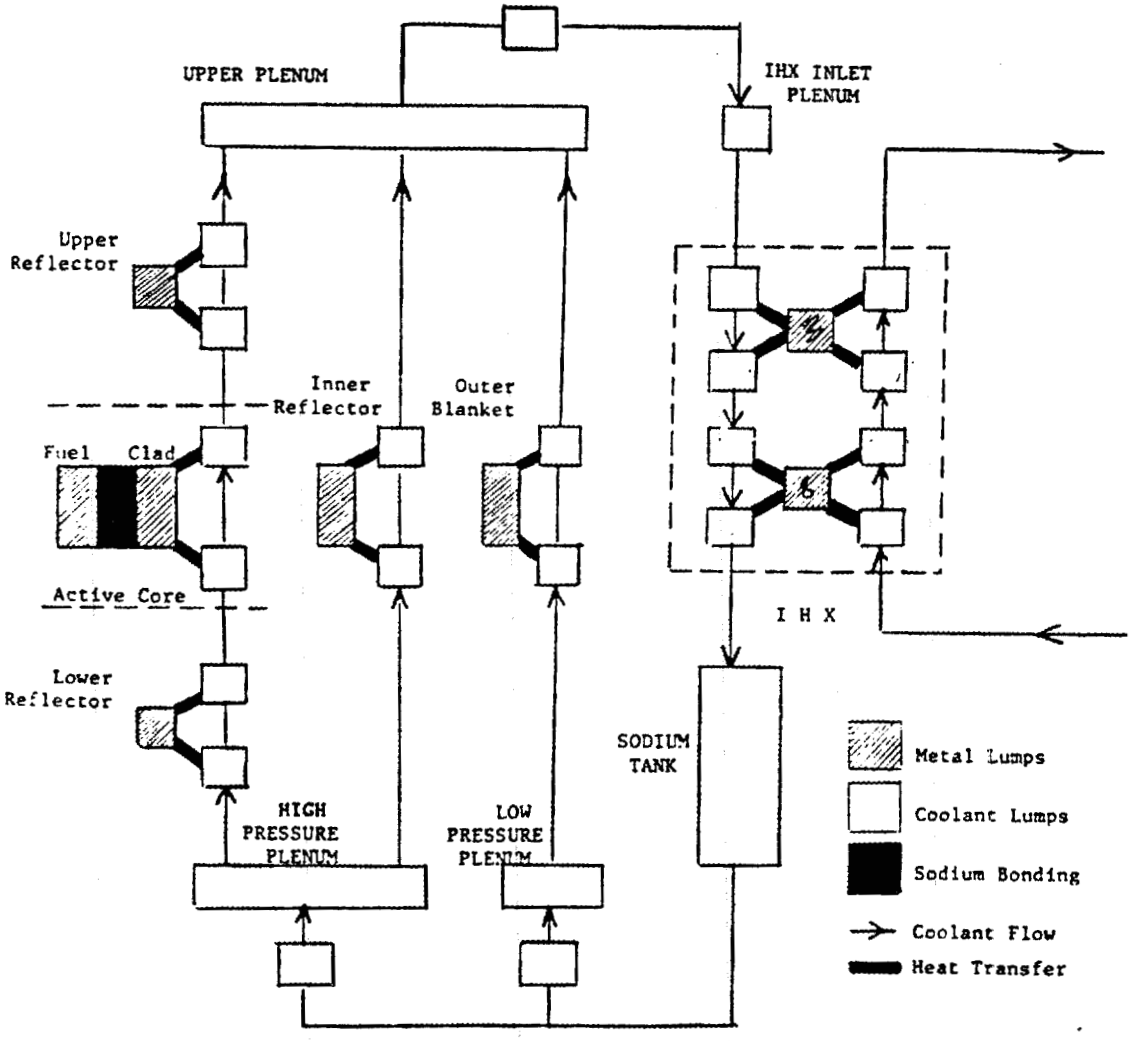

Fig. 3.1. Nodal representation of the EBR-II primary system model.

Λ = neutron generation time,

C = precursor concentration,

α_i = temperature reactivity feedback coefficient corresponding to temperature T_i,

ρ_{ext} = external reactivity,

$\bar{\lambda}$ = precursor average decay constant,

T_i = temperature of the ith region.

The neutronic data and the reactivity feedback coefficients are given in Tables 3.1 and 3.2, respectively. The core bowing reactivity effect becomes significant at high temperatures. The structural material inside the vessel expands radially when some critical temperature point is exceeded and replaces a corresponding amount of coolant volume. Resultant effects are less heat removal, because the coolant volume is reduced, and a contribution to the temperature reactivity feedback phenomena. Compared to the other reactivity mechanisms, however, this behavior is complicated and not as dominant as other feedback effects. Figure 3.2 shows the core bowing reactivity effect temperature dependence with respect to other reactivity effects.[13] A recent study at ANL[13] reports that the uncertainty in predicting a numerical value for the thermal bowing coefficient is high (the reactivity effects have been verified by data from rod drop, reactor oscillator, or power reactivity decrement tests). In the EBR-II core, another significant reactivity feedback effect comes from the control rod expansion at high temperatures. Expansion of a control rod introduces more neutron absorber into the core, which is a negative reactivity effect and improves the safety margins.

For low-order modeling purposes, these mechanisms may be ignored without losing much information about system behavior for small transients around the steady state. Thermal bowing cannot be handled without increasing the order of the model by introducing some radial lumps. At steady state conditions, we assume that the control rod expansion reactivity effect is negligible.

Using the data given in Table 3.1 and averaging the mean lifetime over the six precursor groups, we obtain

$$\bar{\ell} = \frac{\sum_{i=1}^{6} \beta_i \ell_i}{\beta_T} \quad . \tag{3.3}$$

Using Eq. (3.3), an average precursor equation is replaced with the six-group equations of the Greene model. This is a well known physical model reduction technique[2] that gives accurate results when low-order kinetic models are needed. Reducing the order of a model saves

Table 3.1. EBR-II neutronic data

Precursor decay constant (s^{-1})	Delayed neutron fraction	Mean lifetime (s)
$\lambda_1 = 0.0127$	$\beta_1 = 0.000252$	$\ell_1 = 78.74$
$\lambda_2 = 0.0317$	$\beta_2 = 0.00147$	$\ell_2 = 31.5457$
$\lambda_3 = 0.1150$	$\beta_3 = 0.001344$	$\ell_3 = 8.6957$
$\lambda_4 = 0.311$	$\beta_4 = 0.002941$	$\ell_4 = 3.2154$
$\lambda_5 = 1.4$	$\beta_5 = 0.001024$	$\ell_5 = 0.7143$
$\lambda_6 = 3.78$	$\beta_6 = 0.000237$	$\ell_6 = 0.2645$

Total delayed neutron fraction	$\beta_T = 0.007278$
Neutron generation time	$\Lambda = 1.55 \times 10^{-7}$ s
Average precursor mean lifetime	$\bar{\ell} = 12.1077$ s
Average decay constant	$\bar{\lambda} = 1/\bar{\ell} = 0.08259\ s^{-1}$

Table 3.2. EBR-II reactivity feedback coefficients

Coefficient	$\delta\rho/°F$	Coupled parameter
Doppler	$+0.222 \times 10^{-6}$	Fuel temperature
Steel expansion	-0.720×10^{-5}	Clad temperature
Core Na expansion	-0.481×10^{-5}	Core Na temperature
Upper reflector expansion	-0.223×10^{-5}	Upper reflector Na temperature
Lower reflector expansion	-0.223×10^{-5}	Lower reflector Na temperature
Inner reflector expansion	-0.120×10^{-5}	Inner reflector Na temperature
Fuel expansion	-0.200×10^{-5}	Fuel temperature

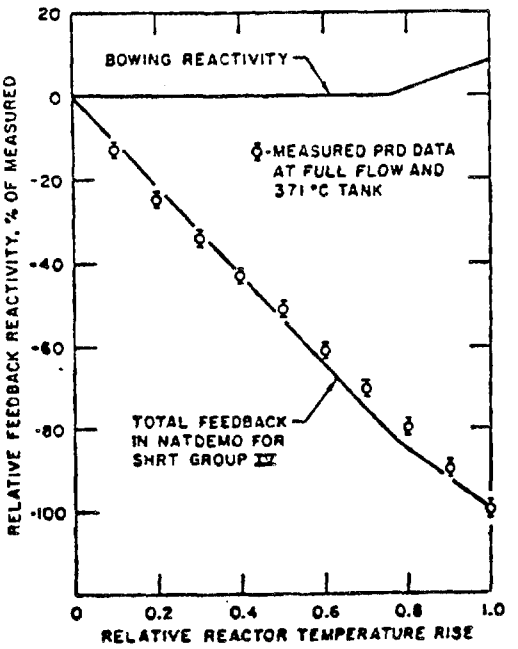

Fig. 3.2. Measured and calculated feedback reactivity in EBR-II for SHRT Group IV.

computational time and associated cost. The calculated parameters are listed in Table 3.1.

3.2.2 Core Heat Transfer

The heat transfer in the active core region is modeled by using five differential equations corresponding to five lumps, as shown in Fig. 3.3. These nodes represent the fuel, sodium bond, cladding, inlet coolant, and outlet coolant regions. The heat transfer dynamics between cladding and coolant regions is represented using Mann's model.[7] In Mann's model, the lower coolant lump outlet temperature is assumed to represent the average lump temperature, which is a coupling parameter for the heat transfer driving force between the metal and the coolant regions.

Table 3.3 shows the core heat transfer parameters. The perturbation forms of the state equations are given below.[4]

$$\frac{d}{dt}\,\delta T_F = \frac{P_F P_o}{(MC_p)_F}\,\frac{\delta P}{P_o} - \frac{1}{R_1 (MC_p)_F}\,(\delta T_F - \delta T_B) \quad , \tag{3.4}$$

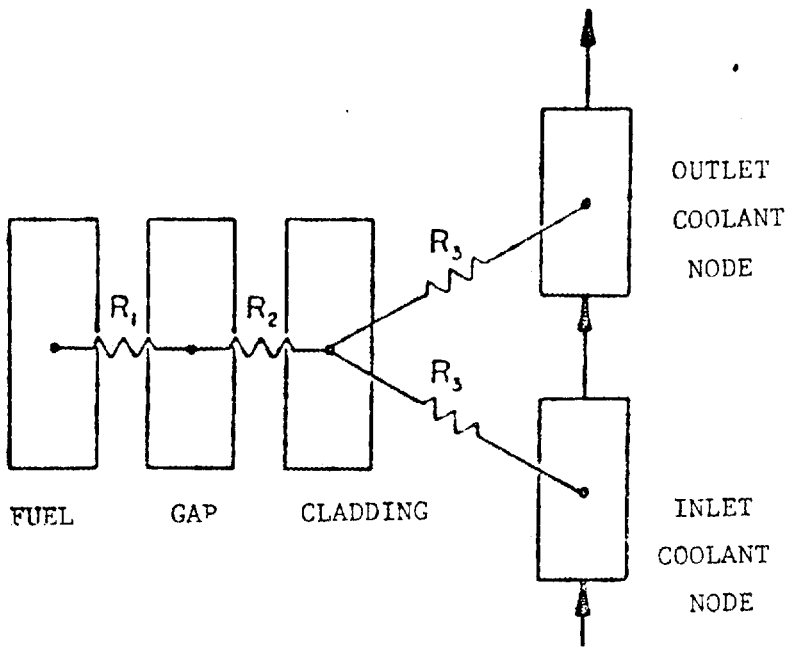

Fig. 3.3. Mann's core heat transfer model.

Table 3.3. Core heat transfer parameters

Power (Btu/s)	Heat capacity (Btu/°F)(°C)	Heat resistance (s-°F/Btu)(°C)
$P_o = 59267$	$MC_f = 34.8$	$R_1 = 6.585$
	$MC_c = 13.33$	$R_3 = 12.5879$
$P_f = 49547.1$	$MC_B = 2.03$	$R_2 = 7.0973$
	$MC_O = 16.69$	$\tau = 0.075$

$$\frac{d\delta T_B}{dt} = \frac{1}{R_1(MC_p)_B}(\delta T_F - \delta T_B) - \frac{1}{R_2(MC_p)_B}(\delta T_B - \delta T_c) \quad , \tag{3.5}$$

$$\frac{d\delta T_C}{dt} = \frac{1}{R_2(MC_p)_B}(\delta T_B - \delta T_C) - \frac{1}{R_3(MC_p)_B}(\delta T_B - \delta \Theta_1) \quad , \tag{3.6}$$

$$\frac{d\delta\Theta_1}{dt} = \frac{1}{R_2(MC_p)_\Theta}(\delta T_C - \delta\Theta_1) + \frac{2}{\tau}(\delta\gamma_2 - \delta\Theta_1) \quad , \tag{3.7}$$

$$\frac{d\delta\Theta_2}{dt} = \frac{1}{R_3(MC_p)_\Theta}(\delta T_C - \delta\Theta_1) + \frac{2}{\tau}(\delta\Theta_1 - \delta\Theta_2) \quad , \tag{3.8}$$

where

T_F = fuel temperature,

T_B = sodium-bond temperature,

T_C = fuel cladding temperature,

Θ_i = temperature of the ith coolant node,

R_1, R_2, R_3 = heat transfer resistances,

γ_2 = lower axial-reflector coolant outlet temperature,

τ = resident time of the coolant in the active core region,

P_F = fraction of power deposited in the fuel,

$(C_p)_B$ = specific heat capacity of the blanket material,

$(C_p)_\Theta$ = specific heat capacity of the coolant,

M_B = mass of the blanket material,

M_Θ = mass of the coolant.

3.2.3 Reflector and Blanket Models

The active core in the EBR-II is surrounded by reflector and blanket materials, as explained in Sect. 2. The complete core model includes 12 nodes representing the axial and the radial reflector zones and radial blanket region. The same heat transfer principle is carried out in developing the state equations as in the core heat transfer model. The general equations for reflector and blanket regions are described by a set of three equations for each. The parameter values are listed in Table 3.4.[4]

$$\frac{d\delta T_M}{dt} = \frac{P_i}{(MC_p)_M}\frac{\delta P}{P_o} - \frac{U \cdot A}{(MC_p)_M}(\delta T_M - \delta T_1) \quad , \tag{3.9}$$

$$\frac{d\delta T_1}{dt} = \frac{U \cdot A}{(MC_p)_T}(\delta T_M - \delta T_1) + \frac{2}{\tau}(\delta\Theta_{in} - \delta T_1) \quad , \tag{3.10}$$

Table 3.4. Reflector and blanket region data

Upper and lower reflector	Inner reflector	Outer blanket
P_f = 711.2025 Btu/s	P_f = 5808.15 Btu/s	P_f = 1303.87 Btu/s
$(MC_p)_m$ = 54.70 Btu/°F	$(MC_p)_m$ = 378.18 Btu/°F	$(MC_p)_m$ = 1797.85 Btu/°F
$(MC_p)_T$ = 27.10 Btu/°F	$(MC_p)_T$ = 14.26 Btu/°F	$(MC_p)_T$ = 217.36 Btu/°F
UA_L = 71.08 Btu/s-°F	Resident time = 0.27 s	Resident time = 1.09 s
UA_U = 4.62 Btu/s-°F	UA = 32.03 Btu/s-°F	UA = 14.89 Btu/s-°F
Resident time = 0.106 s		

$$\frac{d\delta T_2}{dt} = \frac{U \cdot A}{(MC_p)_T} (\delta T_M - \delta T_1) + \frac{2}{\tau} (\delta T_1 - \delta T_2) \ , \tag{3.11}$$

where

T_M = temperature of the metal node,

T_1 = temperature of the first region coolant node,

T_2 = temperature of the second region coolant node,

A = total heat transfer area,

τ = residence time of the coolant in reflector or blanket region,

U = metal to coolant heat transfer coefficient,

θ_{in} = inlet coolant temperature,

$(C_p)_M$ = specific heat capacity of the metal,

$(C_p)_T$ = specific heat capacity of the coolant.

3.2.4 Piping and Plenum Models

The model includes six lumps representing the low-pressure plenum, the high-pressure plenum, the upper plenum, and the three core inlet-outlet piping regions. A first-order transport lag has been assumed for all piping. The other assumptions are: (1) constant coolant density, (2) no axial heat conduction, and (3) no heat gain or loss in the

piping. The perturbation forms of the state equations are as follows. The design parameters are given in Table 3.5.[4]

$$\frac{d\delta T_U}{dt} = \frac{M_1 . C_{p1}}{(MC_p)_u} (\delta\gamma_4 - \delta T_u) + \frac{M_2 . C_{p2}}{(MC_p)_u} (\delta\gamma_6 - \delta T_u) + \frac{M_3 . C_{p3}}{(MC_p)_u} (\delta\gamma_8 - \delta T_u), \quad (3.12)$$

$$\frac{d\delta T_{out}}{dt} = \frac{1}{\tau_1} (\delta T_U - \delta T_{out}) \quad , \quad (3.13)$$

$$\frac{d\delta T_{LI}}{dt} = \frac{1}{\tau_3} (\delta\theta_p - \delta T_{LI}) \quad , \quad (3.14)$$

$$\frac{d\delta T_{HI}}{dt} = \frac{1}{\tau_4} (\delta\theta_p - \delta T_{HI}) \quad , \quad (3.15)$$

$$\frac{d\delta T_H}{dt} = \frac{1}{\tau_5} (\delta T_{HI} - \delta T_H) \quad , \quad (3.16)$$

$$\frac{d\delta T_L}{dt} = \frac{1}{\tau_6} (\delta T_{LI} - \delta T_L) \quad , \quad (3.17)$$

where

T_U = upper plenum temperature,

T_{out} = reactor outlet temperature,

θ_p = primary sodium tank temperature,

T_{LI} = low-pressure plenum inlet temperature,

T_{HI} = high-pressure plenum inlet temperature,

T_H = high-pressure plenum temperature,

γ_4 = upper reflector outlet temperature,

γ_6 = inner reflector outlet temperature,

γ_8 = blanket region outlet temperature,

T_L = low-pressure plenum temperature,

τ_1 = resident time of sodium in reactor outlet piping,

τ_2 = resident time of sodium in the pot,

τ_3 = resident time of sodium in the pot-to-reactor low-pressure piping,

Table 3.5. Primary piping and plenum data

Time constants (s^{-1})	Resident times (s)
$\dot{M}_1/M_1 = 0.1198$	$\tau_1 = 1.54$
$\dot{M}_2/M_2 = 0.0288$	$\tau_2 = 552.6$
$\dot{M}_3/M_3 = 0.0246$	$\tau_3 = 1.8$
	$\tau_4 = 1.78$
	$\tau_5 = 1.49$
	$\tau_6 = 16.28$

τ_4 = resident time of sodium in the pot-to-reactor high-pressure piping,

τ_5 = resident time of sodium in the high-pressure plenum,

τ_6 = resident time of sodium in the low-pressure plenum.

3.2.5 Intermediate Heat Exchanger (IHX) Model

The sodium tank and the IHX are represented by 12 nodes in the model, as shown in Fig. 3.1. The primary inlet plenum and the sodium tank are represented by first-order transport-lag approximations. The heat transfer from the primary to the secondary sodium is modeled using Mann's technique.[7]

For a low-order counterflow heat exchanger model, the system may be divided into five regions, each representing an average temperature (as implemented in Greene's model). The configuration of the model includes two equal lumps for primary and secondary coolant regions and a single lump for the tube wall region, as shown in Fig. 3.4. However, there are cases for which the five-lump configuration becomes insufficient in representing the system behavior, and some unphysical responses may be encountered. An analytical identification of the problem has already been studied,[7] and it has been proven that a transfer function written for the input output pair (T_{out},T_{in}) becomes nonminimum phase if the corresponding time constants of the five-lump model exceed a certain limit. One approach to avoid such an unphysical behavior in system responses is to define average temperatures for smaller portions of the system by dividing the system into more lumps.

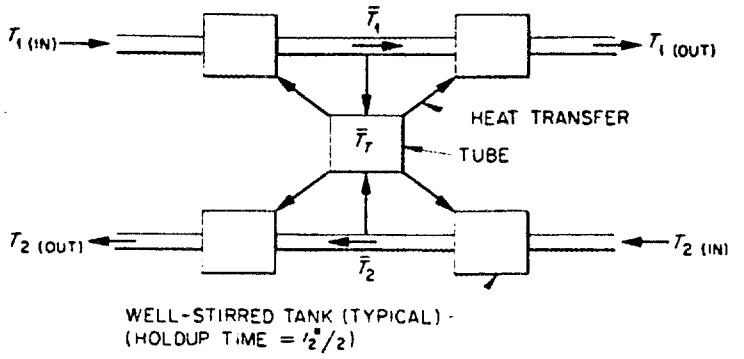

Fig. 3.4. Lumped-parameter approximation of a counterflow heat exchanger. *Source*: S. J. Ball, "Approximate Models for Distributed-Parameter Heat-Transfer Systems," *ISA Trans.* 3, 38-47 (Jan. 1964).

The EBR-II intermediate heat exchanger data for the ratio $(U_{pm}A_{pm}/M_pC_p)$ is 0.216 s^{-1}, and the corresponding time constant is 4.62 s, thus exceeding the acceptable value of 2 s as stated in ref. 7. Therefore, the IHX model is formulated using two five-lump models connected in series, as suggested by Ball. The simulation results presented in Sect. 5 verify that the modification improved the overall heat exchanger behavior.

Five-lump model state equations are described below.[4]

$$\frac{d\delta P_1}{dt} = \frac{2}{T_8}\,\delta P_{in} - \left[\frac{(UA)_p}{(MC_p)_p} + \frac{2}{\tau_8}\right]\delta P_1 + \frac{(UA)_p}{(MC_p)_p}\,\delta M \quad ; \tag{3.18}$$

$$\frac{d\delta P_2}{dt} = \left[\frac{2}{\tau_8} - \frac{(UA)_p}{(MC_p)_p}\right]\delta P_1 - \frac{2}{\tau_8}\,\delta P_2 + \frac{(UA)_p}{(MC_p)_p}\,\delta M \quad ; \tag{3.19}$$

$$\frac{d\delta M}{dt} = \frac{(UA)_p}{(MC_p)_M}\,\delta P_1 - \left[\frac{(UA)_p + (UA)_s}{(MC_p)_M}\right]\delta M + \frac{(UA)_s}{(MC_p)_M}\,\delta S_1 \quad ; \tag{3.20}$$

$$\frac{d\delta S_1}{dt} = \frac{(UA)_s}{(MC_p)_s}\,\delta M - \left[\frac{(UA)_s}{(MC_p)_s} + \frac{2}{\tau_9}\right]\delta S_1 + \frac{2}{\tau_9}\,\delta S_{in} \quad ; \tag{3.21}$$

$$\frac{d\delta S_2}{dt} = \frac{(UA)_s}{(MC_p)_s}\,\delta M - \left[\frac{(UA)_s}{(MC_p)_s} - \frac{2}{\tau_9}\right]\delta S_1 - \frac{2}{\tau_9}\,\delta S_2 \quad ; \tag{3.22}$$

The primary inlet plenum and the sodium tank regions are represented by the following equations.

$$\frac{d\delta P_{in}}{dt} = \frac{1}{\tau_7}\,\delta T_{out} - \frac{1}{\tau_7}\,\delta P_{in} \quad , \tag{3.23}$$

$$\frac{d\delta\Theta_p}{dt} = \frac{1}{\tau_2}\,(\delta P_2 - \delta\Theta_p) \quad , \tag{3.24}$$

where

P_{in} = primary inlet plenum temperature,

T_{out} = reactor outlet temperature,

P_1 = first primary node temperature,

M = tube wall temperature,

P_2 = second primary node temperature,

S_1 = first secondary node temperature,

S_{in} = secondary sodium inlet temperature,

S_o = secondary outlet plenum temperature,

Θ_p = sodium tank temperature,

τ_7 = resident time in primary outlet plenum,

τ_8 = resident time in both primary nodes,

τ_9 = resident time in both secondary nodes,

τ_{10} = sodium resident time in secondary outlet plenum.

The design parameters are given in Table 3.6.

The corresponding nonzero elements of the linearized system matrix A are given in Table 3.7.

Table 3.6. IHX design data

Heat transfer (Btu/s-°F)	Heat capacity (Btu/°F)	Resident times (s)
$(UA)_s = 598.94$	$(MC_p)_p = 1168$	$\tau_7 = 1.91$
$(UA)_p = 505.03$	$(MC_p)_m = 420.83$	$\tau_8 = 7.29$
	$(MC_p)_s = 282.125$	$\tau_9 = 2.86$
		$\tau_{10} = 0.25$

Table 3.7. Nonzero elements of system matrix *A* of the EBR-II primary system model (see Table 5.1, list of state variables)

I	J	A(I,J)	I	J	A(I,J)
1	1	-46955	1	7	-13.282
2	1	46955	7	7	-26.66
3	1	1165.7	16	7	18.867
12	1	4.59			
15	1	4.59	8	8	-0.5555
18	1	5.32	9	8	0.614
21	1	0.107			
			9	9	-0.614
1	2	0.0826	22	9	1.834
2	2	-0.0826			
			10	10	-0.5617
1	3	-9.8179	11	10	0.6711
3	3	-24.612	11	11	-0.6711
4	3	422.29	13	11	18.867
			19	11	7.406
3	4	24.612			
4	4	-812.12	12	12	-1.299
5	4	59.652	13	12	2.622
			14	12	2.622
1	5	-46.4516			
4	5	391.82	1	13	-0.08632
5	5	-93.285	12	13	1.299
6	5	26.838	13	13	-21.489
			14	13	16.245
1	6	-13.282			
5	6	33.633	1	14	-0.08632
6	6	-53.505	6	14	26.66
7	6	-0.171	14	14	-18.867

Table 3.7. (continued)

I	J	A(I,J)	I	J	A(I,J)
15	15	-0.0844	26	26	-0.5235
16	15	0.1704	27	26	0.549
17	15	0.1714			
			27	27	-0.765
1	16	-0.08632	28	27	0.333
15	16	0.0844	29	27	0.300
16	16	-19.038			
17	16	18.696	28	28	-0.549
			32	28	0.549
1	17	-0.08632			
17	17	-18.867	27	29	0.216
24	17	0.1198	28	29	0.216
			29	29	-0.655
18	18	-0.0846	30	29	1.060
19	18	2.2461	31	29	1.060
20	18	2.2461			
			30	30	-1.398
1	19	-0.3795			
18	19	0.0846	29	31	0.355
19	19	-9.66	30	31	0.337
20	19	5.1611	31	31	-2.458
1	20	-0.37935	32	32	-0.765
20	20	-7.407	33	32	0.333
24	20	0.0288	34	32	0.300
21	21	-0.00828	33	33	-0.549
22	21	0.068	37	33	0.0018
23	21	0.0685			
21	22	0.00828	32	34	0.216
22	22	-1.903	33	34	0.216
23	22	1.7654	34	34	-0.655
			35	34	1.060
23	23	-1.834	36	34	1.060
24	23	0.0246			
			31	35	1.398
24	24	-0.1732	35	35	-1.398
			34	36	0.355
25	24	0.6493	35	36	0.337
			36	36	-2.458
25	25	-0.6493			
26	25	0.5235	8	38	0.5555
			10	38	0.5617
			37	37	-0.0018

4. EBR-II STEAM GENERATOR MODEL DEVELOPMENT

4.1 INTRODUCTION

The EBR-II steam generator is a natural circulation, recirculation steam drum/evaporator system, extracting heat from the sodium to produce superheated steam at 820°F (~438°C) at full power. The entire system is divided into 13 lumps, each representing average physical quantities. The nodal representation is shown in Fig. 4.1. On the evaporator side, the primary tube wall and the secondary lumps are divided with a moving boundary determined by the subcooled height. The primary phenomena included in the model are the homogeneous flow in the boiling region, the mass and energy dynamics for both primary and secondary regions, the distribution of mass between downcomer, subcooled, boiling, and drum regions on the secondary side, and the momentum equation for the flow from the downcomer to subcooled regions and flow leaving the boiling region. System dynamics are assumed to be a function of two pressures: drum pressure and pressure inside the tubes of the evaporator.

Thermodynamic properties are determined at these two pressures. Primary assumptions used in this model are phase equilibrium, no superheating in the boiling region, and 100% effectiveness (outlet quality ≈1) for the separators. The superheater model considers a single-phase heat transfer regime. The primary sodium flow is assumed to be constant. A summary of assumptions used in the model is listed in Table 4.1.

The steam generator is represented by 20 differential equations using the state-space technique. The evaporator side consists of 13 state variables, including downcomer and drum water temperatures, drum and boiling region pressures, drum inlet steam quality, subcooled and drum levels, primary sodium and tube wall temperatures, and two flows for the downcomer and rising mixture in the boiling region. Five state variables of the superheater model are temperatures of the primary sodium, superheated steam, tube wall, control input, and feedwater flow. Design parameters are shown in Tables 4.2 through 4.4. The nonzero elements of the system matrix A are listed in Table 4.5.

4.2 EVAPORATOR AND DRUM BALANCE EQUATIONS

The operation of the EBR-II evaporator is quite similar to that of U-tube type steam generators; therefore, similar problems are encountered in modeling these two steam generators. One of the recent U-tube type steam generator models[9] suggests that the unknown flow at the moving boundary between subcooled and boiling regions is a linear function of the latent heat and the heat transfer rate into the subcooled region. The assumption used here is the linear dependence between flow and enthalpy increase caused by the heat transfer into this region. Another study[8] suggests that the unknown flows can be eliminated by algebraic manipulations. Two momentum equations are used for the unknown flows such as the downcomer flow and the flow leaving the evaporators, and the boundary flow is approximated as suggested in

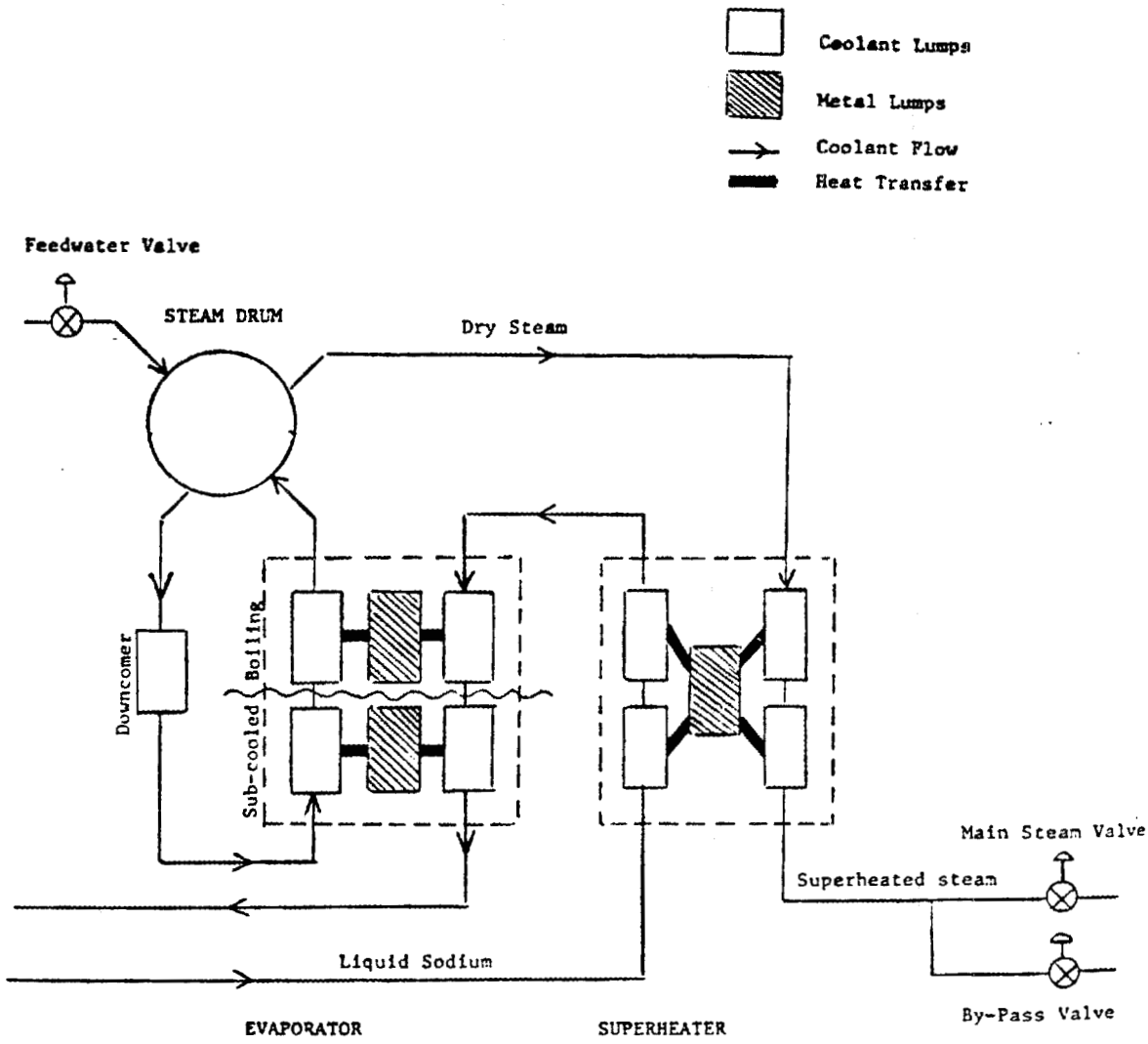

Fig. 4.1. Nodal representation of the EBR-II steam generator model.

Table 4.1. List of assumptions used in the EBR-II steam generator model

Assumption	Corresponding region
Phase equilibrium	Evaporator
No superheating	Drum, evaporator
No counterflow	Recirculation loop
Constant thermal conductivity	All
Constant heat transfer coefficient	All
No axial heat transfer	All
Linear relationship between boiling height and rising mixture steam quality	Boiling
Linear relationship between heat transfer rate into subcooled and flow rate	Subcooled
Linear approximation to thermodynamic variables around saturation conditions	Drum, evaporator
100% effective moisture separation	Drum
First-order dynamics	Feedwater valve
Critical flow assumption	Drum steam outlet
Single-phase regime	Superheaters

Table 4.2. Evaporator design data[a]

100% power level	From ref. a
Recirculation ratio	1/7
Primary sodium flow rate, lb_m/s	626
Feedwater flow rate, lb_m/s	75
Secondary flow rate, lb_m/s	525
Heat capacity of sodium, Btu/lb_m-°F	0.3003
Heat capacity of tube wall, Btu/lb_m-°F	0.1098
Heat capacity of water, Btu/lb_m-°F	1.012
Heat capacity of steam, Btu/lb_m-°F	0.639
Number of duplex tubes	72
Number of evaporator units	7
Secondary cross-sectional area, ft^2 (m^2)	2.56 (~0.23)
Primary cross-sectional area, ft^2 (m^2)	5.04 (~0.45)
Heat transfer area (sodium-metal), ft^2 (m^2)	6260 (563.4)
Heat transfer area (metal-secondary), ft^2 (m^2)	3338 (300.42)
Density of subcooled water, lb_m/ft^3	45.45
Density of dry steam (at 579°F, ~303.8°C), lb_m/ft^3	3.10
Density of liquid sodium, lb_m/ft^3	48.88
Average density in boiling region, lb_m/ft^3	40.97
Saturation temperature, °F (°C)	579 (~303.8)
Temperature at downcomer outlet, °F (°C)	542 (~283.3)
Evaporator steam exit quality	0.1428

Table 4.2 (continued)

100% power level	From ref. a
Overall heat transfer coefficient (liquid sodium-tube wall), Btu/ft^2-h	1241
Overall heat transfer coefficient (tube, wall-subcooled water), Btu/ft^2-h	988
Overall heat transfer coefficient (tube wall-boiling region), Btu/ft^2-h	1973
Total mass of primary sodium, lb_m	6290
Total mass of tube wall, lb_m	80604
Friction factor of downcomer piping	0.02
Average friction multiplier (boiling)	4.01
Height of downcomer piping, ft (m)	35 (~10.5)
Height of evaporator, ft (m)	27 (8.1)
$(\partial/\partial P_B)T_{sat}$ (around saturation, °F/psi	0.099
$(\partial/\partial P_B)V_{fg}$ (around saturation), ft^3/psi-lb_m	-0.0003
$(\partial/\partial P_B)h_{fg}$ (around saturation), Btu/lb_m-psi	-0.1848
$(\partial/\partial P_B)\rho_{sc}$ (around saturation), lb_m/ft^3-psi	-0.0093
$(\partial/\partial P_B)h_f$ (around saturation), Btu/lb_m-psi	0.1332
$(\partial/\partial P_B)\rho_b$ (around saturation), lb_m/ft^3-psi	0.1400

[a]*Source*: *EBR-II System Design Descriptions*, Vols. 1 through 5, Argonne National Laboratory, Argonne, Ill., June 1972.

Table 4.3. Superheater design data

100% power level	From ref. a
Total height, ft	27
Number of duplex tubes	72
Number of units	2
Temperature of inlet steam °F (°C)	579 (~303.8)
Temperature of superheated steam, °F (°C)	872 (~466.6)
Temperature of primary inlet sodium, °F (°C)	883 (~482.7)
Temperature of primary outlet sodium, °F (°C)	703 (~372.7)
Overall heat transfer coefficient (tube wall-steam), Btu/ft^2-h	1973
Overall heat transfer coefficient (sodium-tube wall), Btu/ft^2-h	1241
Total mass of primary sodium, lb_m	6290
Total mass of tube wall, lb_m	80604
Cross-sectional area (steam), ft^2 (m^2)	2.56 (~0.23)
Cross-sectional area (sodium), ft^2 (m^2)	5.04 (~0.45)
Total heat transfer area (tube wall-steam), ft^2 (m^2)	3338 (300.42)
Total heat transfer area (sodium-tube wall), ft^2 (m^2)	6260 (563.4)
Primary sodium flow, lb_m/s	626
Superheated steam flow, lb_m/s	75

[a]*Source*: *EBR-II System Design Descriptions*, Vols. 1 through 5, Argonne National Laboratory, Argonne, Ill., June 1972.

Table 4.4. Steam drum design data

100% power level	From ref. a
Inlet steam quality	0.1428
Outlet steam quality	1
Total length, ft (m)	42 (12.6)
Diameter, ft (cm)	4.26 (127.8)
Drum level (below centerline), in. (cm)	8 (~20)
Density of drum water, lb_m/ft^3	45.45
Blowdown flow, lb_m/h	20,000
Pressure drop across feedwater valve, psi	100

[a]*Source*: *EBR-II System Design Descriptions*, Vols. 1 through 5, Argonne National Laboratory, Argonne, Ill., June 1972.

ref. 9. The following sections describe the derivation of the model and the nonzero elements of the coefficient matrix.

4.2.1 Drum Liquid

All water properties in the drum and downcomer regions are evaluated at the drum pressure. The assumption of perfectly mixed liquids is applied. The energy balance equations for the water in the drum can be written as follows:

$$\frac{d}{dt}\,[h_{\ell d}M_{\ell d}] = W_{FW}h_{FW} - W_{DC}h_{DC} + (1 - X_e)\,W_{RM}h_F \quad . \tag{4.1}$$

The mass of the water is

$$M_{\ell D} = L \cdot A_D \cdot \rho_{\ell D} \tag{4.2}$$

where

$h_{\ell D}$ = enthalpy of the liquid in the drum,

$M_{\ell D}$ = total mass of the liquid inside the drum,

Table 4.5. Nonzero elements of system matrix *A* of the EBR-II steam generator model

I	J	A(I,J)	I	J	A(I,J)
1	1	-2.2898	7	6	-0.0033246
2	1	0.10631			
3	1	-0.000039615	1	7	5.689
5	1	0.89941	2	7	-0.58015
6	1	0.30745	3	7	-0.0010111
7	1	0.29215	5	7	-3.765
8	1	0.01635	6	7	-1.5921
9	1	0.56	7	7	-1.9124
12	1	0.00778			
16	1	0.094	1	8	1.5386
			2	8	0.0070115
1	2	1.6993	3	8	-0.00006987
2	2	-0.34648	5	8	0.059318
3	2	-0.0013382	6	8	0.018931
4	2	7.221	7	8	0.018931
5	2	-3.6272	8	8	-0.089
6	2	-0.9355	12	8	0.00027894
7	2	-0.9355	18	8	-0.00026
9	2	-0.9166	20	8	0.00091
1	3	-365.22	1	9	-1.67474
2	3	0.41627	2	9	0.0019087
3	3	-0.068836	3	9	0.000075753
5	3	3.5217	5	9	0.016148
6	3	1.1239	6	9	0.0051536
7	3	1.1239	7	9	0.0051536
10	3	468.75	10	9	0.1275
12	3	-0.68753	12	9	0.0011131
18	3	-0.13	18	9	0.00022
20	3	0.4589	20	9	-0.00076894
4	4	-1.343	8	10	-0.01635
5	4	0.1992	9	10	-0.02104
6	4	0.243	10	10	-0.053
			20	10	-2.49 E-8
5	5	-1.343			
7	5	0.243	1	11	1.2542
			2	11	-0.047415
1	6	1.0803	3	11	-0.000011807
2	6	-0.0012313	5	11	-0.40113
3	6	0.00020362	6	11	-0.12802
4	6	1.143	7	11	-0.13318
5	6	-0.010417	11	11	-0.11057
6	6	-0.45232	12	11	-0.068753

Table 4.5. (continued)

I	J	A(I,J)	I	J	A(I,J)
1	12	-0.28545	15	16	0.49
2	12	-0.0013008	16	16	-137.00
3	12	0.000012963	17	16	-15.90
5	12	-0.011005			
6	12	-0.0035122	17	17	-79.0
7	12	-0.0035122			
11	12	0.11057	20	18	-0.175
13	13	-4.40000	12	19	-0.0054872
14	13	4.00000	18	19	0.000262
15	13	1.00000	19	19	-0.200000
			20	19	-0.00089705
4	14	0.1994			
14	14	-37.8000	19	20	14.87
			20	20	-0.0019777
13	15	5.3913			
14	15	5.5013			
15	15	-1.6504			
16	15	84.5000			
17	15	84.5000			

W_{FW} = feedwater mass flow rate,

h_{FW} = enthalpy of the feedwater,

L = level in the drum,

$\rho_{\ell D}$ = density of the liquid in the drum,

A_D = longitudinal area of the drum,

X_e = steam exit quality,

W_{DC} = downcomer flow rate,

W_{RM} = rising water/steam mixture flow rate,

h_F = saturation enthalpy of the water,

h_{DC} = downcomer water enthalpy.

The perturbation form of the final state equation is

$$C_P M_{\ell d} \frac{d\delta T_{\ell d}}{dt} + [h_{\ell D} \cdot A_D \ \rho_{\ell D}] \frac{d\delta L}{dt} = [C_P \cdot W_{FW}] \ \delta T_{FW}$$

$$+ [h_{FW}] \ \delta W_{FW} - W_{DC} C_P T_{DC} - h_{DC} \delta W_{DC}$$

$$+ (1 - x_e) \ W_{RM} \ \frac{\partial h_F}{\partial P_B} \ \delta P_B + (1 - X_e) \ h_F \ \delta W_{RM} - W_{RM} h_F \ \delta X_e , \tag{4.3}$$

where

$T_{\ell D}$ = temperature of the liquid in the drum,

T_{DC} = downcomer temperature,

T_{FW} = feedwater temperature.

4.2.2 Drum Steam

It is assumed that the rising steam is at saturation temperature and there is no superheating. The mass balance equation for the steam in the drum is

$$\frac{dM_{sd}}{dt} = X_e W_{RM} - W_{SO} \quad . \tag{4.4}$$

The dry steam flow leaving the drum can be stated in terms of the drum pressure and the steam valve coefficient. The assumption behind this simplification is called the "critical flow" assumption.[10] "It is assumed that the pressure drop in the downstream or turbine pressure will not change the steam flow rate from the steam generator":

$$\delta W_{SO} = C_L \delta P_D + P_D \delta C_L \quad . \tag{4.5}$$

Neglecting the effect of steam density deviation on the drum water level, the mass of the steam can be expressed as the product of steam volume and steam density. Using the chain rule, it is possible to restate the density deviation in terms of the pressure deviation in the drum. Using Eq. (4.5) in Eq. (4.4) and applying the chain rule, the following is obtained.

$$V_{SD} \ \frac{\partial \rho_{ST}}{\partial P_D} \ \frac{d\delta P_D}{dt} = X_e \delta W_{RM} + W_{RM} \delta X_e + C_L \delta P_D + P_D \delta C_L \quad , \tag{4.6}$$

where

V_{SD} = volume of steam drum,

P_D = pressure inside steam drum,

ρ_{ST} = density of steam,

C_L = steam valve coefficient.

4.2.3 Primary Coolant Lumps

The first primary coolant lump has the dimensions determined by the subcooled height. The mass balance is written as follows.

$$\frac{d(M_{P1})}{dt} = W_{PE} - W_{P1} \quad . \tag{4.7}$$

As indicated above, the mass of the coolant can be restated in terms of its density and volume. Using a cross-sectional area that is constant through the tube, the volume is related to the subcooled height. Then Eq. (4.7) has the following form:

$$\rho_P \cdot A_P \frac{dZ_{sc}}{dt} = W_{PE} - W_{P1} \quad . \tag{4.8}$$

The energy balance for the same lump is written as

$$C_P \frac{d(M_{P1}T_{P1})}{dt} = W_{PE}C_PT_{PE} - W_{P1}C_PT_{P1} - \dot{Q}_{PM1} \quad , \tag{4.9}$$

where

M_{P1} = mass of primary sodium,

W_{PE} = mass flow rate at the entrance of the lump,

W_{P1} = mass flow rate at the exit of the lump,

ρ_P = density of primary sodium,

A_P = flow area of primary sodium,

Z_{SC} = subcooled height,

T_{M1} = average metal temperature,

T_{P1} = bulk mean temperature of the node,

Q_{PM1} = heat transfer rate between primary-1 and metal-1 regions,

T_{PE} = entrance sodium temperature.

The heat transfer rate from the first sodium lump into the first metal lump is expressed as

$$\dot{Q}_{PM1} = U_{PM}\, A_{PM1}\, (T_{P1} - T_{M1}) \quad , \tag{4.10}$$

where

U_{PM} = overall heat transfer coefficient between the primary and metal lumps,

A_{PM1} = heat transfer area between the first metal and primary regions ($A_{PM1} = A_{PM2}$ for this model).

The unknown flow W_{P1} can be eliminated between Eqs. (4.8) and (4.9) leading to the following final state equation:

$$\frac{d\delta T_{P1}}{dt} = \frac{1}{\tau_{P1}} \delta T_{PE} - \frac{1}{\tau_{P1}} + \frac{U_{PM} \cdot A_{PM1}}{M_{P1} \cdot C_P} \delta T_{P1} + \frac{U_{PM} A_{PM1}}{M_{P1} C_P} \delta T_{M1}$$

$$+ \frac{U_{PM} L_{PM}}{M_{P1} C_P} (T_{P1} - T_{M1}) \delta Z_{SC} \quad . \tag{4.11}$$

where

L_{PM} = unit heat transfer length between primary and metal nodes,

The second primary coolant lump is treated in a manner similar to the first primary lump. Since the total height of the evaporator is constant, the following relation exists:

$$\frac{dZ_{SC}}{dt} = -\frac{dZ_B}{dt} \quad . \tag{4.12}$$

The entrance flow for the first coolant lump is the outlet flow of the second coolant lump:

$$W_{P2} = W_{PE} \quad . \tag{4.13}$$

The energy balance for the second lump is

$$C_P \frac{d(M_{P2} T_{P2})}{dt} = W_{P1} C_P T_{P1} - W_{P2} C_P T_{P2} - Q_{PM2}^{\bullet} \quad , \tag{4.14}$$

where

T_{P2} = bulk mean temperature of the lump,

Q_{PM2} = heat transfer rate between primary-2 and metal-2 lumps,

T_{M2} = average metal temperature.

The heat transfer rate from the second sodium lump into the second metal lump is given by

$$Q_{PM2} = U_{PM} A_{PM2} (T_{P2} - T_{M2}) \quad . \tag{4.15}$$

The perturbation form of the final state equation is given by

$$\frac{d\delta T_{P2}}{dt} + \left(\frac{T_{P2} - T_{P1}}{Z_{SC}}\right) \frac{d\delta Z_{SC}}{dt} = \frac{1}{\tau_{P2}} \delta T_{P1} - \left[\frac{1}{\tau_{P2}} + \frac{U_{PM}A_{PM2}}{M_{P2}C_{P2}}\right] \delta T_{P2}$$

$$+ \frac{U_{PM}A_{PM2}}{M_{P2}C_P} \delta T_{M2} - \frac{U_{PM}L_{PM}}{M_{P2} \cdot C_P} (T_{P2} - T_{M2}) \delta Z_{SC} \quad , \tag{4.16}$$

where

A_{PM2} = heat transfer area between primary-2 and metal-2 lumps,

τ_{P2} = residence time of the sodium in primary-2 lump,

M_{P2} = mass of sodium in primary-2 lump.

4.2.4 Tube Wall Lumps

Using the moving boundary approach introduces a complexity into the metal regions. In order to write a proper energy balance equation, the mass transfer caused by the moving border between the metal lumps has to be taken into consideration. In this model, it is assumed that the variation in the boundary contributes some amount of energy to the total energy balance, which can be written in terms of the average metal temperature and the time derivative of the subcooled height.[9] The last term of the energy balance equation stated below emphasizes this contribution.

$$C_M \frac{d(M_{M1}T_{M1})}{dt} = \dot{Q}_{PM1} - \dot{Q}_{MS1} + \rho_M A_M C_M \bar{T}_M \frac{dZ_B}{dt} \quad , \tag{4.17}$$

where

$$\bar{T}_M = \frac{T_{M1} + T_{M2}}{2} \quad , \tag{4.18}$$

ρ_M = density of tube metal,

A_M = cross-sectional area of tube metal lump,

C_M = specific heat capacity of tube metal,

$\bar{T}_M$ = average temperature at the boundary,

M_{M1} = mass of the tube metal in lump-1,

Q_{MS1} = heat transfer rate between metal-1 and secondary-1 lumps,

T_{sat} = saturation temperature of the secondary water,

T_{M1} = bulk mean temperature of metal lump-1,

T_{M2} = bulk mean temperature of metal lump-2.

The heat transfer rate from the first tube region to the boiling region is written as

$$\dot{Q}_{MS1} = U_{MS1}\ A_{MS1}\ (T_M - T_{S1}) \quad . \tag{4.19}$$

Note that the temperature in the boiling region is at the saturation value,

$$T_{S1} = T_{sat} \quad . \tag{4.20}$$

The saturation temperature is related to the pressure in the boiling region (using the chain rule), provided that it is evaluated about the steady state. In other words, the saturation temperature deviation is governed only by the boiling pressure in a linear manner:

$$\delta T_{sat} = \frac{\delta T_{sat}}{\delta P_B}\ \delta P_B \quad . \tag{4.21}$$

The perturbation form of the final state equation is expressed below.

$$\frac{d\delta T_{M1}}{dt} - \frac{T_{M1} - T_{M2}}{2Z_{SC}}\ \frac{d\delta Z_{SC}}{dt} = \frac{U_{PM}A_{PM1}}{M_{M1}C_M}\ \delta T_{P1} - \frac{U_{PM}A_{PM} + U_{MS1}A_{MS1}}{M_{M1}C_M}\ \delta T_{M1}$$

$$+ \frac{U_{MS1}A_{MS1}}{M_{M1}C_M}\ \frac{\partial T_{sat}}{\partial P_B}\ \delta P_B \quad , \tag{4.22}$$

where

U_{MS1} = heat transfer coefficient between metal and secondary-1 lumps,

A_{MS1} = heat transfer area between metal and secondary-1 lumps.

The second metal lump is treated in a manner similar to the first one. The energy balance equation is:

$$C_M\ \frac{d(M_{M2}T_{M2})}{dt} = \dot{Q}_{PM2} - \dot{Q}_{MS2} + \rho_M A_M C_M \bar{T}_M - \frac{dZ_{SC}}{dt} \quad . \tag{4.23}$$

The heat transfer rate into the second metal region is expressed as

$$\dot{Q}_{MS2} = U_{MS2}\ A_{MS2}\ (T_{S2} - T_{M2}) \quad . \tag{4.24}$$

The subcooled water temperature T_{s2} is not taken as a state variable in this model; instead it is assumed to be an average temperature which can be written approximately as an arithmetic average of the inlet and outlet temperatures of the lump:

$$T_{s2} = \frac{T_{pc} + T_{sat}}{2} \quad . \tag{4.25}$$

The final state equation is written as

$$\frac{d\delta T_{M2}}{dt} - \left[\frac{T_{M1} - T_{M2}}{2Z_{SC}}\right] \frac{d\delta Z_{SC}}{dt} = \frac{U_{PM}A_{PM2}}{M_{M2}C_M} \delta T_{P2} + \frac{U_{MS2}A_{MS2}}{2M_{M2} \cdot C_M} \delta T_{DC}$$

$$+ \left[\frac{U_{MS2}A_{MS2}}{2M_{M2}C_M}\right] \left[\frac{\partial T_{sat}}{\partial P_B}\right] \delta P_B - \left[\frac{U_{PM}A_{PM2} + U_{MS2}A_{MS2}}{M_{M2}C_M}\right] \delta T_{M2} \quad , \tag{4.26}$$

where

T_{DC} = downcomer outlet temperature,

U_{MS2} = heat transfer coefficient between metal and secondary-2 lumps,

A_{MS2} = heat transfer area between metal and secondary-2 lumps,

M_{M2} = mass of the tube metal in lump 2.

4.2.5 Subcooled Region

The total heat delivered by the primary sodium system is transferred into the steam system by three different heat transfer mechanisms. Most of the source heat is absorbed in the superheaters, and the remaining produces steam in the evaporator. Steam production starts at some elevation in the evaporator as the subcooled water at the bottom reaches the saturation temperature. Above the boundary where saturation starts, heat transfer from the primary provides increase in steam quality until the steam water mixture reaches the top of the evaporator.

The phase change in the secondary coolant can be modeled using the moving boundary approach. The relationship between several thermodynamic parameters is summarized as follows. The saturation temperature is a function of the pressure inside the tubes. The subcooled height is determined by downcomer flow, heat transfer rate from the primary side, and inlet coolant temperature of the evaporator. There is also interdependence between the heat transfer rate and the saturation pressure because the heat transfer driving force parameter T_{sat} is a function of the pressure; therefore, the saturation pressure influences the moving boundary also.

The subcooled water enters the evaporator at downcomer outlet temperature T_{DC} and leaves the moving boundary at T_{sat}. As mentioned earlier, the average temperature of the subcooled region is assumed to be equal to the arithmetic mean of the inlet and outlet temperatures. The inlet flow is equal to the downcomer flow W_{DC}. The flow at the

boundary is approximated (see Appendix A) and assumed to be a function of the heat transfer rate and the latent heat.

The mass balance equation for the subcooled region can be written as

$$\frac{d(M_{SC})}{dt} = W_{DC} - W_2 = \frac{d(\rho_{SC} \cdot S_{SC} \cdot Z_{SC})}{dt} \quad . \tag{4.27}$$

Equation (4.27) above is manipulated to obtain subcooled height as a state variable:

$$\frac{d\delta Z_{SC}}{dt} = \frac{1}{\rho_{SC} A_{SC}} (\delta W_{DC} - \delta W_2) \quad . \tag{4.28}$$

The energy balance equation for the subcooled region is

$$\frac{d(M_{SC1} C_{PW} T_{SC})}{dt} = \dot{Q}_{MS2} + W_{DC} C_{PW} T_{sat} \quad , \tag{4.29}$$

where

M_{SC} = mass of subcooled water,

C_{PW} = specific heat capacity of subcooled water,

W_{DC} = downcomer mass flow rate,

W_2 = mass flow rate of water leaving subcooled region,

ρ_{SC} = density of subcooled water,

A_{SC} = cross-sectional area of subcooled region,

$\dot{Q}_{MS2}$ = heat transfer rate between metal-2 and subcooled lumps.

The unknown flow W_2 leaving the lump is expressed by the following linear relationship (see Appendix A):

$$W_2 = WB1 \ \delta T_{M2} + WB2 \ \delta T_{DC} + WB3 \ \delta P_B + WB4 \ \delta Z_{SC} \ , \tag{4.30}$$

where $WB1$, $WB2$, $WB3$, $WB4$ = constant coefficients.

Substituting W_2 in the balance equations and using simple algebra relating the mass and energy balance equations yield the following final state equation:

$$\left[\frac{A_{SC}\rho_{SC}Z_{SC}C_{PW}}{2}\right]\left[\frac{D\delta T_{DC}}{dt} + \frac{A_{SC}\rho_{SC}Z_{SC}C_{PW}}{2} \cdot \left(\frac{\partial T_{sat}}{\partial P_B}\right)\right]\frac{d\delta P_B}{dt}$$

$$+ \left[A_{SC}\cdot\rho_{SC}\cdot C_{PW}\left(\frac{T_{DC} + T_{sat}}{2}\right)\right]\frac{d\delta Z_{SC}}{dt}$$

$$= [U_{MS1}\cdot L_{MS}\cdot Z_{SC} - C_{PW}\cdot T_{sat}\cdot WB1]\ \delta T_{M2}$$

$$- [U_{MS1}\cdot L_{MS}\cdot Z_{SC} - W_{DC}C_{PW} + C_{PW}T_{sat}\cdot WB2]\ \delta T_{DC}$$

$$- \left[U_{MS1}\cdot A_{MS1}\left(\frac{\delta T_{sat}}{\delta P_B}\right) + W_2C_{PW}\left(\frac{\delta T_{sat}}{\delta P_B}\right) + C_{PW}T_{sat}\cdot WB3\right]\delta P_B$$

$$+ \left[U_{MS1}\cdot L_{MS}\cdot\ T_{M1} - \left(\frac{T_{DC} + T_{sat}}{2}\right) - C_{PW}T_{sat}\cdot WB4\right]\delta Z_{SC}$$

$$+ [C_{PW}\cdot T_{DC}]\ \delta W_{DC}\ . \tag{4.31}$$

4.2.6 Boiling Region

As indicated above, the two-phase regime in the evaporator can be modeled using at least three thermodynamic variables, namely the moving boundary, saturation pressure, and steam quality. To complete the model for the evaporator dynamics, we need two more state equations to handle these three unknowns.

Boiling starts at the moving boundary and ends at the end of the heat transfer region near the top of the evaporator. It is assumed that the two-phase mixture is homogeneous with an average enthalpy, quality, and density represented by the following equations.

$$\bar{X} = \frac{X_e}{2}\ ; \tag{4.32}$$

$$\rho_B = \rho_F(1 - \bar{X}) + \rho_G\ \bar{X}\ ; \tag{4.33}$$

$$h_B = h_F(1 - \bar{X}) + h_G\ \bar{X}\ . \tag{4.34}$$

The mass balance equation for the boiling region is

$$\frac{d(\rho_B A_B Z_B)}{dt} = W_2 - W_{RM}\ . \tag{4.35}$$

This can be rewritten in terms of the density and the boiling height as

$$A_B\left[Z_B\frac{d\delta\rho_B}{dt} + \rho_B\frac{d\delta Z_B}{dt}\right] = \delta W_2 - \delta W_{RM}\ . \tag{4.36}$$

The perturbation form of the average density in the boiling region is expressed by the following relationship:[9]

The perturbation form of the average density in the boiling region is expressed by the following relationship:[9]

$$\delta\rho_B = K_1\delta P + K_2\delta X_e \quad , \tag{4.37}$$

where

$$K_1 = \frac{-\bar{X}}{(\nu_f + \bar{X}\nu_{FG})^2}\left(\frac{\delta\nu_{FG}}{\delta P_B}\right) \quad , \tag{4.38}$$

$$K_2 = \frac{-\nu_{FG}}{2(\nu_F + \bar{x}\nu_{FG})^2} \quad . \tag{4.39}$$

Note that the time derivative of the boiling height is equal to the time derivative of the subcooled height with a negative sign. Using the chain rule for the partial derivatives, the equations above yield the following final state equation:

$$-A_B\ \rho_B\ \frac{d\delta Z_{SC}}{dt} + A_B Z_B \cdot K_1\ \frac{d\delta P_B}{dt} + A_B Z_B K_2\ \frac{d\delta X_e}{dt} =$$

$$(WB1)\ \delta T_{M2} + (WB2)\delta T_{DC} + (WB3)\delta P_B + (WB4)\delta Z_{SC} - \delta W_{RM} \quad , \tag{4.40}$$

where

$WB1$, $WB2$, $WB3$, $WB4$ = coefficients of approximated flow equation,

W_{RM} = mass flow rate of rising mixture,

ν_F = specific volume of the liquid phase,

ν_G = specific volume of the vapor,

$\bar{X}$ = average steam quality,

$\bar{X}_e$ = exit steam quality.

A third state equation can be generated considering the energy balance throughout the boiling region.

$$\frac{d[\rho_B A_B Z_B h_B]}{dt} = \dot{Q}_{MS1} + W_2 h_F - W_{RM} h_e \quad , \tag{4.41}$$

where the outlet enthalpy

$$h_{Xe} = h_F + X_e h_{FG} \quad . \tag{4.42}$$

The algebraic manipulations yield the following final state equation.

$$\left[A_B \cdot \rho_B \cdot Z_B \left(\frac{\partial h_F}{\partial P_B} + X_e \frac{\partial h_{FG}}{\partial P_B}\right) + h_B A_B Z_B K_1\right] \frac{d\delta P_B}{dt}$$

$$+ \left[A_B \ \rho \cdot Z_B \ \frac{h_{FG}}{2} - h_B A_B Z_B K_2\right] \frac{d\delta X_e}{dt} - [h_B \cdot A_B \cdot \rho_B] \frac{d\delta Z_{SC}}{dt} = [U_{MS1} A_{MS1}] \ \delta T_{M1}$$

$$+ \left[W_2 \left(\frac{\partial h_F}{\partial P_B}\right) - U_{MS1} A_{MS1} \left(\frac{\partial T_{sat}}{\partial P_B}\right) - W_{RM} X_e \left(\frac{\partial h_{FG}}{\partial P_B}\right) + WB3 \cdot h_F\right] \delta P_B$$

$$- [U_{MS1}, \ L_{MS}(T_{M1} - T_{sat}) - h_F WB4] \ \delta Z_{SC}$$

$$- [h_{Xe}] \ \delta W_{RM} - [W_{RM} \cdot h_{FG}] \ \delta X_e + [WB1 \cdot h_F] \ \delta T_{MZ} + [h_F WB2] \ \delta T_{DC} \quad , \qquad (4.43)$$

where

Q_{MS1} = heat transfer rate between metal-1 and boiling region lumps.

L_{MS} = unit heat transfer length between metal and secondary nodes.

h_{FG} = latent heat of evaporation.

4.2.7 Downcomer Region

Unlike the U-tube type steam generators, the secondary coolant enters the evaporators directly through piping. The downcomer region, therefore, is the piping between the steam drum and the evaporators. It is assumed that there is no axial heat transport through the pipes and no radial heat loss. A transport lag is used to formulate the dynamics. Note that the downcomer inlet temperature is the temperature of the well mixed drum liquid T_{1d}:

$$\frac{d\delta T_{DC}}{dt} = \frac{1}{\tau_{DC}} \ (\delta T_{\ell D} - \delta T_{DC}) \quad , \qquad (4.44)$$

where

τ_{DC} = resident time in the downcomer piping.

4.2.8 Momentum Equations

In the development of the evaporator model, inlet and outlet coolant flows are the two unknowns to be modeled. In a simple study such as using a tea kettle model for the steam generator, these flows might be considered to be constant and equal. However, when the drum dynamics is a subject of study, then the deviations in flows cannot be avoided. The momentum equation for the downcomer piping is

$$\frac{Z_{DC}}{g_c \cdot A_{DC}} \cdot \frac{dW_{DC}}{dt} = \Delta P + \rho_{DC} \cdot Z_{DC} - \frac{f_{DC}}{2 g_C \cdot D_{DC} A_{DC}^2} \cdot \frac{Z_{DC}}{\rho_{DC}} \ |W_{DC}| \cdot W_{DC} \quad , \qquad (4.45)$$

where

Z_{DC} = height of the downcomer pipes,

A_{DC} = cross-sectional area of the downcomer pipes,

W_{DC} = mass flow rate in the downcomer,

ΔP = pressure drop across the piping,

ρ_{DC} = density of downcomer fluid,

f_{DC} = friction factor in downcomer piping,

D_{DC} = hydraulic diameter,

g_C = gravitational constant.

Linearization about the steady state yields the following final form:

$$\frac{d\delta W_{DC}}{dt} = \left[\frac{g_C \cdot A_{DC}}{Z_{DC}}\right] \delta P_B - \left[\frac{g_C \cdot A_{DC}}{Z_{DC}}\right] \delta P_D - \left[\frac{f_{DC} W_{DC}}{D_{DC} A_{DC} \rho_{DC}}\right] \delta W_{DC} \quad . \tag{4.46}$$

The momentum equation for the outgoing flow is somewhat more complicated because of the two-phase regime. To obtain an equation for the flow of the water/steam mixture, the following momentum equation is used:

$$\left[\frac{Z_{EV}}{g_C \cdot A_T}\right] \frac{dW_{RM}}{dt} = \Delta P - \rho_{SC} Z_{SC} - \bar{\rho}_B Z_B - \left[\frac{f_{SC} Z_{SC}}{2 g_C D_T \rho_{SC}} - \frac{f_B Z_B}{2 g_C D_T \rho_F}\right] \bar{\phi}^2 \cdot G^2 \quad , \tag{4.47}$$

where

Z_{EV} = height of the evaporator,

W_{RM} = mass flow rate of rising mixture,

A_T = cross-sectional area of the duplex tubes,

ΔP = driving pressure drop,

f_{SC} = friction factor through the subcooled region,

f_B = friction factor through the boiling region,

D_T = total hydraulic diameter,

$\bar{\phi}$ = integral average two-phase friction multiplier.

An approximated Martinelli-Nelson friction multiplier is used.[10]

$$\bar{\phi}^2 = 1.0 + \pi(G,P)\ 1.2 \left(\frac{\rho_F}{\rho_G}\right) - 1 \quad X^{0.824} \quad . \tag{4.48}$$

The integral average is taken as follows:

$$\bar{\phi}^2 = \frac{1}{Z_b} \int_{Z_{SC}}^{Z_{EV}} \phi^2 \, dZ \quad . \tag{4.49}$$

Using the relationship between steam quality and the height,

$$X(Z) = \frac{X_e}{Z_B} \ (Z - Z_{SC}) \quad . \tag{4.50}$$

The resultant average can be written as

$$\bar{\phi}^2 = 1.0 + \frac{1.2\pi(G,P)\left(\frac{\rho_F}{\rho_G} - 1\right) X_e^{0.824}}{1.824} \quad , \tag{4.51}$$

where

$\pi(G,P) = 1.36 + (5.E\text{-}4)P + (3.6\ E\text{-}4)G - (2.57\ E\text{-}6)PG$ for $\leq 194.4\ lb_m/ft^2\text{-}s$,

$\pi(G,P) = 1.26 - (4.E\text{-}4)P + (33.6/G) + [(7.777E\text{-}2_p)/G]$ for $G > 194.4\ lb_m/ft^2\text{-}s$,

G = mass flux through the evaporator,

G = 205.07 lb_m/ft^2-s (for EBR-II evaporator),

Z_B = boiling height.

The final state equation for W_{rm} is

$$\frac{d\delta W_{RM}}{dt} = C_1\delta P_D + C_2\delta P_B + C_3\delta Z_{SC} + C_4\delta W_{RM} \quad , \tag{4.52}$$

where

$$C_1 = -\frac{g_C A_T}{Z_{EV}} \quad ,$$

$$C_2 = \frac{g_{CZ}A_T}{Z_{EV}} - \frac{g_C A_T}{Z_{EV}} Z_{SC} \frac{\partial \rho_{SC}}{\partial P_B} + Z_B \frac{\partial \rho_B}{\partial P_B}$$

$$+ \frac{A_t \phi_{FO}^2}{2Z_{EV}D_T} \frac{f_{SC}Z_{SC}}{\rho_{SC}^2} \frac{\partial \rho_{SC}}{\partial P_B} + \frac{f_B Z_B}{\rho^2 F} \frac{\partial \bar{\rho}_F}{\partial P_B} ,$$

$$C_3 = (\bar{\rho}_B - \rho_{SC}) \frac{g_C A_T}{Z_{EV}} + \frac{A_T \phi_{FO}^2}{2Z_{EV}D_T} \frac{f_B}{\rho_F} - \frac{f_{SC}}{\rho_{SC}} ,$$

$$C_4 = - \frac{f_{SC}Z_{SC}W_{RM}}{A_T Z_{EV} D_T \rho_{SC}} - \frac{f_b Z_b W_{rm}}{A_T Z_{EV} D_T \rho_F} \phi^2 .$$

4.3 SUPERHEATER STATE EQUATIONS

The two superheater units in EBR-II are identical in construction to the evaporators. Their design data, therefore, are exactly the same as those for the evaporators. The entering dry steam flows through the duplex tubes and is heated by the primary sodium flowing in the shell side of the superheaters, producing superheated steam at 875°F (~468°C) at full power.

Since the fluids on either side do not change phase during their residence in the superheaters, the modeling becomes simple. Thus the EBR-II superheater is nothing but a counterflow single-phase heat exchanger. Using Mann's technique in five-lump configuration, the superheater dynamics is represented by the heat exchanger Eqs. (3.18) through (3.22). The data assure that the five-lump model is efficient in representing the system dynamics. (MC_p/UA ratios are 0.87 s for primary and 0.67 s for secondary, both smaller than the 2-s limit.)

4.4 THREE-ELEMENT CONTROLLER

In the actual plant, the drum level controller uses four signals. These are the blowdown flow, feedwater flow, steam outlet flow, and drum level signals. Since the ratio of the blowdown flow to other flows is small, it is assumed to be negligible on the system performance. Using three signals, the control signal is generated by the following formula.

$$u = [K_1(L_{set} - L) + K_2(W_{FW} - W_{ST})] \quad 1 + \frac{K_I}{s} , \qquad (4.53)$$

where

K_I = proportional gain corresponding to the ith signal,

u = control signal,

L = level signal,

L_{set} =drum level set point,

K_I = integral gain,

s = Laplace transform variable.

$K_1 = k_1/\Delta L_{full}$

$K_2 = k_2/(W_{FW},100\%)$

ΔL_{full}=full range of level variations,

$W_{FW},100\%$=100% feedwater flow,

k_I = gain for the ith error signal.

Outlet steam flow is not a state variable in this model; therefore, the steam flow is related to the drum pressure using the critical flow assumption.[9] The final state equation can be obtained by taking the inverse Laplace transform of Eq. (4.53):

$$\frac{d\delta u}{dt} + K_1 \frac{d\delta L}{dt} - K_2^* \frac{d\delta P_D}{dt} + K_2 \frac{d\delta W_{FW}}{dt} = -K_1 \cdot K_I \delta L + K_2^* K_I \delta P_D - K_2 K_I \delta W_{FW}, \quad (4.54)$$

where

$$K_2^* = K_2 \cdot C_L \quad .$$

It can be seen from Eq. (4.54) that the implementation of the controller needs two more state equations, one for the actuator (W_{FW}) and the other for the drum level variable.

The actuator dynamics denoted by z is related to the control input u in the following manner:

$$\frac{dz}{dt} = \frac{1}{\tau_{pos}} (u - z) \quad . \quad (4.55)$$

The feedwater flow is a function of the actuator dynamics,

$$W_{FW} = f(z) \cdot K_{CV} \cdot \sqrt{\rho_{FW} \cdot \Delta P} \quad . \quad (4.56)$$

Assuming $f(z)$ to be a linear function of z,

$$W_{FW} = K_{TOT} \cdot z \quad . \quad (4.57)$$

Substituting Eq. (4.57) into Eq. (4.55) leads to the following state equation:

$$\frac{1}{K_{TOT}} \frac{d\delta W_{FW}}{dt} = \frac{1}{\tau_{pos}} \delta u - \frac{1}{K_{TOT}\tau_{pos}} \delta W_{FW} \quad , \tag{4.58}$$

where

K_{CV} = feedwater valve coefficient,

ρ_{FW} = feedwater density,

ΔP = pressure drop across the feedwater valve,

z = intermediate variable representing the value dynamics,

τ_{pos} = time constant of the feedwater valve positioning,

C_L = steam value coefficient.

Finally, the drum level is formulated using the mass balance equation for the drum water.

$$\frac{dM_{\ell D}}{dt} = W_{FW} - W_{DC} + (1 - X_e)\, W_{RM} \quad . \tag{4.59}$$

Assuming a simple geometry for the drum, the final state equation can be stated as follows.

$$\rho_{\ell d} \cdot A_D \frac{d\delta L}{dt} = \delta W_{FW} - \delta W_{DC} + (1 - X_e)\, \delta W_{RM} - W_{RM}\delta X_e \quad . \tag{4.60}$$

5. TRANSIENT SIMULATIONS USING OPEN-LOOP MODELS

5.1 CALCULATION PROCEDURE

The linear dynamic models are represented using matrix notation and are given by

$$\dot{\underline{X}} = A\,\underline{X} + B\,\underline{u} \quad ,$$

$$\underline{Y} = C\,\underline{X} + D\,\underline{u} \quad , \tag{5.1}$$

where

$\underline{X}$ = vector of state variables,

$\underline{Y}$ = vector of measurements,

u = vector of forcing functions,

A = coefficient matrix,

B = input matrix,

C = observation matrix,

D = disturbance matrix.

The use of a set of coupled first-order differential equations in the development of system models often requires an extensive algebraic manipulation to achieve a compact representation, as in Eq. (5.1). When the number of derivative terms per equation exceeds one, the cumbersome algebra can be avoided by representing the system in the following form:

$$M\,\dot{\underline{X}} = N\,\underline{X} + E\,\underline{u} \quad . \tag{5.2}$$

Then the corresponding A and B system matrices are calculated as

$$A = M^{-1}.N \quad ,$$

$$B = M^{-1}.E \quad , \tag{5.3}$$

provided $\underline{M}^{-1}$ exists. However, taking the inverse of a large system matrix may result in some numerical problems. The possibility of encountering "ill behaved" matrices also exists. Thus care must be exercised in dealing with these problems.

In the present model of the EBR-II primary and steam generator systems, the two different representations stated above are used. The system matrix A of the steam generator model listed in Sect. 4 is calculated as shown in Eq. (5.3). All calculations in this study are performed using the commercially available software package MATRIX_x.[14] The default

integration algorithm invoked by the $Matrix_x$ is the "variable step Kutta-Merson" method[14] which is used for transient calculations.

Equation (5.1) is a standard mathematical form used in simulation studies. Obtaining open-loop system responses to a given step perturbation requires the definition of matrices A, B, C, and D. Since the purpose of this study does not include the multiple input case, the input and disturbance matrices are single-column vectors. We assume that there is no disturbance at the output for open-loop transients; hence all of the D vector elements are equal to zero. We also assume that all the state variables are available for measurement and that the observation matrix C is an identity matrix of order equal to that of the system matrix A. A list of state variables of the two models is given in Table 5.1.

5.2 PRIMARY SYSTEM DYNAMIC SIMULATION

5.2.1 Reactivity Perturbation Results

An isolated primary system model includes the reactor core, IHX, and the sodium tank, as explained in Sect. 3. A typical perturbation of small reactivity insertion is applied to the open-loop model. Figure 5.1 shows a comparison between the fractional power responses of the primary system model and ANL rod drop test[13] for a −5-cent step reactivity insertion. As can be seen from Fig. 5.1, the linear model gives a reasonable prediction of the actual power response. Figure 5.2 shows the fractional power responses of the primary model and the Greene model for a −5-cent step reactivity insertion. The difference in the responses is about 1% at 40 s, which verifies that, by replacing six precursor equations of the Greene model with one "averaged" precursor equation, the model reduction is a very good approximation. Using the two models, the temperature responses of the IHX coolant lumps for the same perturbation differ significantly because of the "five-lump to ten-lump" modification. Figure 5.3 shows the temperature responses of the IHX model used in the Greene model. As the figure indicates, the secondary outlet sodium temperature exceeds the tube wall temperature, which is a physically inconsistent result. (Note that there is no heat input to the IHX secondary inlet lump, and a −5-cent reactivity insertion to the core produces a heat input at the primary side of the IHX.) Figure 5.4 shows the temperature responses of the modified model for the same perturbation. The dynamic behavior of the IHX model is improved using the ten-lump configuration.

The power production is distributed among the active core fuel and several other reflector materials. The heat removal from these regions is carried out by the liquid sodium flowing upward. Any sudden temperature change in cladding is expected to be reflected in the uppercoolant nodes of the corresponding lumps. The liquid sodium carrying the sudden energy increment will flow out of the core and pass through the shell side of the IHX. The excess heat will partially be removed from the primary loop as it passes through the IHX, and some remaining amount of heat will return to the sodium tank. Since the

Table 5.1. List of state variables

Row No. of matrix *A*	State variable
	Primary system model
1	Fractional reactor power
2	Precursor concentration
3	Fuel temperature
4	Sodium bond temperature
5	Cladding temperature
6	Core inlet sodium temperature
7	Core outlet temperature
8	Low-pressure plenum inlet temperature
9	Low-pressure plenum temperature
10	High-pressure plenum inlet temperature
11	High-pressure plenum temperature
12	Lower reflector metal temperature
13	Lower reflector inlet sodium temperature
14	Lower reflector outlet sodium temperature
15	Upper reflector metal temperature
16	Upper reflector inlet sodium temperature
17	Upper reflector outlet sodium temperature
18	Inner reflector metal temperature
19	Inner reflector inlet sodium temperature
20	Inner reflector outlet sodium temperature
21	Outer blanket metal temperature
22	Outer blanket inlet sodium temperature
23	Outer blanket outlet sodium temperature
24	Reactor upper plenum temperature
25	Reactor outlet piping temperature
26	IHX inlet plenum temperature
27	IHX first primary node temperature
28	IHX second primary node temperature
29	IHX upper metal node temperature
30	IHX secondary outlet temperature
31	IHX third secondary node temperature
32	IHX third primary node temperature
33	IHX primary outlet temperature
34	IHX lower metal node temperature
35	IHX second secondary node temperature
36	IHX secondary inlet temperature
37	Sodium tank temperature

Table 5.1 (continued)

Row No. of matrix *A*	State variable
	Steam generator model
1	Boiling region pressure
2	Evaporator subcooled height
3	Evaporator steam exit quality
4	Evaporator sodium temperature
5	Evaporator sodium outlet temperature
6	Evaporator upper metal node temperature
7	Evaporator lower metal node temperature
8	Downcomer flow
9	Evaporator rising mixture flow
10	Steam drum pressure
11	Drum water temperature
12	Downcomer temperature
13	Superheater inlet sodium temperature
14	Superheater outlet sodium temperature
15	Superheater metal temperature
16	Superheater first steam node temperature
17	Superheated steam outlet temperature
18	Drum level
19	Feedwater flow
20	Control input (3-element controller)

dimensions of the sodium tank are large (resulting in large sodium volume), the new steady state temperature of the sodium in the tank will be established after a long time, compared with the sudden temperature change of the upper lumps. Figure 5.5 shows the temperature response of the tank sodium to a sudden flow reduction test.[13] Figure 5.5 indicates that the time constant is quite large. For the step reactivity perturbation of −5 cents, Fig. 5.6 indicates that the temperature response of the tank sodium settles down at about 2500 s with a large time constant resembling the time constant obtained in the flow reduction test. This delayed temperature deviation will affect the core and reflector regions as the recycling sodium temperature reaches the tank temperature. The effect of the tank sodium temperature on the reactivity can be seen in Fig. 5.7. The time response of the primary system model is observed to be in three modes: the prompt jump (0 to 1 s), the reactivity feedback settlement (1 to 200 s), and delayed thermohydraulic effects (200 to 3000 s). The temperature responses of

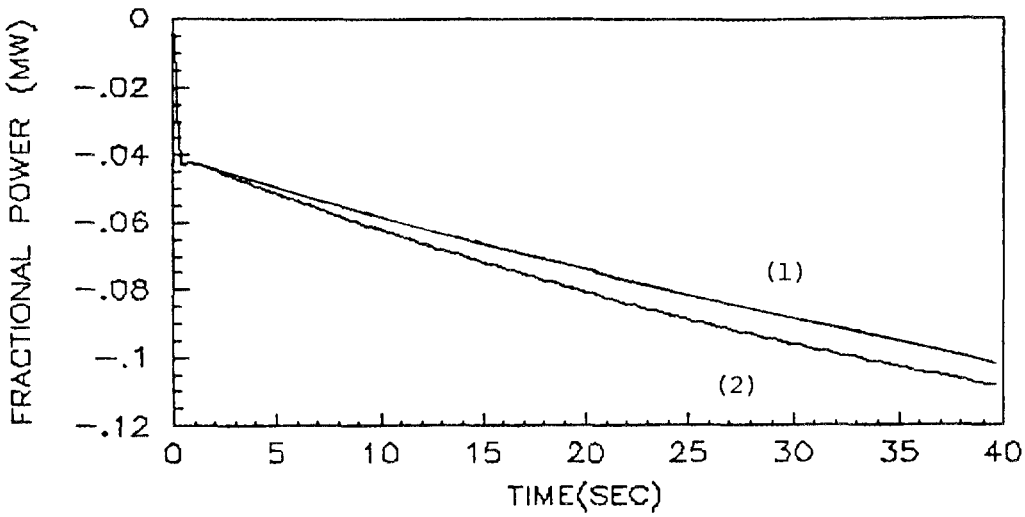

Fig. 5.1. Step response of fractional reactor power to a -5-cent reactivity perturbation. (Deviations from steady state.) (1) Open-loop primary model. (2) ANL rod drop test results. *Source: Guide for Irradiation Experiments in EBR-II*, Argonne National Laboratory, Argonne, Ill., March 1975.

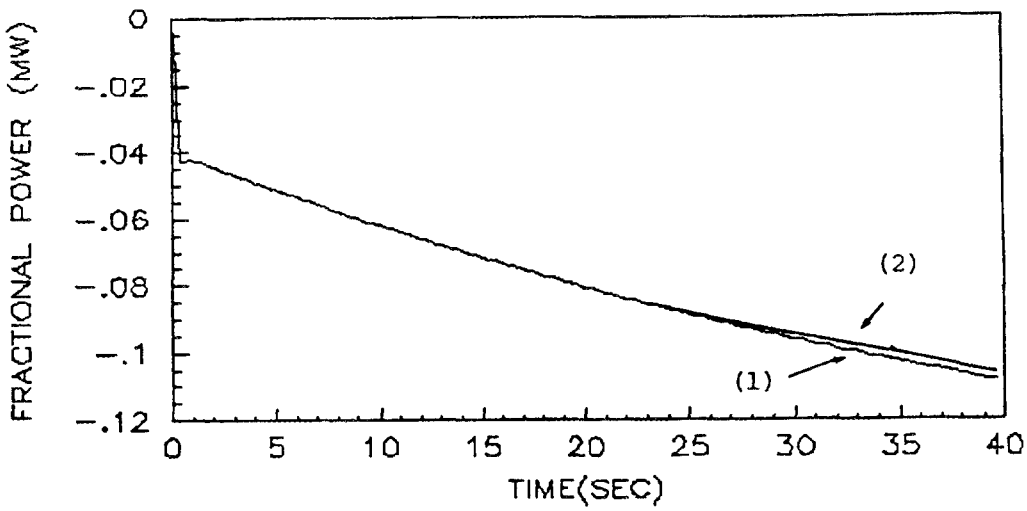

Fig. 5.2. Step response of fractional power to a -5-cent reactivity perturbation. (Deviations from steady state.) (1) Open-loop primary model. (2) Greene's model. *Source*: S. R. Greene, "The Design, Implementation and Cost-Benefit Analysis of a Dynamic Testing Program in the Experimental Breeder Reactor II," M.S. thesis, The University of Tennessee, 1979.

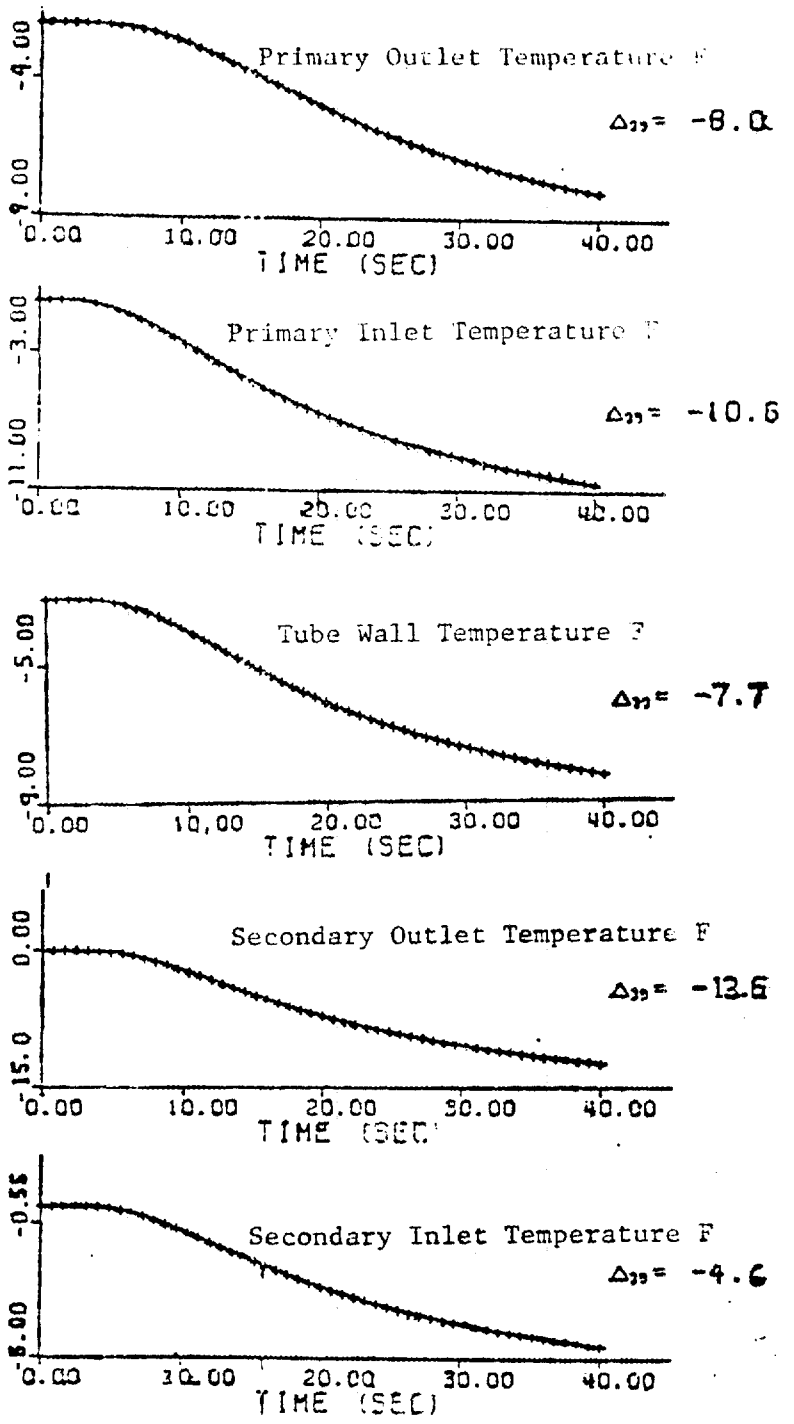

Fig. 5.3. Temperature responses of the IHX coolant lumps to a −5-cent step reactivity perturbation (Greene's model).

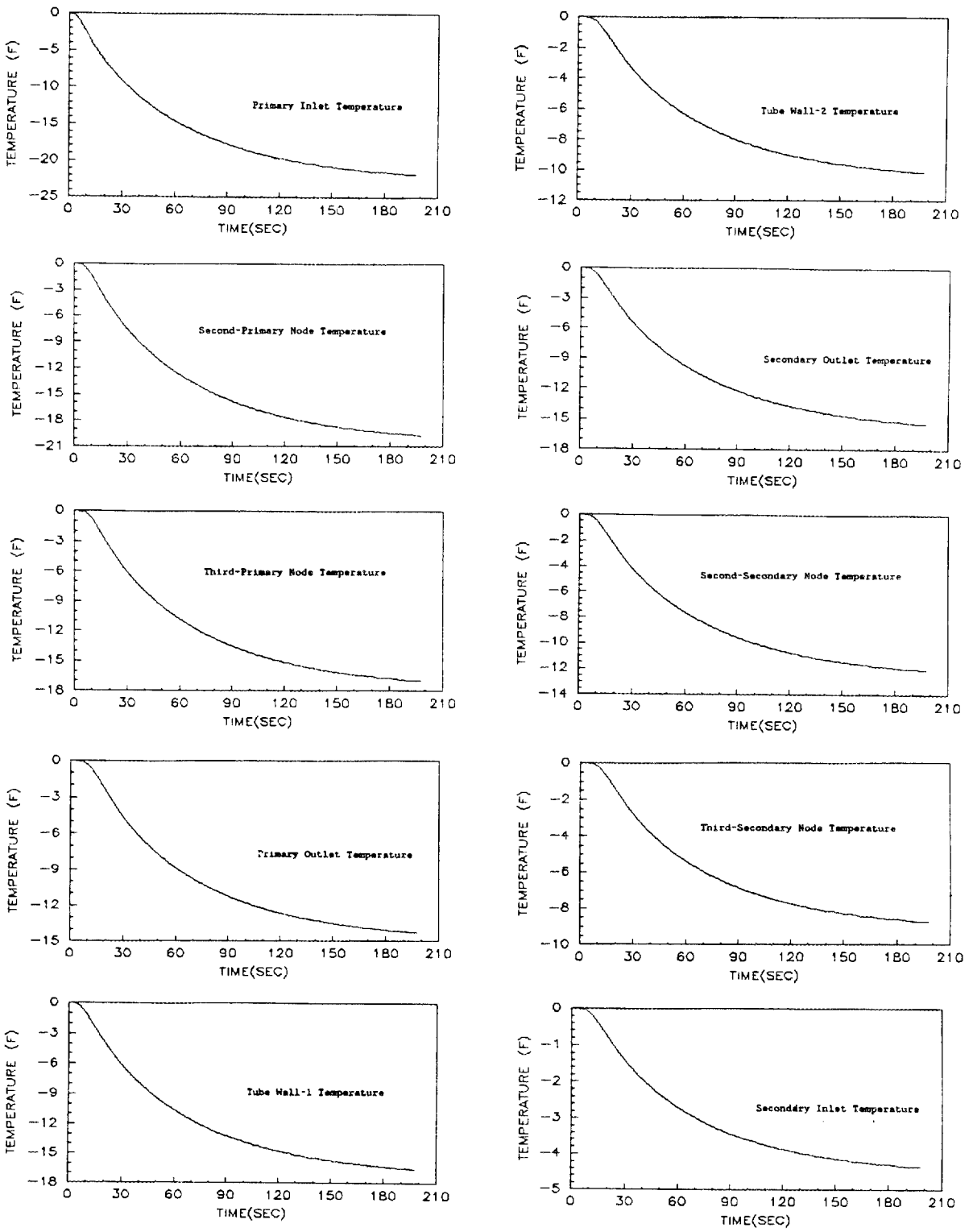

Fig. 5.4. Temperature responses (deviations from steady state) of the IHX coolant lumps to a -5-cent step reactivity perturbation (open-loop primary model).

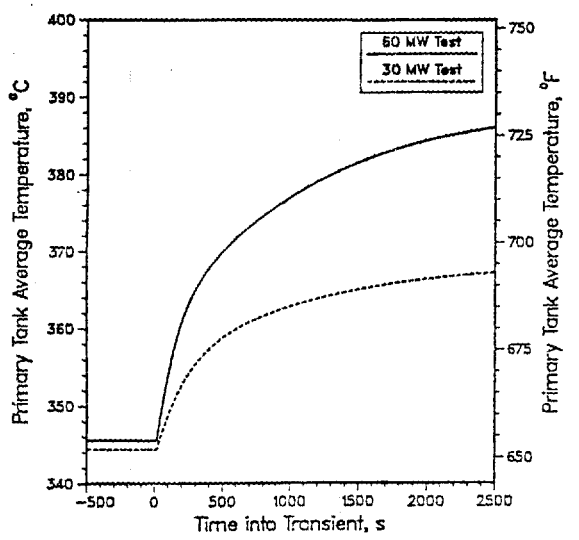

Fig. 5.5. Temperature response of tank sodium to a sudden flow reduction test.

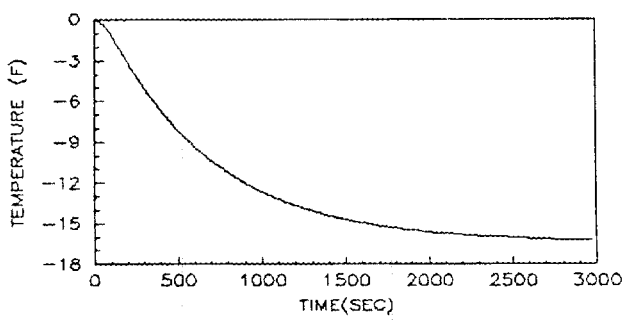

Fig. 5.6. Step response of tank sodium temperature to a -5-cent reactivity perturbation. (Deviations from steady state.)

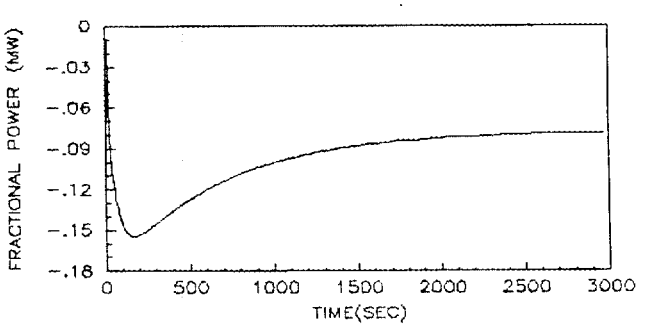

Fig. 5.7. Step response of fractional reactor power to a -5-cent reactivity perturbation. (Deviations from steady state.)

the fuel, cladding, core coolant, and reflector wall lumps verify that the overall heat transfer mechanism is represented reasonably by the primary model. A complete set of system responses to a −5-cent step reactivity insertion is listed in Appendix B.

5.2.2 Sodium Inlet Temperature Perturbation Results

To verify that the ten-lump IHX model provides a good representation of the dynamics when the heat transfer occurs in the opposite direction (from secondary to primary), a secondary sodium loop inlet temperature perturbation is applied. This input will exist when the coupling of the primary system model to the steam generator is implemented. A step perturbation of +10°F (+5.5°C) to the IHX secondary sodium inlet resulted in the system responses shown in Figs. 5.8 through 5.11. Figure 5.12 shows the temperature response of the sodium in the tank to the same input. The fractional power deviation indicates the temperature reactivity feedback effect as shown in Fig. 5.13. The core outlet coolant temperature first increases as the hot sodium enters the corresponding region, then starts decreasing because of the small late power decrease caused by the reactivity feedback effect. Note that the time delay is a result of a large sodium mass in the tank. Figure 5.14 shows the step response of the core outlet coolant temperature to a +10°F temperature perturbation at the IHX inlet. A set of system responses for this perturbation is shown in Appendix C. Table 5.2 includes a list of numerical values corresponding to the two input vectors of −5-cent reactivity insertion and the 10°F IHX secondary inlet sodium temperature perturbation.

5.3 ISOLATED STEAM GENERATOR DYNAMIC SIMULATION

The EBR-II steam generator open-loop model contains 18 state variables (first 18 in Table 5.1) including the level dynamics. There is no control action on the drum level for open-loop simulations. The drum level is expected to diverge for any kind of disturbance to the system. Four standard step perturbations applied to the model are:

1. +10°F (+5.5°C) feedwater temperature,

2. +10°F inlet sodium temperature,

3. +10 lb_m/s feedwater flow, and

4. +10% steam valve opening.

The corresponding input vectors are listed in Table 5.2.

5.3.1 Feedwater Temperature Perturbation Results

In the first case, an increase in the feedwater temperature increases the drum water and the downcomer temperatures, as shown in Figs. 5.15 and 5.16, respectively. As the water enters the evaporator, the subcooled water temperature also increases and the bubble formation

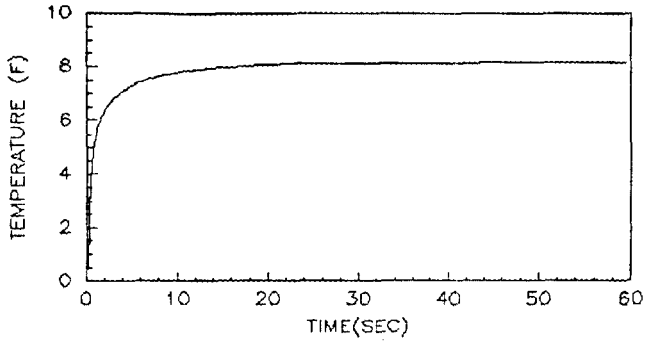

Fig. 5.8. Step response of IHX secondary inlet temperature to a +10°F (+5.5°C) IHX secondary inlet temperature perturbation. (Deviations from steady state.)

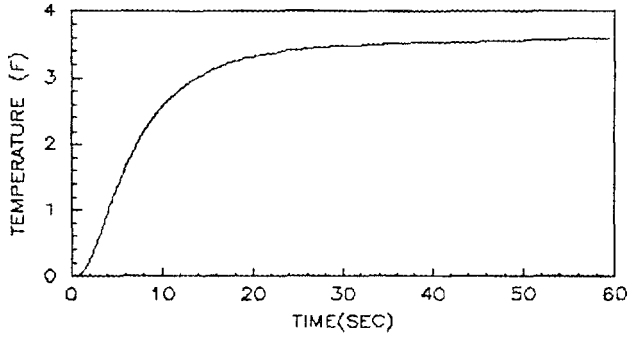

Fig. 5.9. Step response of IHX secondary outlet temperature to a +10°F (+5.5°C) IHX secondary inlet temperature perturbation. (Deviations from steady state.)

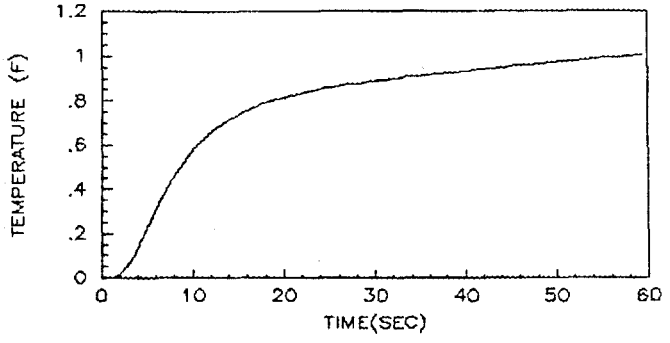

Fig. 5.10. Step response of IHX primary inlet temperature to a +10°F (+5.5°C) IHX secondary inlet temperature perturbation. (Deviations from steady state.)

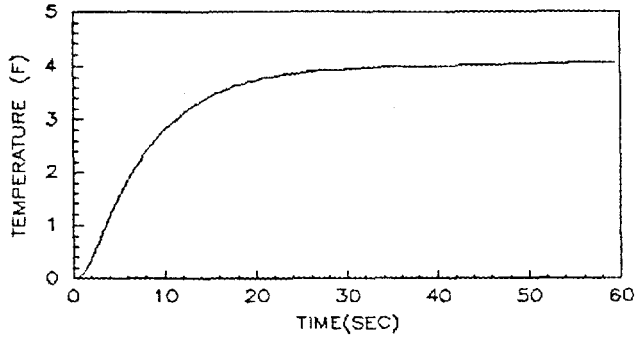

Fig. 5.11. Step response of IHX primary outlet temperature to a +10°F (+5.5°C) IHX secondary inlet temperature perturbation. (Deviations from steady state.)

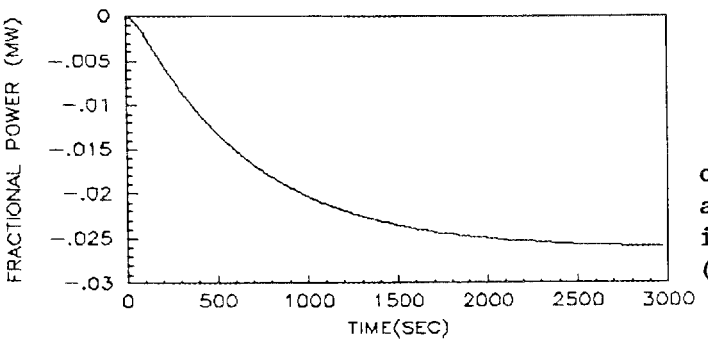

Fig. 5.12. Step response of fractional reactor power to a +10°F (+5.5°C) IHX secondary inlet temperature perturbation. (Deviations from steady state.)

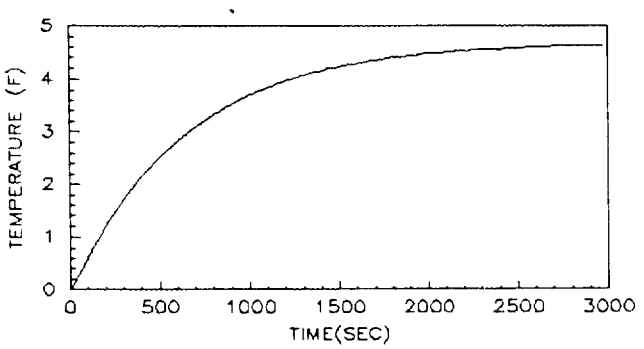

Fig. 5.13. Step response of sodium tank temperature to a +10°F (+5.5°C) IHX secondary inlet temperature perturbation. (Deviations from steady state.)

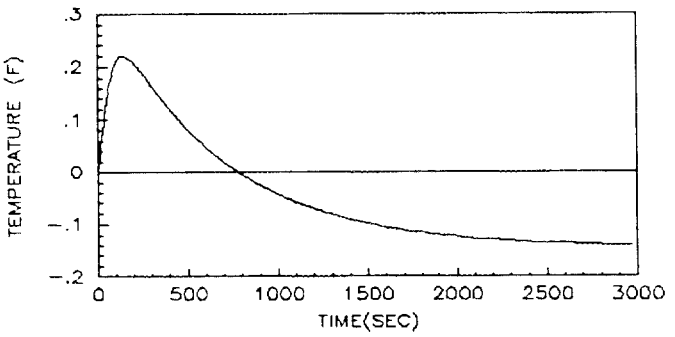

Fig. 5.14. Step response of core outlet temperature to a +10°F (+5.5°C) IHX secondary inlet temperature perturbation. (Deviations from steady state.)

Table 5.2. Forcing functions used in the EBR-II subsystem model simulation studies

Primary system model	Steam generator model
Reactivity (cent) B(1,1) = -475.4	Feedwater temperature (°F) B(12,1) = 0.009821
IHX inlet temperature B(36,1) = 1.398	Feedwater flow (lb_m/s) B(12,1) = -0.0054872 B(18,1) = 0.000262
	Steam valve opening (%) B(10,1) = -0.36
	Inlet sodium temperature (°F) B(13,1) = 0.4

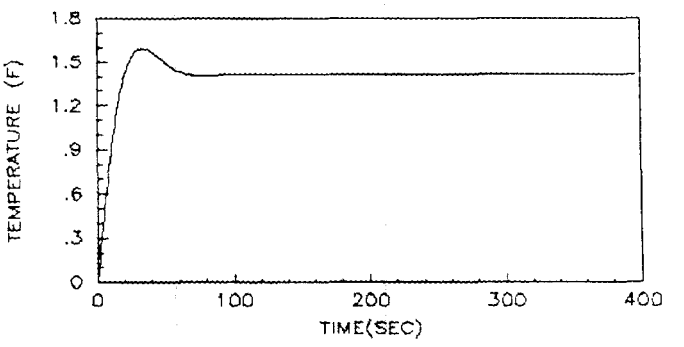

Fig. 5.15. Step response of drum water temperature to a +10°F (+5.5°C) feedwater temperature perturbation. (Deviations from steady state.)

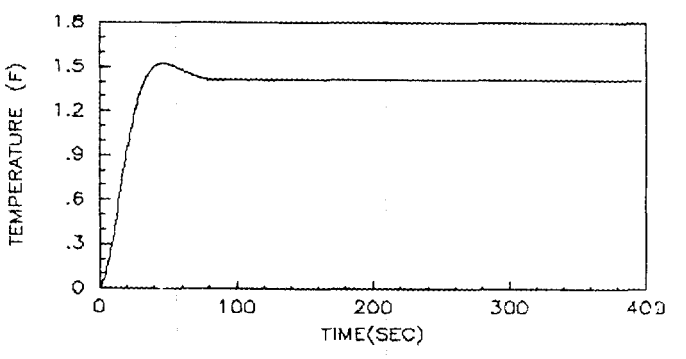

Fig. 5.16. Step response of downcomer temperature to a +10°F (+5.5°C) feedwater temperature perturbation. (Deviations from steady state.)

starts at lower elevations. The reason for the moving boundary to drop in level is the average temperature of the subcooled water which approaches the saturation temperature by the positive heat increment carried in by the entering downcomer water. Figure 5.17 indicates the deviation in the moving boundary. The height of the boiling region gets bigger as the subcooled height lowers; consequently, the amount of energy transfer into the boiling region increases, as does the steam quality (see Fig. 5.18). An increase in the steam quality results in more steam and an increase in the steam pressure, as shown in Fig. 5.19. The step responses to a +10°F feedwater temperature are shown in Appendix B.

5.3.2 Sodium Inlet Temperature Perturbation Results

The second case of step perturbation is a 10°F sodium inlet temperature increase at the superheater inlet. The heat increment input is immediately transferred to the secondary side of the superheater as shown in Fig. 5.20. Some remaining portion of the input heat is absorbed by the evaporator, which results in increasing the steam production. The steam quality and subcooled height responses are shown in Figs. 5.21 and 5.22 respectively. The evaporator sodium outlet temperature response (Fig. 5.23) indicates the amount of excess heat carried away without absorption by the steam generator. A complete set of step responses for this case is listed in Appendix B.

5.3.3 Feedwater Flow Perturbation Results

A step perturbation of +10 lb_m/s feedwater flow increase was the third input applied to the isolated steam generator model. The feedwater flow increase introduces some accumulation of additional water mass in the drum during the early stages of the transient. The addition of water mass drops the average drum water temperature, as shown in Fig. 5.24. It also increases the recirculation flow, namely downcomer and rising mixture flows, as shown in Figs. 5.25 and 5.26 respectively. As the secondary water inside the evaporator flows faster, the resident time decreases and the subcooled water retains its single-phase character up to some higher elevation before it reaches the saturation temperature. Figure 5.27 shows the response of the subcooled height to a +10-lb_m/s feedwater flow perturbation. Accordingly, the height of the boiling section shrinks, which results in less steam production and a decrease in steam quality (Fig. 5.28). The resultant steam pressure drop can be seen in Fig. 5.29. A complete set of system responses for the third input case is listed in Appendix B.

5.3.4 Steam Valve Opening Perturbation Results

The last case of a +10% steam valve opening step perturbation was modeled using the critical flow assumption defined in Sect. 4. Mathematically, this perturbation was implemented on the drum steam pressure in our model by assuming a linear relationship between the valve opening and the corresponding pressure drop in the drum. Figure 5.30 shows the steam pressure response to a +10% valve opening perturbation. In the present model, the system was assumed to be driven

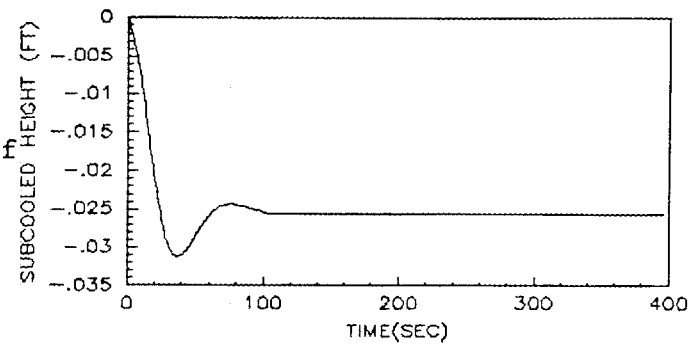

Fig. 5.17. Step response of subcooled height to a +10°F (+5.5°C) feedwater temperature perturbation. (Deviations from steady state.)

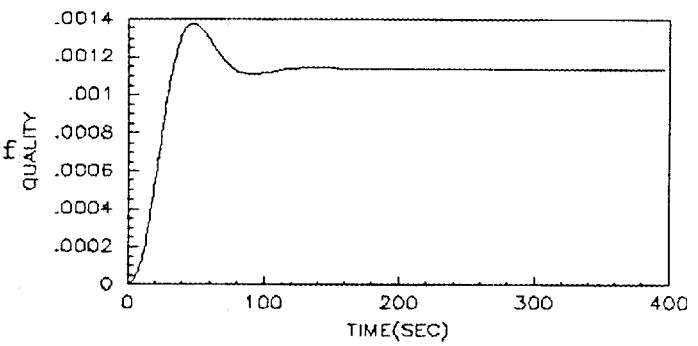

Fig. 5.18. Step response of steam exit quality to a +10°F (+5.5°C) feedwater temperature perturbation. (Deviations from steady state.)

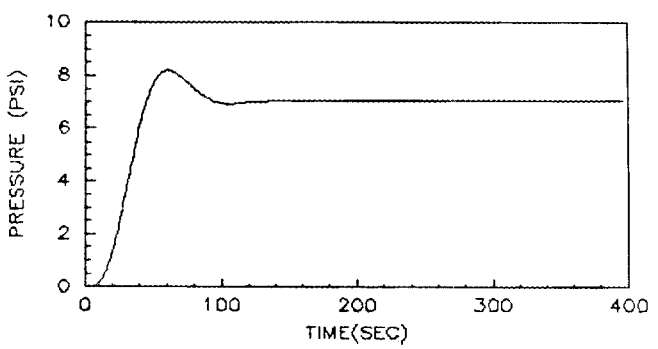

Fig. 5.19. Step response of drum pressure to a +10°F (+5.5°C) feedwater temperature perturbation. (Deviations from steady state.)

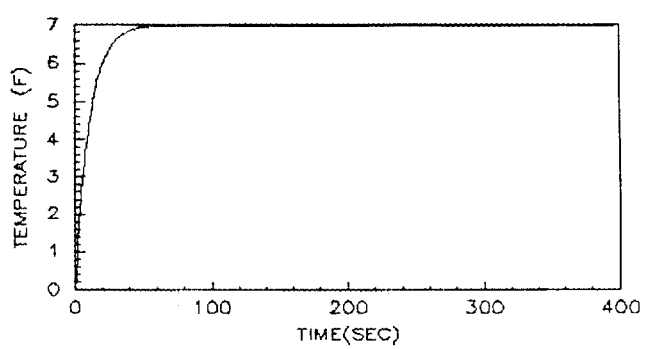

Fig. 5.20. Step response of superheated steam outlet temperature to a +10°F (+5.5°C) inlet sodium temperature perturbation. (Deviations from steady state.)

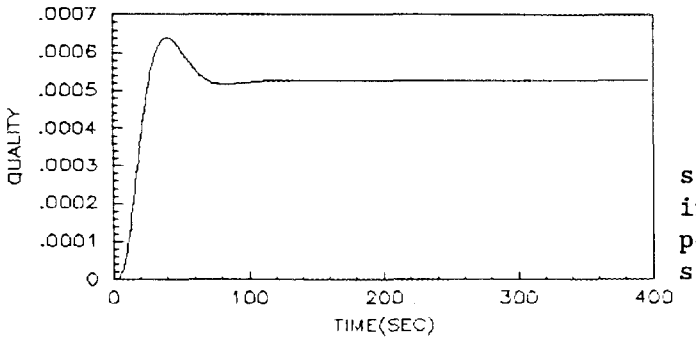

Fig. 5.21. Step response of steam exit quality to a +10°F inlet sodium temperature perturbation. (Deviations from steady state.)

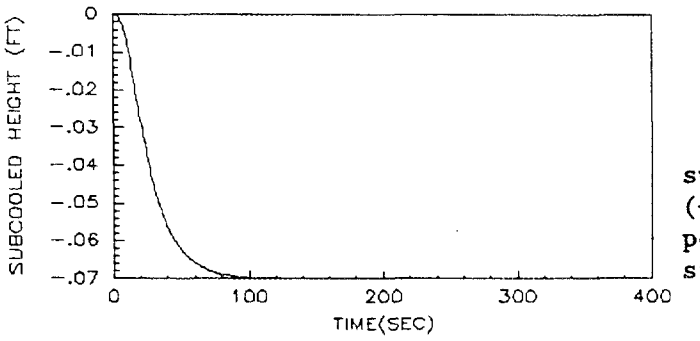

Fig. 5.22. Step response of subcooled height to a +10°F (+5.5°C) inlet sodium temperature perturbation. (Deviations from steady state.)

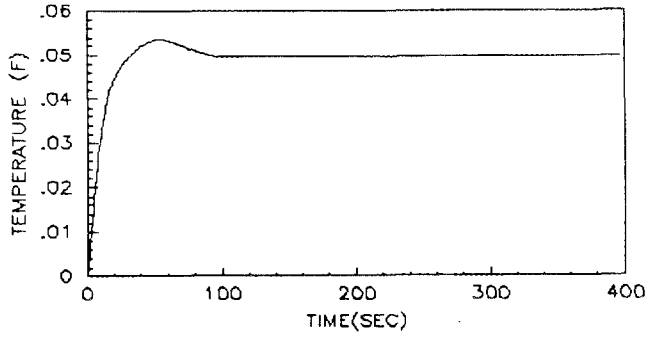

Fig. 5.23. Step response of evaporator sodium outlet temperature to a +10°F (+5.5°C) inlet sodium temperature perturbation. (Deviations from steady state.)

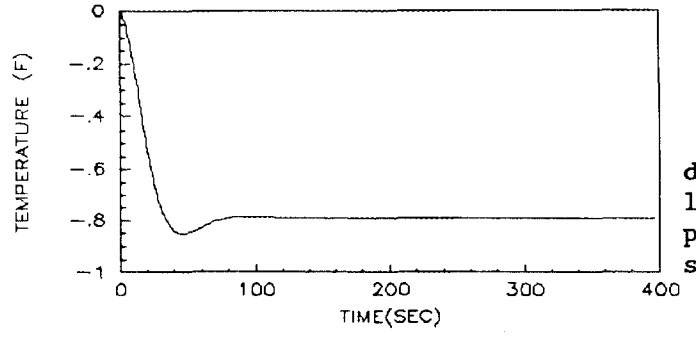

Fig. 5.24. Step response of drum water temperature to a +10-lb_m/s feedwater flow perturbation. (Deviations from steady state.)

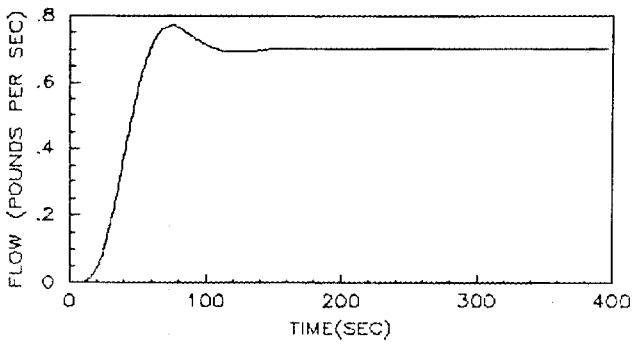

Fig. 5.25. Step response of downcomer flow to a +10-lb_m/s feedwater flow perturbation. (Deviations from steady state.)

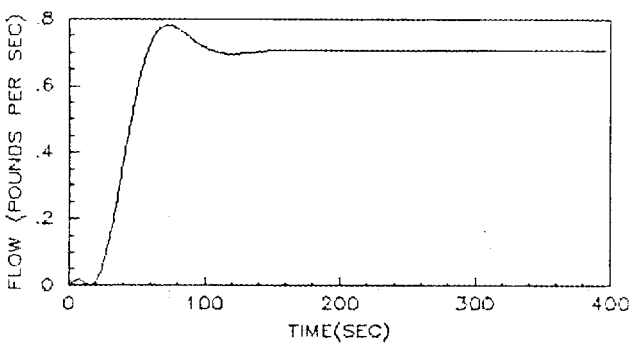

Fig. 5.26. Step response of evaporator flow to a +10-lb_m/s feedwater flow perturbation. (Deviations from steady state.)

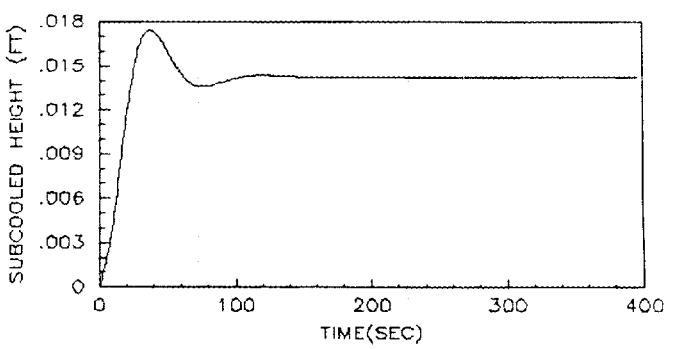

Fig. 5.27. Step response of subcooled height to a +10-lb_m/s feedwater flow perturbation. (Deviations from steady state.)

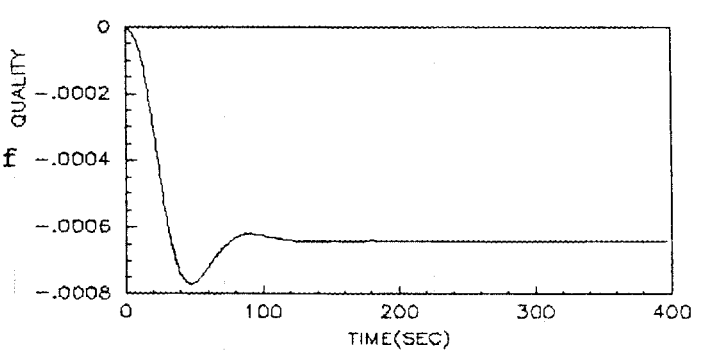

Fig. 5.28. Step response of steam outlet quality to a +10-lb_m/s feedwater flow perturbation. (Deviations from steady state.)

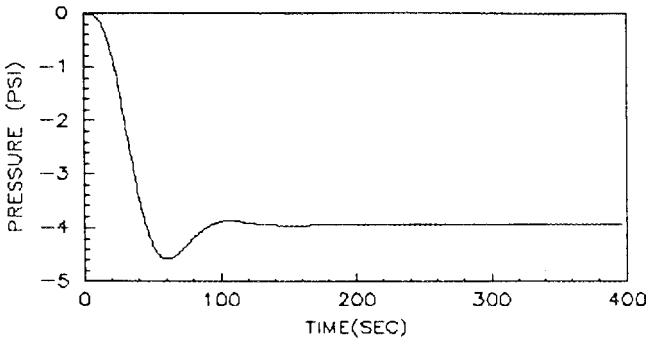

Fig. 5.29. Step response of drum pressure to a +10-lb_m/s feedwater flow perturbation. (Deviations from steady state.)

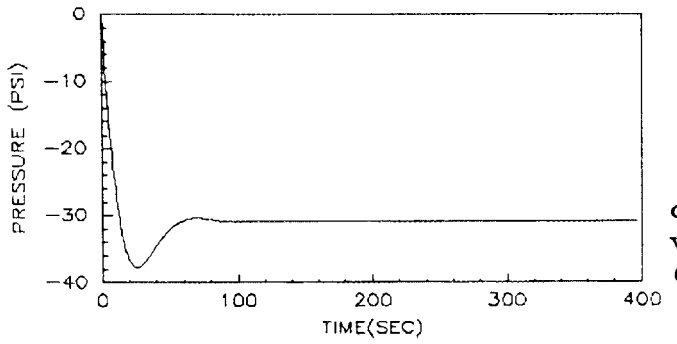

Fig. 5.30. Step response of drum pressure to a +10% steam valve opening perturbation. (Deviations from steady state.)

by the drum pressure and the pressure inside the evaporator tubes. A sudden drop in the drum pressure is followed by a pressure drop inside the evaporator tubes, and it is smaller than the pressure perturbation. Consequently, the pressure difference enforces the rising mixture flow upward, increasing the recirculation flow and the downcomer flow. Note that the net pressure difference creates a driving force toward the drum since the drop in the drum pressure is larger. Figures 5.31 and 5.32 show the downcomer and rising mixture flows respectively. The increment in the flows affects the steam production mechanism in a manner similar to the feedwater flow perturbation case; that is, steam quality decreases, subcooled height increases, and so forth. However, another mechanism for creating a driving force for the steam production appears, which is dominant and in the reverse direction. It is the change in the saturation conditions inside the evaporator tubes. The pressure drop lowers the required saturation temperature for the bubble formation. The subcooled height therefore shrinks and the steam quality tends to increase, as shown in Figs. 5.33 and 5.34. A complete set of step responses is given in Appendix B.

5.3.5 Comparison of the Results with a PWR U-Tube Steam Generator Model

The EBR-II and PWR steam generators are quite different in size, capacity, structure, and range of operation. However, they are steam-generating machines working with the same principles of physics. Thus, a comparison between the responses of the EBR-II steam generator model

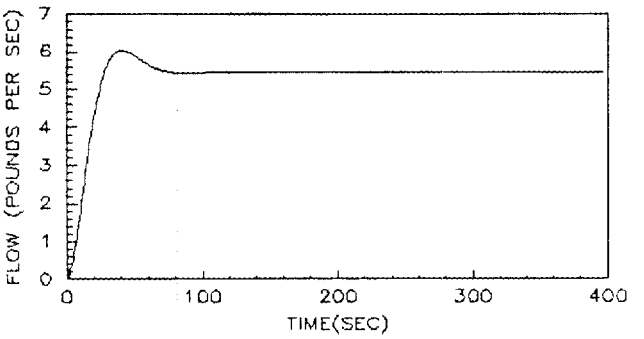

Fig. 5.31. Step response of downcomer flow to a +10% steam valve opening perturbation. (Deviations from steady state.)

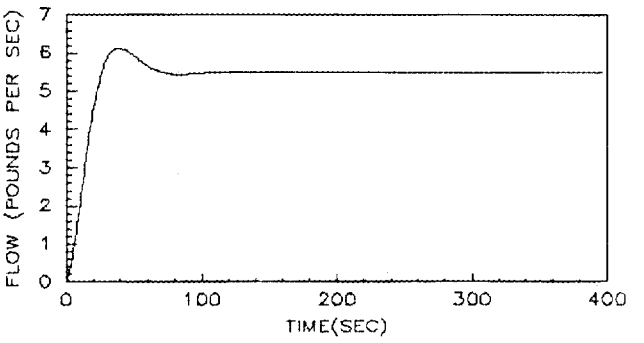

Fig. 5.32. Step response of evaporator flow to a +10% steam valve opening perturbation. (Deviations from steady state.)

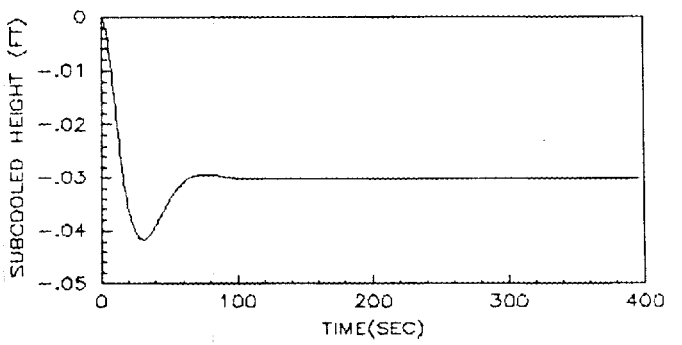

Fig. 5.33. Step response of subcooled height to a +10% steam valve opening perturbation. (Deviations from steady state.)

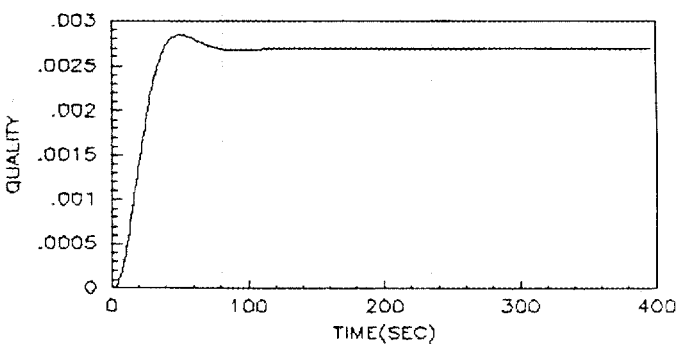

Fig. 5.34. Step responses of steam exit quality to a +10% steam valve opening perturbation. (Deviations from steady state.)

and a previously developed PWR steam generator model is considered to be worthwhile. A linear, U-tube, recirculating-type PWR steam generator model has been developed previously.[9] The Ali model uses typical Westinghouse data, and it is validated.[2] Figure 5.35 shows the responses of several state variables to a 10% step change in steam valve opening using the EBR-II and Ali's PWR steam generator models. Another comparison is shown in Fig. 5.36 for a 10°F step change in feedwater temperature. The figures emphasize that the overall dynamic behavior of the EBR-II model is in physical agreement with Ali's validated PWR U-tube steam generator model.

5.4 SIMULATION OF THE COMBINED SYSTEM

5.4.1 Combining Subsystem Models

There are several different ways of coupling the primary system and the steam generator models using MATRIX_X. A brief description of the methods for coupling different modules is given in Appendix C. In the present model, the coupling is implemented by creating an overall system matrix, including the system matrices of primary system and steam generator models. Using the appropriate coupling terms, an overall system matrix can be formed as follows.

$$A = \begin{bmatrix} A_{pr} & CP_1 \\ CP_2 & A_{sg} \end{bmatrix} , \tag{5.4}$$

where

CP_1, CP_2 = coupling matrices,

A_{pr} = system matrix of the primary model,

A_{sg} = system matrix of the steam generator model.

We can see from Fig. 3.1 that the only input to the primary system model is provided by the sodium temperature connection between the IHX secondary inlet node and evaporator outlet node. The coupling matrix CP_1, therefore, includes the IHX inlet temperature forcing vector as listed in Table 5.2. Similarly, the coupling matrix CP_2 includes the transpose of the steam generator inlet temperature forcing vector as listed in Table 5.2.

5.4.2 Combined Model Simulations

The application of a -5-cent step reactivity perturbation to the combined model yields similar system responses as in the simulation of the isolated primary model. Figure 5.37 shows the fractional power response to a -5-cent step reactivity insertion. The IHX outlet sodium temperature step response is shown in Fig. 5.38, which is an input to

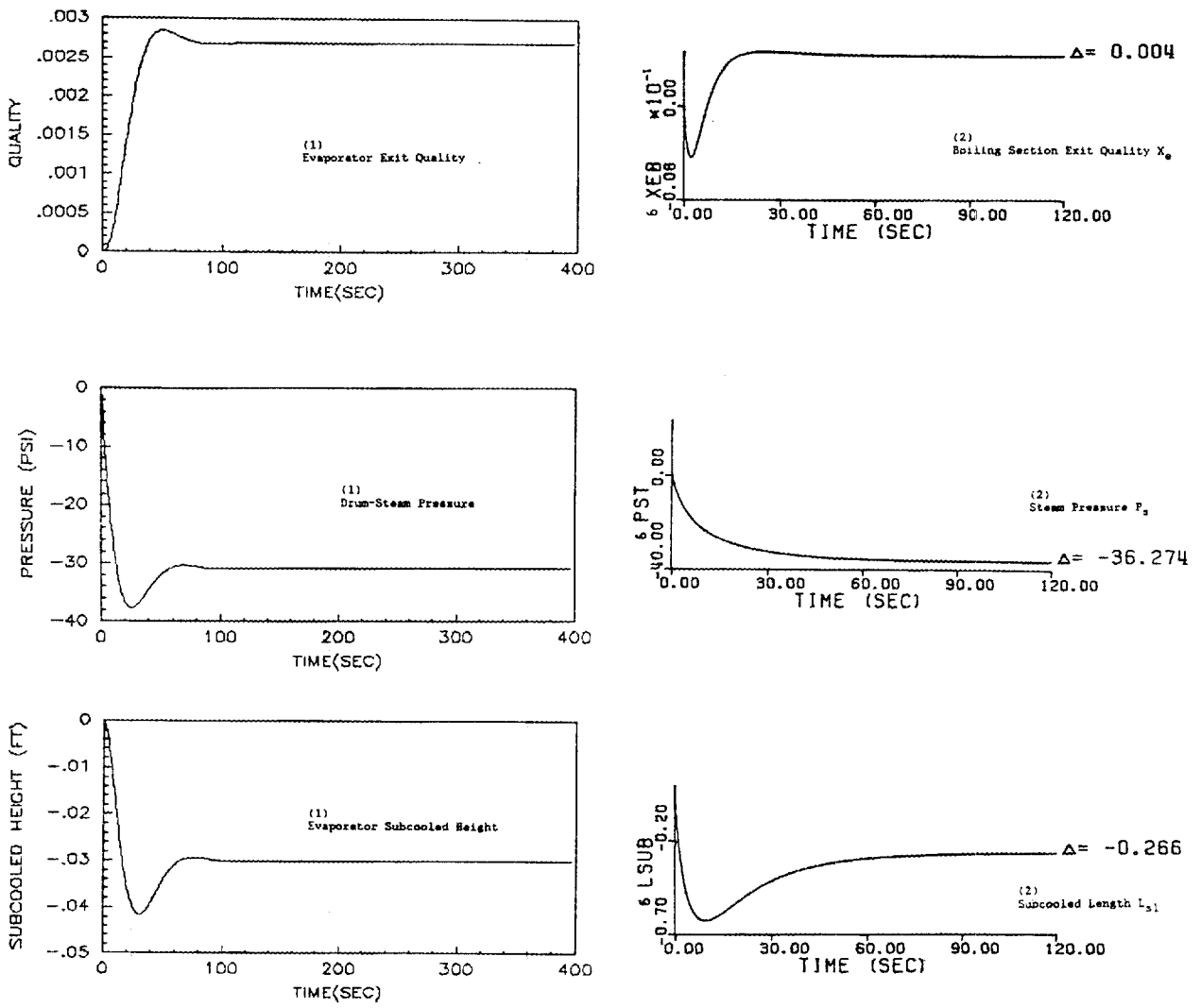

Fig. 5.35. Step responses to a +10% change in steam valve opening. (Deviations from steady state.) (1) EBR-II steam generator model. (2) PWR U-tube steam generator model.

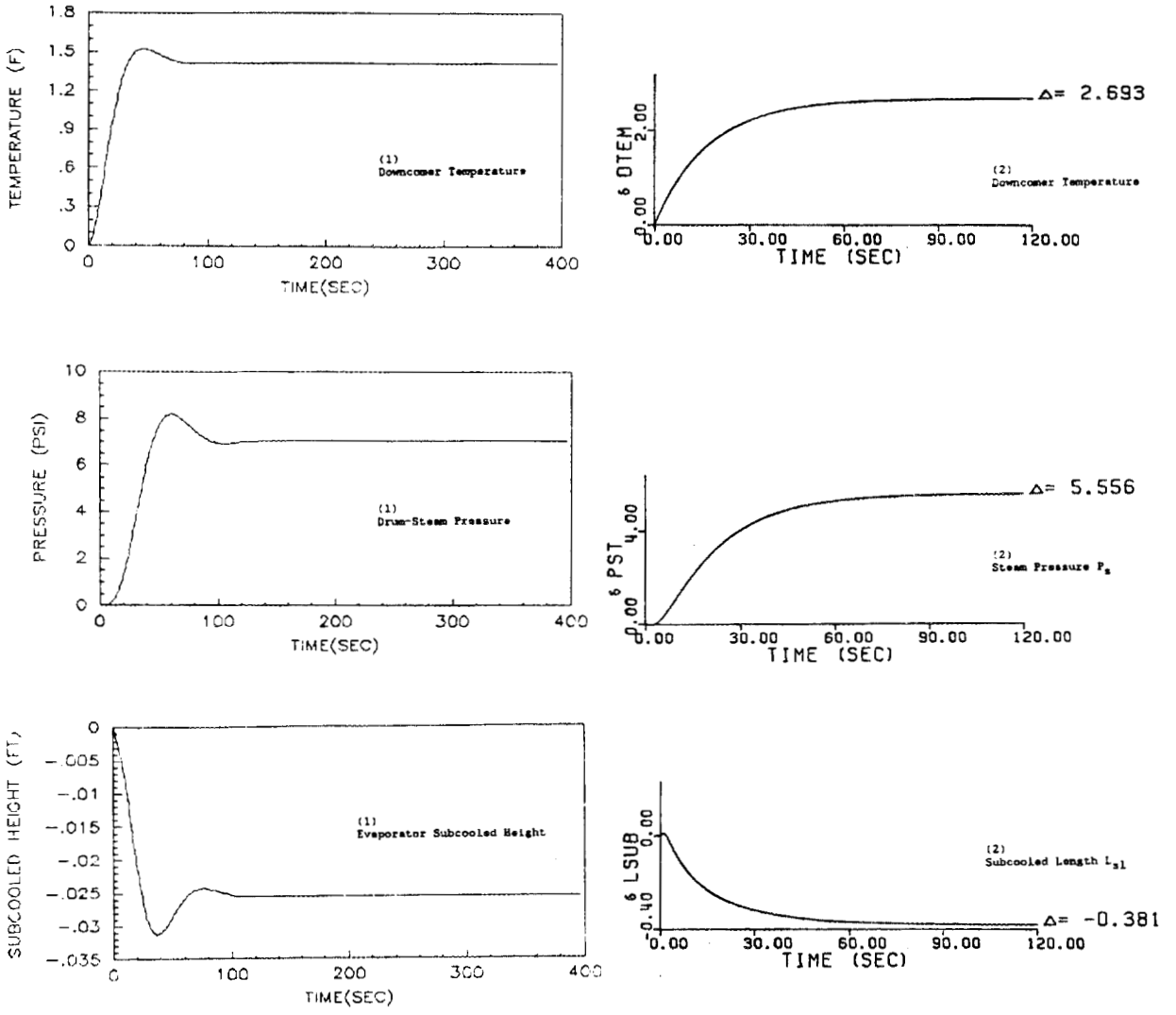

Fig. 5.36. Step responses to a +10°F change in feedwater temperature. (Deviations from steady state.) (1) EBR-II steam generator model. (2) PWR U-tube steam generator model.

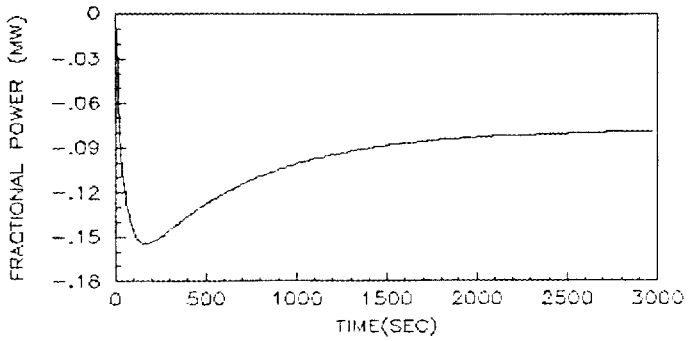

Fig. 5.37. Step response of fractional reactor power to a -5-cent reactivity perturbation. (Deviations from steady state.)

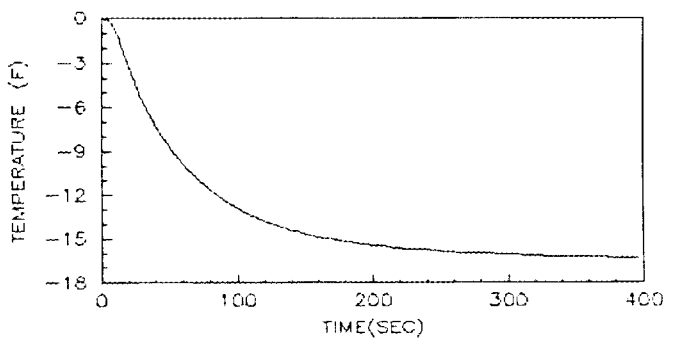

Fig. 5.38. Step response of IHX outlet sodium temperature to a -5-cent reactivity perturbation. (Deviations from steady state.)

the superheater model. The temperature drop in the secondary sodium caused by the reactivity perturbation results in decreasing the superheated steam temperature, as shown in Fig. 5.39. Some amount of temperature drop also appears in the shell side of the evaporators, which slows down the steam production rate, that is, decreased steam quality, increased subcooled height. Consequently, the drum pressure decreases, which is a measure of steam mass flow rate leaving the steam generator. Figure 5.40 shows the drum pressure response to a -5-cent step reactivity perturbation.

The second input case of +10% steam valve opening step perturbation is applied to the combined system model. The steam drum pressure step response is shown in Fig. 5.41. The drop in the steam pressure affects the rest of the steam generator system in a way similar to that of the isolated steam generator case explained in Sect. 5.3. The fractional power response to the same perturbation is shown in Fig. 5.42. The combined EBR-II model does not include the feedwater and condenser systems. In the actual plant, the superheated steam flow deviation changes the feedwater temperature because the feedwater reheaters use some fraction of the superheated steam. A change in the feedwater temperature causes an additional input to the evaporators, which affects the secondary sodium temperature flowing through the shell side of the evaporators. This effect is carried to the primary system as the

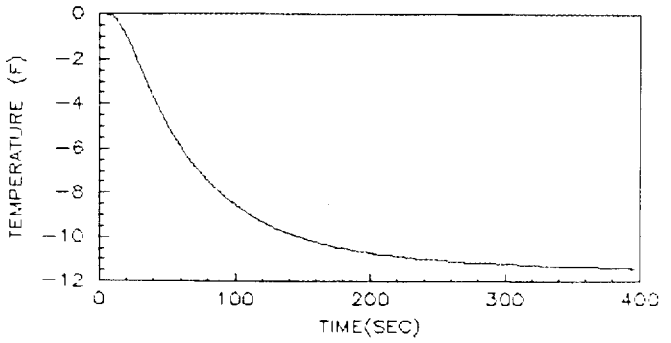

Fig. 5.39. Step response of superheated steam temperature to a -5-cent reactivity perturbation. (Deviations from steady state.)

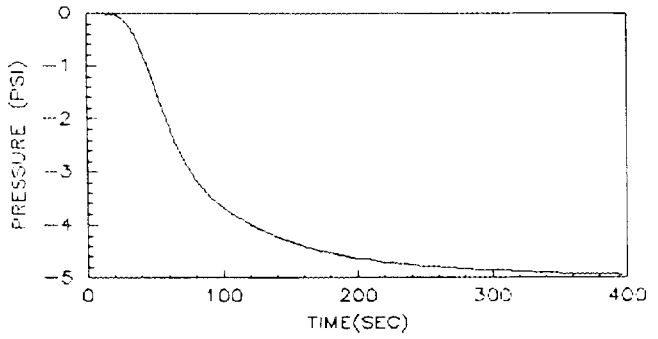

Fig. 5.40. Step response of drum pressure to a -5-cent reactivity perturbation. (Deviations from steady state.)

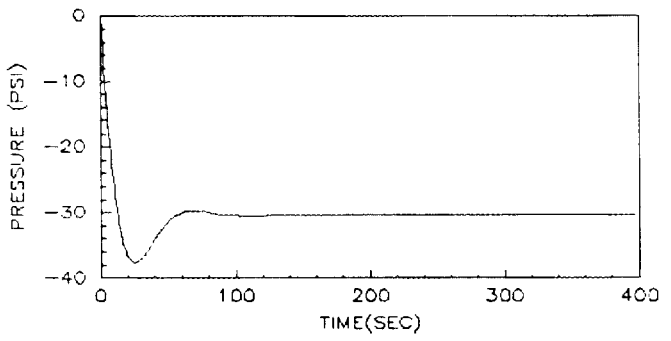

Fig. 5.41. Step response of drum pressure to a +10% steam valve opening perturbation. (Deviations from steady state.)

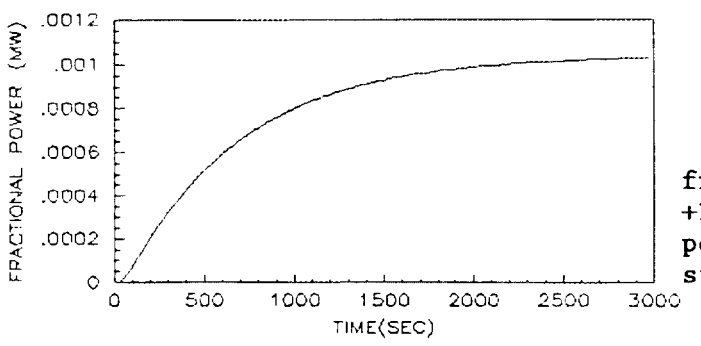

Fig. 5.42. Step response of fractional power response to a +10% steam valve opening perturbation. (Deviations from steady state.)

secondary sodium leaves the evaporators and enters the IHX. As a result, the primary system receives an additional heat input in reality, and the reactor power is to be affected by means of the temperature reactivity feedback mechanism. The power response obtained by the present linear model, therefore, does not include this additional effect. A set of system responses to −5-cent reactivity and +10% steam valve opening step perturbations is given in Appendix B.

5.4.3 Prediction of the ANL Safety Tests

The effectiveness of the reactivity feedback in the EBR-II has been demonstrated through several dynamic testing programs. These tests were planned to simulate possible accidental events, thus the range of transients exceeded the limits of the prediction capability of linear models. However, it is observed that the EBR-II model presented in this report could provide predictions of some of the key state variables for a few test transients. Note that the inputs used in the model are approximations of the real-plant perturbations.

A large steam pressure reduction test (B402) was conducted at EBR-II to demonstrate that it is possible to design an LMR plant in which the reactivity feedback mechanism is capable of protecting the reactor without severe damage in case of a loss-of-heat-sink accident initiated by a large steam pressure loss. The drum pressure is ramped down to about 400 psi, held, and ramped back to its original value in the test. Using the linear model, this case was simulated by ramp opening the steam valve and holding it constant. We aimed at evaluating the feedwater controller performance for which a large steam pressure reduction is one of the most severe transients involving drum level control. Figure 5.43 shows the drum pressure response compared to the measured data and NATDEMO prediction.[15] The controlled drum level response with a similar comparison is shown in Fig. 5.44.[15] As can be seen from Fig. 5.44, the linear model exhibits tightly tuned behavior for the controller. However, the actuator is not overforced to accomplish this task, as can be seen in Fig. 5.45, which compares this response to NATDEMO predictions of feedwater and extraction flows.[15] Note that pressure reduction is held constant after the ramp in the simulation; therefore, the feedwater flow stays constant, as indicated in Fig. 5.45. The test simulates the loss-of-heat-sink phenomenon in which the tank sodium temperature increases, resulting in a negative reactivity feedback effect on the reactor power. The power decrement is observed in the linear model; however, the evaporator sodium outlet prediction is much lower than the measured data because of the exceeded range of acceptable transients that can be used in linear models. The steam generator is the most nonlinear component among EBR-II subsystems; thus such mismatchings in scale are expected in the case of a linear steam generator model simulating large transients.

The purpose of the loss-of-flow-without-scram (LOFWS) test program was to demonstrate that EBR-II neutronics possesses the inherently safe property of a strong reactivity feedback mechanism that would, in loss-of-flow accidents, shut down the reactor naturally without activating the emergency protection systems. In the SHRT-39 test, the primary and

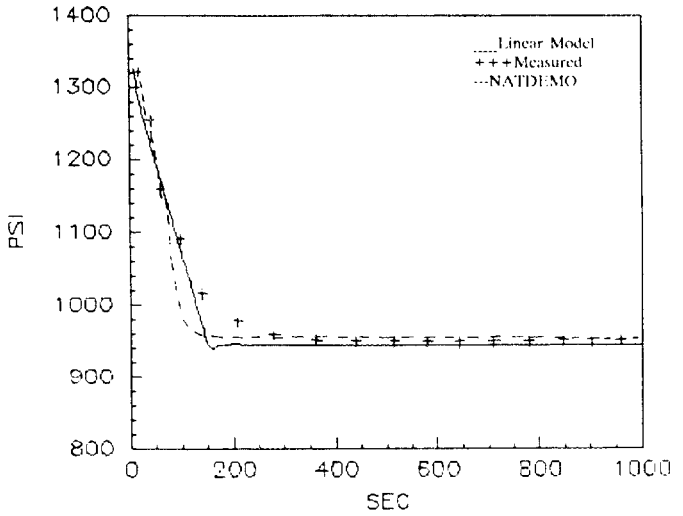

Fig. 5.43. Drum pressure response to a large steam reduction test (B402).

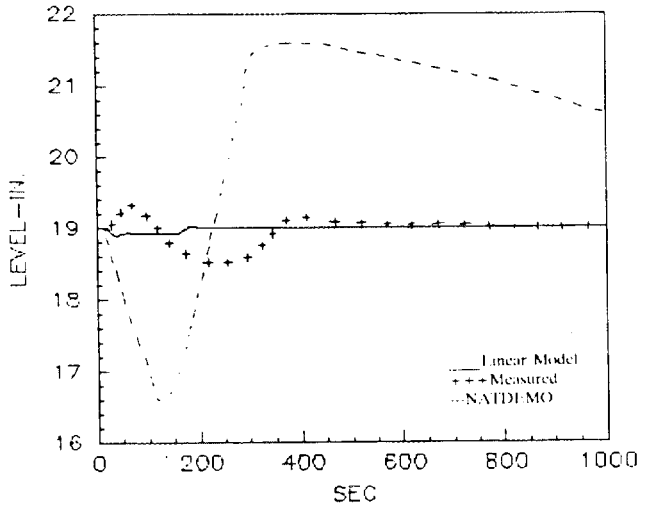

Fig. 5.44. Drum level response to a large steam reduction test (B402).

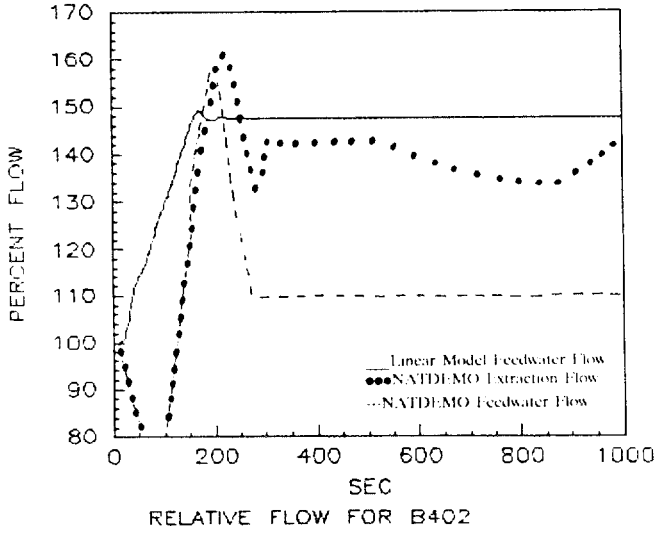

Fig. 5.45. Relative flow response to a large steam reduction test (B402).

secondary pumps were stopped to reduce both flows almost 100%, leaving the reactor in a natural recirculation mode. When the heat removal process slows down, the reactor inlet temperature increases and the neutron power decreases due to reactivity feedback effect. The simulation results using the linear EBR-II model show that the neutron power behavior matches the measured data, as shown in Fig. 5.46.[16] Figure 5.47 shows the intermediate heat exchanger secondary outlet temperature response in the SHRT-39 test.[16]

In the SHRT-26 test, the power rejection through IHX was changed by reducing the secondary flow to obtain a ramp increase in the reactor inlet temperature of approximately 16°C (60.8°F). The simulation of this test was to verify the sensitivity of the reactivity feedback mechanism to a given temperature increase in the reactor inlet. The predictions using the DSNP code[17] were validated by modifying the tank model so that the initial estimate of 40% of the inventory of tank sodium was reduced to 24%. Using the linear model, the same modification was also found to be essential for good agreement. Figure 5.48 shows the high-pressure inlet plenum temperature response.[17] The neutron power response shown in Fig. 5.49 exhibits agreement between the measured data and their prediction using the linear model.

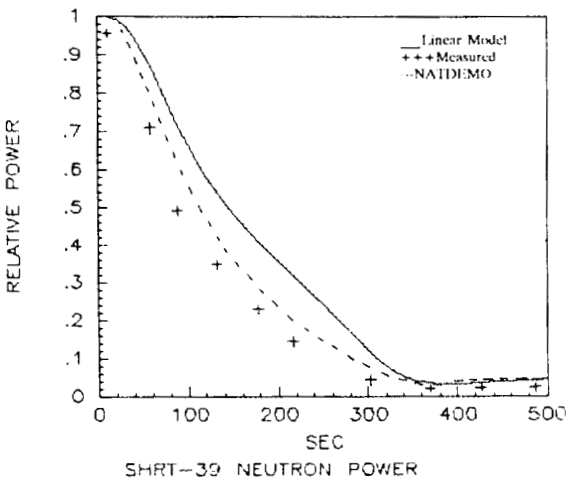

Fig. 5.46. Neutron power response to the SHRT-39 test.

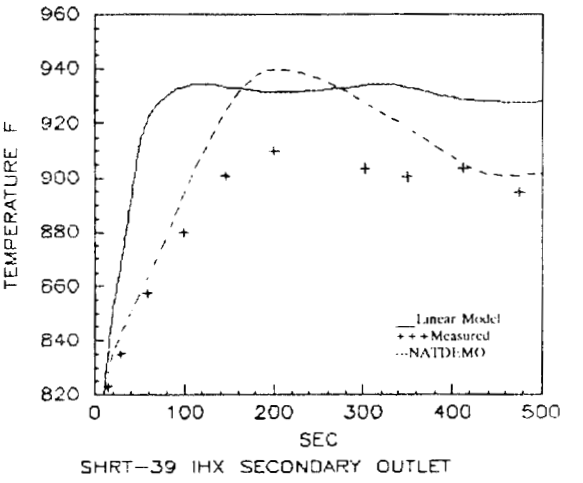

Fig. 5.47. IHX secondary outlet temperature response to the SHRT-39 test.

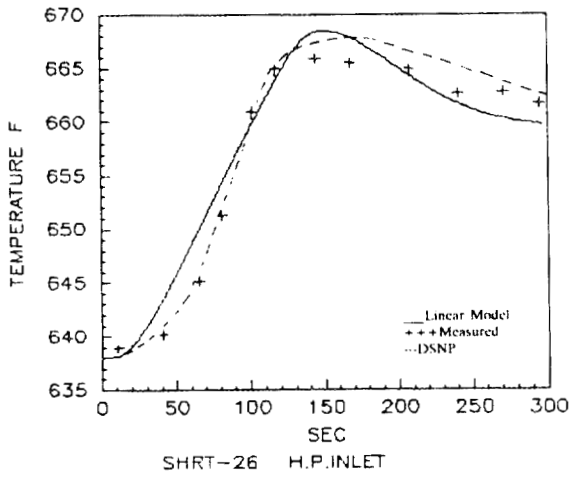

Fig. 5.48. High-pressure plenum inlet temperature response to the SHRT-26 test.

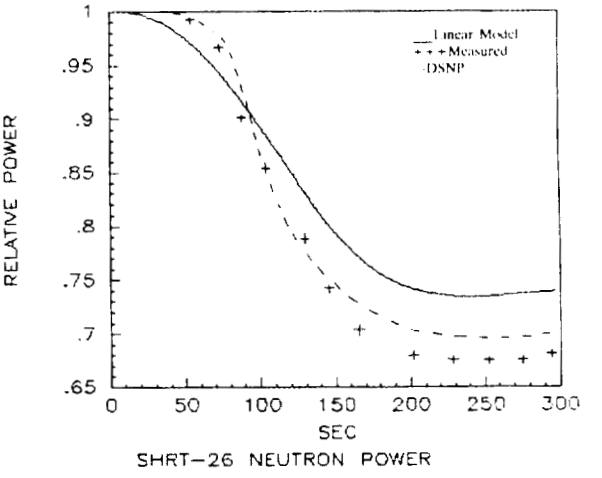

Fig. 5.49. Neutron power response to the SHRT-26 test.

6. CONCLUSIONS

6.1 SUMMARY

This study contains the development of a low-order linear EBR-II system model including the reactor, liquid sodium tank, intermediate heat exchanger, and steam generator subsystems. The model is developed as two separate modules, namely the primary system and the steam generator.

The EBR-II primary system model is taken from an earlier work[4] and modified using a physical model reduction technique,[2] six precursor concentration equations replaced with one "averaged" group equation. The model includes a point reactor kinetics equation, an averaged precursor equation, Mann's heat transfer model, and the first-order transport-lag approximations. The core bowing and control rod expansion reactivity feedback mechanisms are not included in the model because of their negligible effects for small transients around the steady state. The remaining seven reactivity feedback effects are taken into consideration.

Another modification to the Greene model pertains to the use of more lumps for the IHX model. The necessity for this modification comes from the heat transfer limitations of Greene's five-lump IHX model. The step responses to a −5-cent reactivity perturbation are physically consistent and agree with ANL results. The results also agree with the Greene model results. The temperature responses of the IHX coolant lumps verify that increasing the number of lumps provides better results. The IHX model, which is a part of the primary system model, is simulated for a +10°F sodium temperature perturbation at the secondary inlet plenum. The step responses of the primary system model to the inlet sodium temperature perturbation show that the ten-lump IHX model is sufficient in representing the dynamics of the heat exchanger system.

The secondary system of the EBR-II is modeled using the energy and mass balance equations for the evaporator, superheater, and drum regions. Two momentum equations are used for the downcomer and evaporator flows. The phase change in the evaporator is modeled with a moving boundary approach. In the two-phase region, a homogeneous flow assumption is considered.[9] The superheater dynamics is represented by a single-phase heat transfer formulation (Mann's model).[7] A three-element controller is designed for the drum level control problem. The controller uses drum level and feedwater flow and steam flow signals. The steam leaving the drum is assumed to be completely dry, and its representation is based on the critical flow assumption.[2] The step responses of the steam generator model to four different step perturbations show that the drum level is unstable unless the three-element controller is activated. It is also observed that an inherent stability exists in the boiling region dynamics regardless of any control action on the drum level. The overall results are in physical agreement with the results obtained by a previously developed PWR, U-tube (recirculation type) steam generator model.[2]

The linear models of the primary system and the steam generator are coupled. The combined model step responses to a −5-cent reactivity insertion are quite similar to the results obtained using only the primary system model. On the steam generator side, the superheaters receive a sodium temperature decrease input from the primary system that is immediately absorbed by the dry steam flowing through the tube side of the superheaters. There is not much feedback from the steam generator to the primary system for small perturbations around steady state. A +10% steam valve opening perturbation to the steam generator side of the combined model results in step responses that are similar to the isolated steam generator results. The primary system is not very much affected by the steam valve opening perturbation for two reasons. First, the sodium tank in the primary system has a large time constant, and any sudden temperature change in the secondary system will be slowed on its way to the active core region; therefore, the tank-sodium temperature reactivity feedback effect on the reactor power is a slowly varying mechanism. The other reason for the weak coupling between the two modules is as follows. A change in the superheated steam flow affects the heat transfer rate to the feedwater through the feedwater heaters (the heaters use a fraction of the superheated steam). The feedwater heater system belongs to the condenser-turbine system, and the present EBR-II model does not include this feedwater heater system. The missing information about the feedwater dynamics results in an exclusion of the effects of the feedwater temperature variations on evaporator dynamics.

Although the linear models are known to provide reasonable predictions around the linearization point, the EBR-II model could predict few state variables in SHRT-39 and SHRT-26 test transients. A complete agreement was not achieved due to the fact that the test perturbations are too large. The three-element controller performance is verified through simulations of large steam reduction test B402.

Matrix_X is one of the more advanced members of the MATLAB CAD package family. All simulations in this work are performed using the special features of Matrix_X. Using the menu-driven SYSTEM-BUILD option, a number of modules can be coupled regardless of the complexity of input-output relationships among them. There are six integration algorithms; the default "variable Kutta-Merson" method is used in this work.

6.2 RECOMMENDATIONS

The development of a model for the EBR-II condenser turbine system is a natural extension of the study described in this work. The combined system model with this third module can be used to predict system behavior for the test transients. Despite the limited capabilities of linear models, it is believed that a complete EBR-II model will contribute to the development of new control strategies for advanced liquid metal reactors.

An important recommendation is the application of model reduction techniques to the EBR-II model. The present model contains 57 state

variables, including the three-element controller dynamics. Software for the control design algorithms can be made less costly if an appropriate model reduction method is used to eliminate the redundant states.

The present model can be improved by introducing nonlinearities to the linear model. Increasing the number of lumps may provide better temperature predictions for a detailed study. The core bowing and the control rod expansion reactivity feedback effects should be included in a nonlinear version of the model. The three-element controller design is a subject of further investigation, and the actuator dynamics can be represented with an improved model.

Despite the fact that some agreement between the measured safety test results and the linear model responses are observed, the linear model cannot be used for the prediction of a complete set of state variables for test transients. The necessary nonlinearities must be included to complete the model for such applications. Furthermore, successive linearization of the model must be studied, especially for control strategy development.

REFERENCES

1. G. H. Golden et al., "Evolution of Thermal-Hydraulics Testing in EBR-II," *Nucl. Eng. Design* 101, 3-12 (1987).

2. T. W. Kerlin et al., "*Pressurized Water Reactor Modeling for Long-Term Power System Dynamics Simulation*," EPRI EL-3087, Vol. 2, May 1983.

3. J. T. Madell and R. E. Jarka, *Analysis of the Linear Components of the PRD in EBR-II*, ANL-7539, Argonne National Laboratory, October 1969.

4. S. R. Greene, "The Design, Implementation and Cost-Benefit Analysis of a Dynamic Testing Program in the Experimental Breeder Reactor II," M.S. thesis, The University of Tennessee, 1979.

5. G. M. Marshall, "A Dynamic Analysis of the Primary System in Experimental Breeder Reactor II," M.S. thesis, Louisiana State University, 1987.

6. R. C. Berkan, "Dynamic Modeling of EBR-II for Simulation and Control," M.S. thesis, The University of Tennessee, Knoxville, 1987.

7. S. J. Ball, "Approximate Models for Distributed-Parameter Heat-Transfer Systems," *ISA Trans.* 3, 38-47 (January 1964).

8. A. T. Chen, "A Digital Simulation for Nuclear Once-Through Steam Generators," Ph.D. dissertation, The University of Tennessee, 1976.

9. M. R. A. Ali, "Lumped Parameter, State Variable Dynamic Models for U-Tube Recirculation Type Nuclear Steam Generators," Ph.D. dissertation, The University of Tennessee, 1976.

10. N. L. Snidow and T. L. Wilson, "U-Tube Steam Generator Modeling System," Internat. Conf. Power Plant Simulation, Cuernavaca, Mexico, November 19-21, 1984.

11. *EBR-II System Design Descriptions*, Vols. 1 through 5, Argonne National Laboratory, Argonne, Ill., June 1972.

12. L. J. Koch, W. B. Lowenstein, and H. O. Monson, *Addendum to Hazard Summary Report on EBR-II*, Argonne National Laboratory, Argonne, Ill., ANL-5719, January 1964.

13. *Guide for Irradiation Experiments in EBR-II*, Argonne National Laboratory, Argonne, Ill., March 1975.

14. R. E. Crosbie and W. Heyes, "Variable-step Integration Methods for Simulation Applications," *Appl. Math. Model.*, 137-140 (1976).

15. E. E. Feldman, "Predicted and Measured Response of the EBR-II Plant to Large Steam Pressure Changes," *Nucl. Eng. Design* **108**, 331-341 (1988).

16. D. Mohr, "Loss-of-Primary-Flow-Without-Scram Test: Pretest Predictions and Preliminary Results," *Nucl. Eng. Design* **101**, 45-56 (1987).

17. E. M. Dean, W. K. Lehto and H. A. Larson, "System Modeling and Simulation at EBR-II," Proceedings, 6th Power Plant Dynamics, Control and Testing Symposium, Knoxville, Tenn., 1986.

SELECTED BIBLIOGRAPHY

1. A. V. Campise, *Dynamic Simulation and Analysis of EBR-II Rod-Drop Experiments*, ANL-7664, Argonne National Laboratory, March 1970.

2. J. C. Cherng, "An Investigation of Feedwater Control and Nonlinear Effects for a U-Tube Steam Generator Model," M.S. thesis, The University of Tennessee, 1978.

3. H. P. Planchon, J. I. Sackett, G. H. Golden, and R. H. Sevy, "Implications of the EBR-II Inherent Safety Demonstration Test," *Nucl. Eng. Design* **101**, 75-90 (1987).

4. Shih-Jen Wang, "Modeling And Simulation of Pressurized Water Reactor Power Plant," Ph.D. dissertation, The University of Tennessee, 1983.

APPENDIX A

AUXILIARY CALCULATIONS

A.1 BOUNDARY FLOW APPROXIMATION

The development of a lumped-parameter steam generator model includes formulation of the two-phase flow phenomenon. To use the energy balance equation for the boiling region, the coolant flows (in and out) must be known in the form of state or algebraic variables. For a simple linear model such as the tea kettle model, these flows can be assumed to be constant; however, this assumption is not applicable for detailed studies because of an unacceptable compromise in the accuracy. One of the practical methods for the treatment of the boundary flow (between boiling and subcooled regions) is to express the unknown boundary flow in terms of available state variables, such as heat transfer rate and latent heat of evaporation. Assuming a linear relationship, the boundary flow W_2 is written as follows.

$$W_2 = \frac{Q_{SC}}{h_F - h_{DC}} = \frac{U_{MS} \cdot A_{MS} \ (2T_{M2} - T_{DC} - T_F)}{2C_P(T_F - T_{DC})} \quad , \tag{A.1}$$

where

Q_{SC} = heat transfer rate into the subcooled region,

h_F = saturation enthalpy,

h_{DC} = subcooled region inlet enthalpy,

U_{MS} = heat transfer coefficient for tube metal subcooled water interface,

A_{MS} = heat transfer area,

T_{M2} = tube metal temperature.

Using the chain rule, the linearization around steady state results in the following algebraic form.

$$W_2 = [WB1] \ T_{M2} + [WB2] \ T_{DC} + [WB3] \ P_B + [WB4] \ Z_{SC} \quad , \tag{A.2}$$

where

$$WB1 = \frac{\partial W_2}{\partial T_{M2}} = \frac{U_{MS} \cdot A_{MS}}{C_P(T_F - T_{DC})} \quad ,$$

$$WB2 = \frac{\partial W_2}{\delta T_{DC}} = \frac{4C_P U_{MS} \cdot A_{MS} \cdot (T_{M2} - T_F)}{(h_F - h_{DC})^2} \quad ,$$

$$WB3 = \frac{\partial W_2}{\partial T_F}\left(\frac{\partial T_F}{\partial P_B}\right) = \frac{-4C_P U_{MS} \cdot A_{MS}\ (T_{M2} - T_{DC})}{(h_F - h_{DC})^2}\left(\frac{\partial T_F}{\partial P_B}\right) ,$$

$$WB4 = \frac{\partial W_2}{\partial Z_{SC}} = \frac{U_{MS} \cdot P_R\ (2T_M - T_{DC} - T_F)}{2(h_F - h_{DC})} .$$

A.2 HEAT TRANSFER

When the mean temperature of the tube metal lump is considered as a state variable, the effective heat transfer coefficient can be expressed using the classical analogy between the flow of heat energy through thermal resistance to the flow of electrical current in an electrical resistor.

Referring to Fig. A.1, the heat transfer rates are

$$\dot{Q}_{PM} = \frac{T_P - T_N}{R_O + R_M\ (A_{M2}/A_O)} = U_{PM}A_O(T_P - T_M) \tag{A.3}$$

and

$$\dot{Q}_{MS} = \frac{T_n - T_s}{R_I + R_M\ (A_{M2}/A_I)} = U_{MS}A_I\ (T_M - T_S) . \tag{A.4}$$

From Eqs. (A.3) and (A.4),

$$\frac{1}{U_{PM}} = \frac{1}{U_O} + \left(\frac{A_O}{A_{M2}}\right) \cdot \frac{1}{U_M} , \qquad A_{M1} = \frac{A_M - A_I}{\ell n\ (A_M/A_I)} ,$$

$$\frac{1}{U_{MS}} = \frac{1}{U_I} + \left(\frac{A_I}{A_{M1}}\right) \frac{1}{U_M} , \qquad A_{M2} = \frac{A_O - A_M}{\ell n\ (A_O/A_M)} .$$

The six different cases of heat resistances are calculated as follows.

1. No internal heat generation:

$$R = \frac{\ell n ro/r_I}{4\pi kL} .$$

2. Annular rings with the same thermal conductivity; Q^{111} = constant:

$$R_{I,I+1} = \frac{(r_{I+1}^2 - r_{I-1}^2)/r_I^{\ 2}}{8\pi kL} .$$

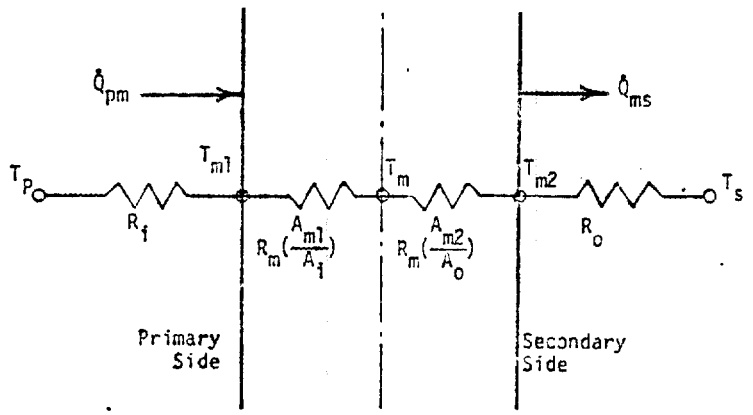

Fig. A.1. Heat transfer.

3. Annular rings with different thermal conductivity; Q^{111} = constant:

$$R_{I,I+1} = \frac{1}{8\pi L} \frac{r_{I+1}^2 + r_I^2}{k_{I+1} r_I^2} - \frac{r_I^2 + r_{I-1}^2}{k_I r_I^2} .$$

4. Annular ring closest to the surface of the cylinder; Q^{111} = constant:

$$R_{SO} = \frac{(r_S^2 - r_{S-1}^2)/r_S^2}{8\pi k L} .$$

5. Clad node average-to-clad surface:

$$R_{CAS} = \frac{\ell u \; r_O/r_I}{r\pi k L} .$$

6. Fluid film resistance:

$$R_F = \frac{1}{h2^7 r_O L} ,$$

where

r_O = outer diameter,

r_I = inner diameter,

k = thermal conductivity,

L = length of heat transfer area.

The overall heat transfer coefficients are calculated using the following correlations:

1. Chen's correlation[1] for the boiling region,

2. the Dittus-Boelter correlation[2] for the single-phase heat transfer regimes, and

3. the Lyon-Martinelli correlation[2] for the liquid sodium.

APPENDIX A REFERENCES

1. A. T. Chen, "A Digital Simulation for Nuclear Once-Through Steam Generators," Ph.D. dissertation, The University of Tennessee, 1976.

2. M. M. El-Wakil, *Nuclear Heat Transport*, The American Nuclear Society Press, La Grange Park, Ill. (May 1978).

APPENDIX B

SUMMARY OF TRANSIENT RESPONSES

The outputs of the transient simulations performed in this study are presented in this section. The organization of the figures is explained in Table B.1.

Table B.1. Organization of the results

Figure	Title
B.1	Step responses of primary model to a -5-cent reactivity perturbation
B.2	Step responses of primary model to a +10°F (+5.5°C) IHX inlet sodium temperature perturbation
B.3	Step responses of steam generator model to a +10°F feedwater temperature perturbation
B.4	Step responses of steam generator model to a +10°F inlet sodium temperature perturbation
B.5	Step responses of steam generator model to a +10% steam valve opening perturbation
B.6	Step responses of steam generator model to a +10-lb_m/s feedwater flow perturbation
B.7	Step responses of combined model to a -5-cent reactivity perturbation
B.8	Step responses of combined model to a +10% steam valve opening perturbation

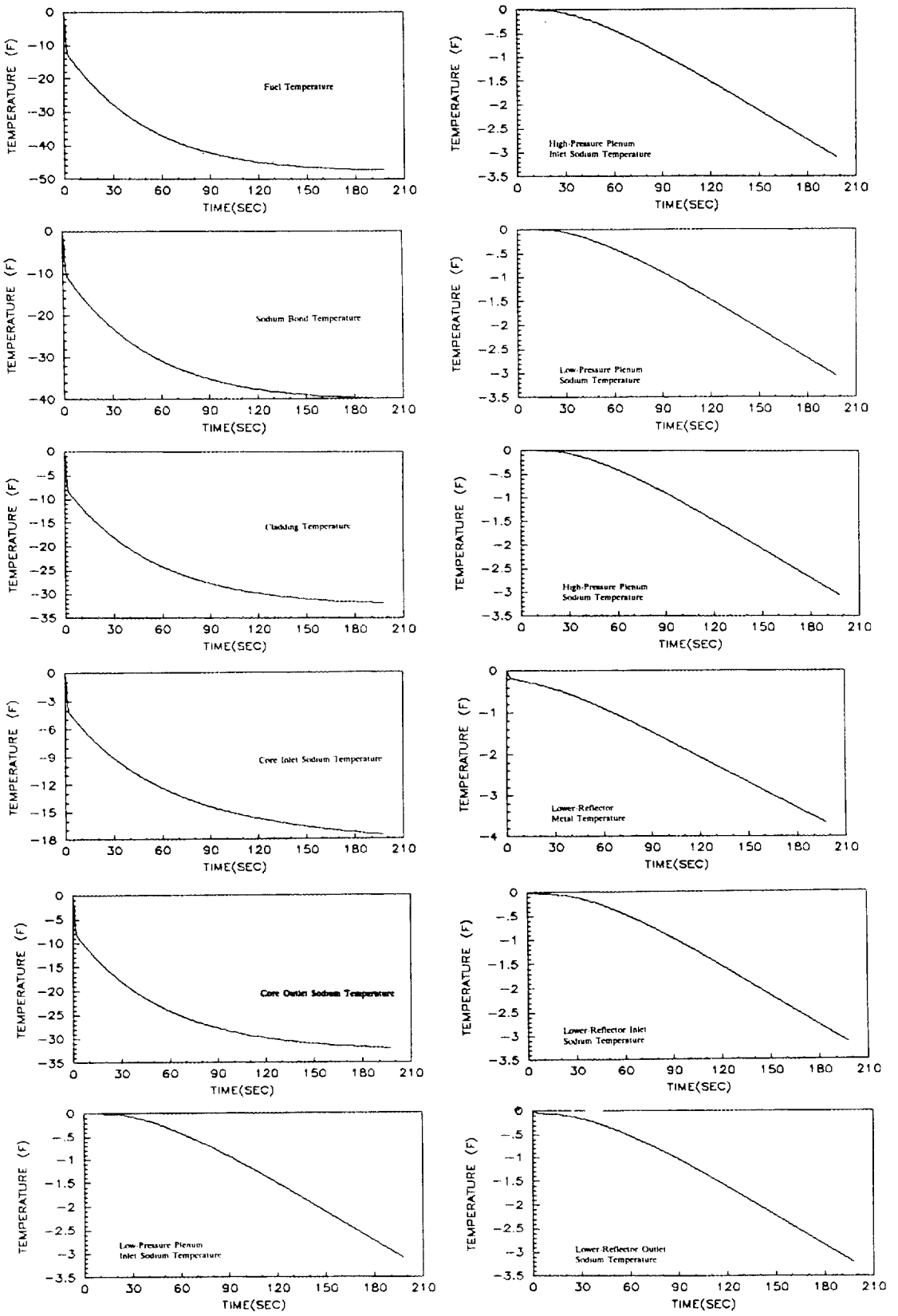

Fig. B.1. Step responses of primary model to a -5-cent reactivity perturbation. (Deviations from steady state.)

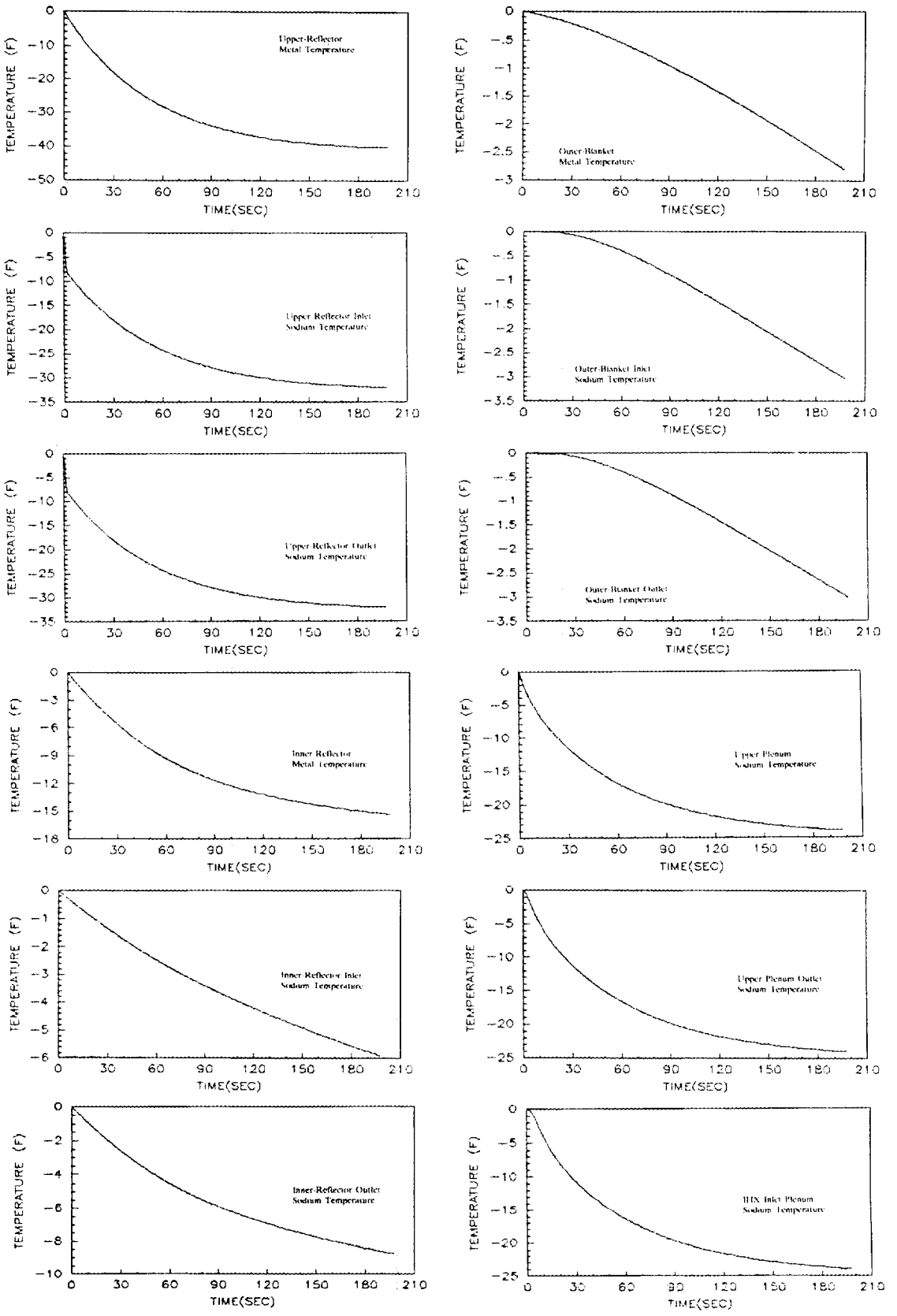

Fig. B.1. (continued).

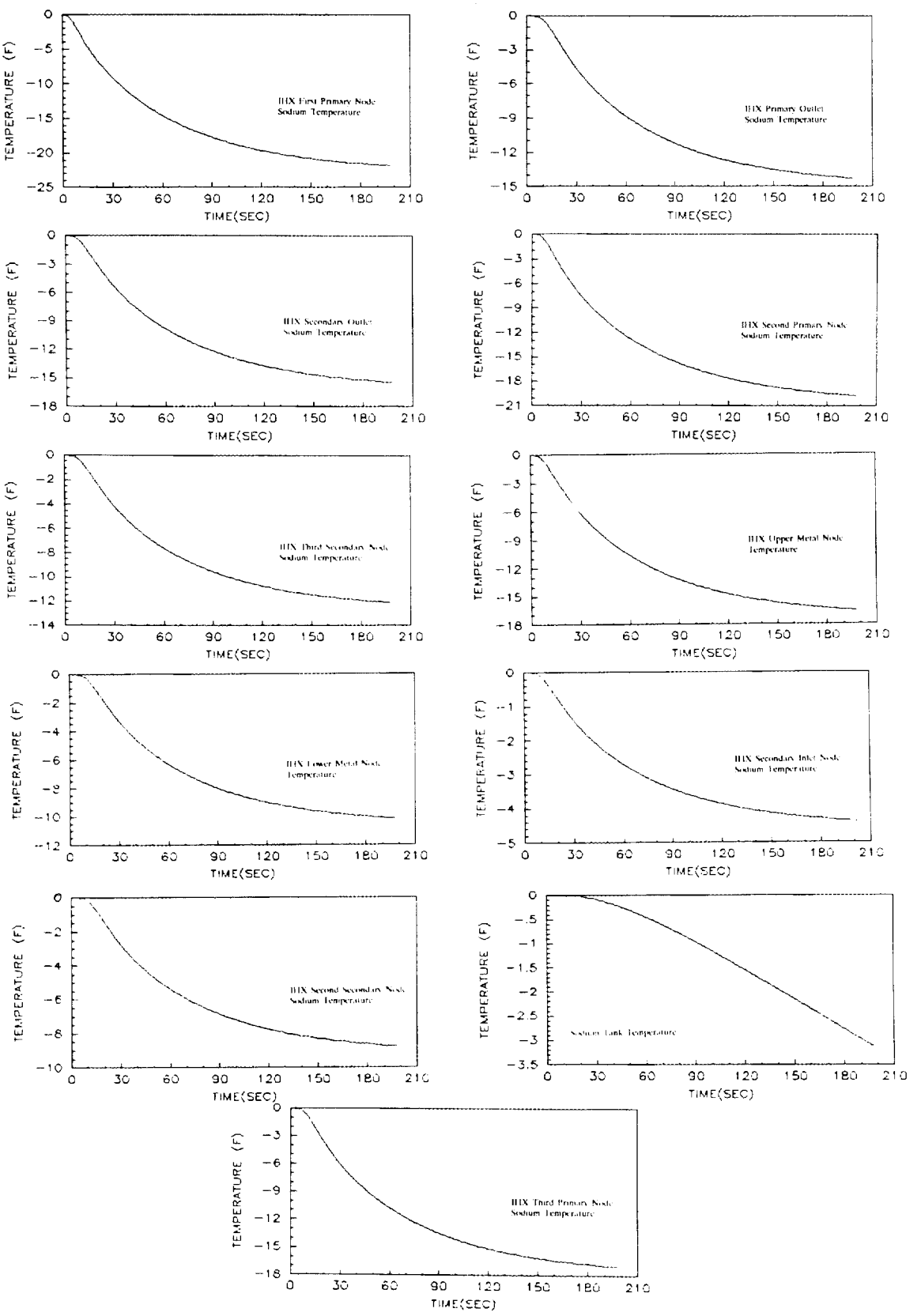

Fig. B.1. (continued).

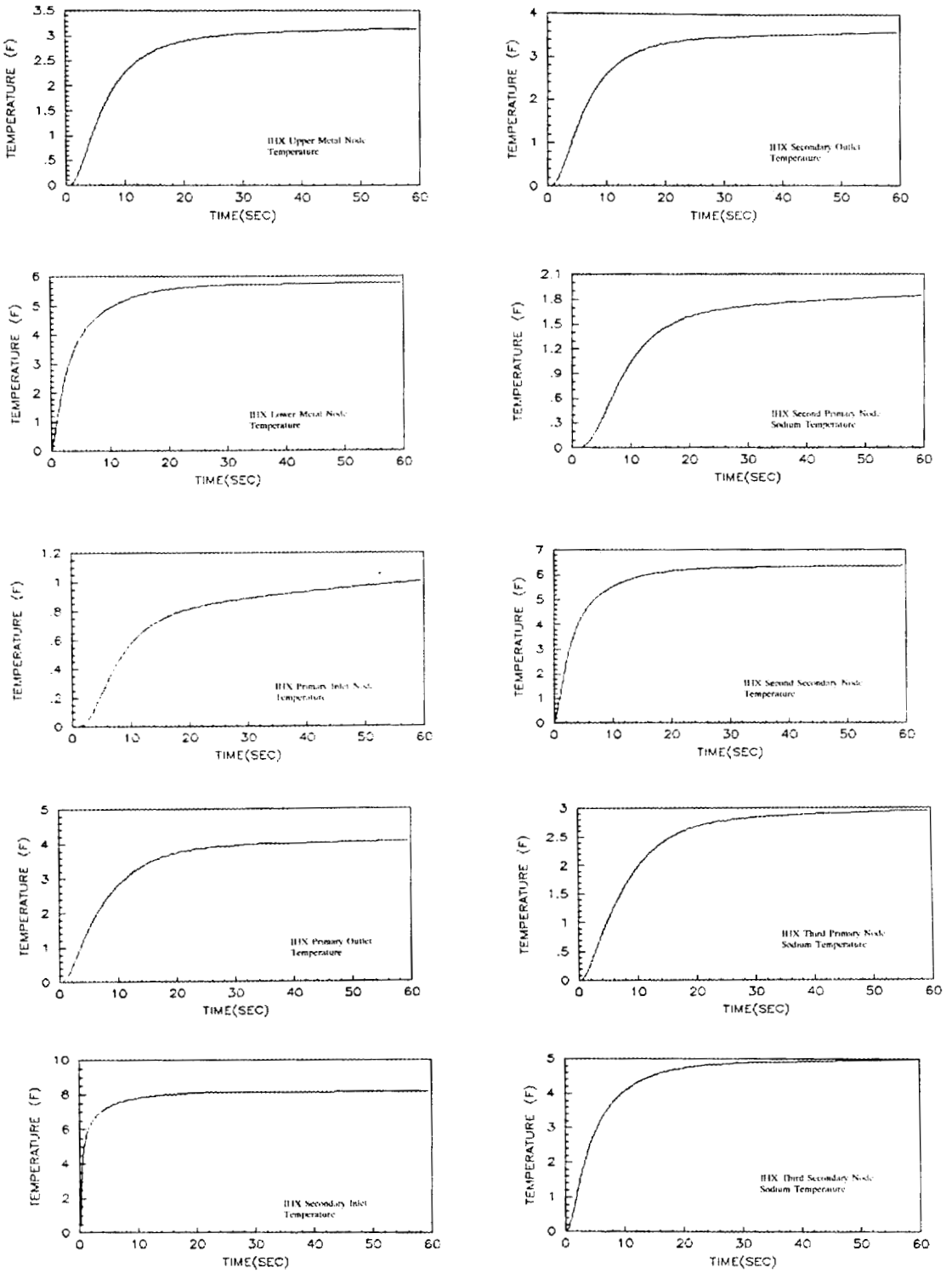

Fig. B.2. Step responses of primary model to a +10°F IHX inlet sodium temperature perturbation. (Deviations from steady state.)

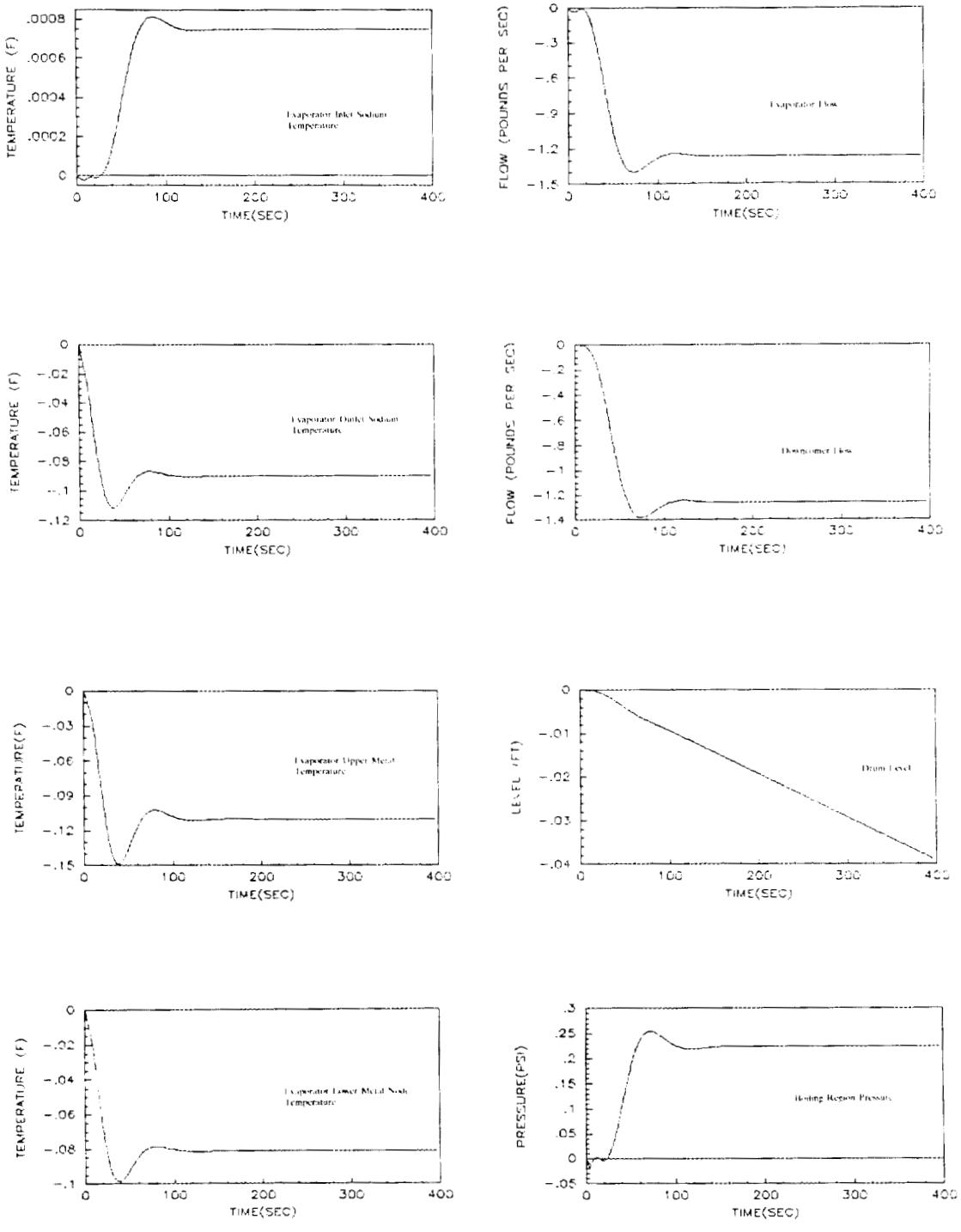

Fig. B.3. Step responses of steam generator model to a +10°F feedwater temperature perturbation. (Deviations from steady state.)

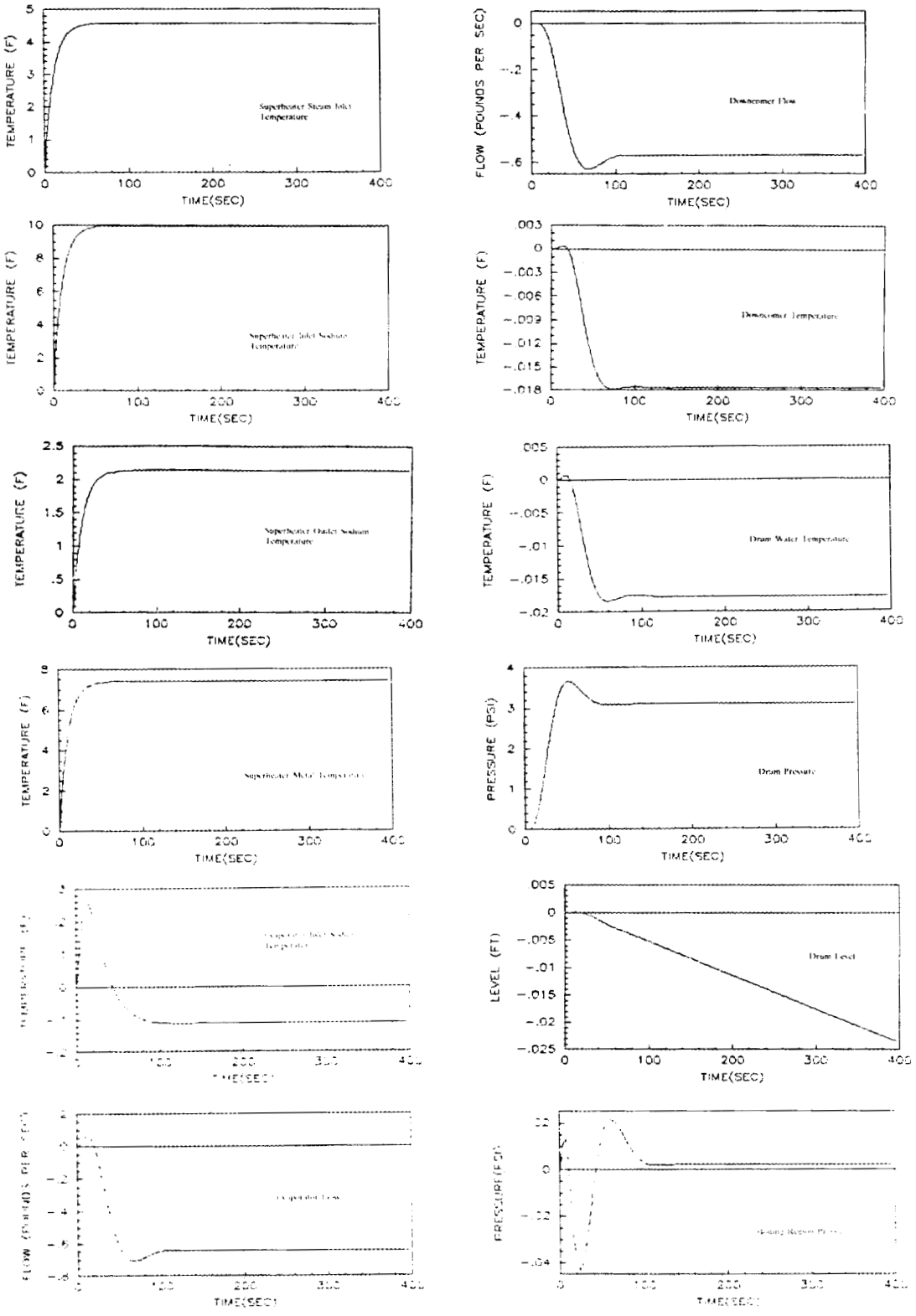

Fig. B.4. Step responses of steam generator model to a +10°F inlet sodium temperature perturbation. (Deviations from steady state.)

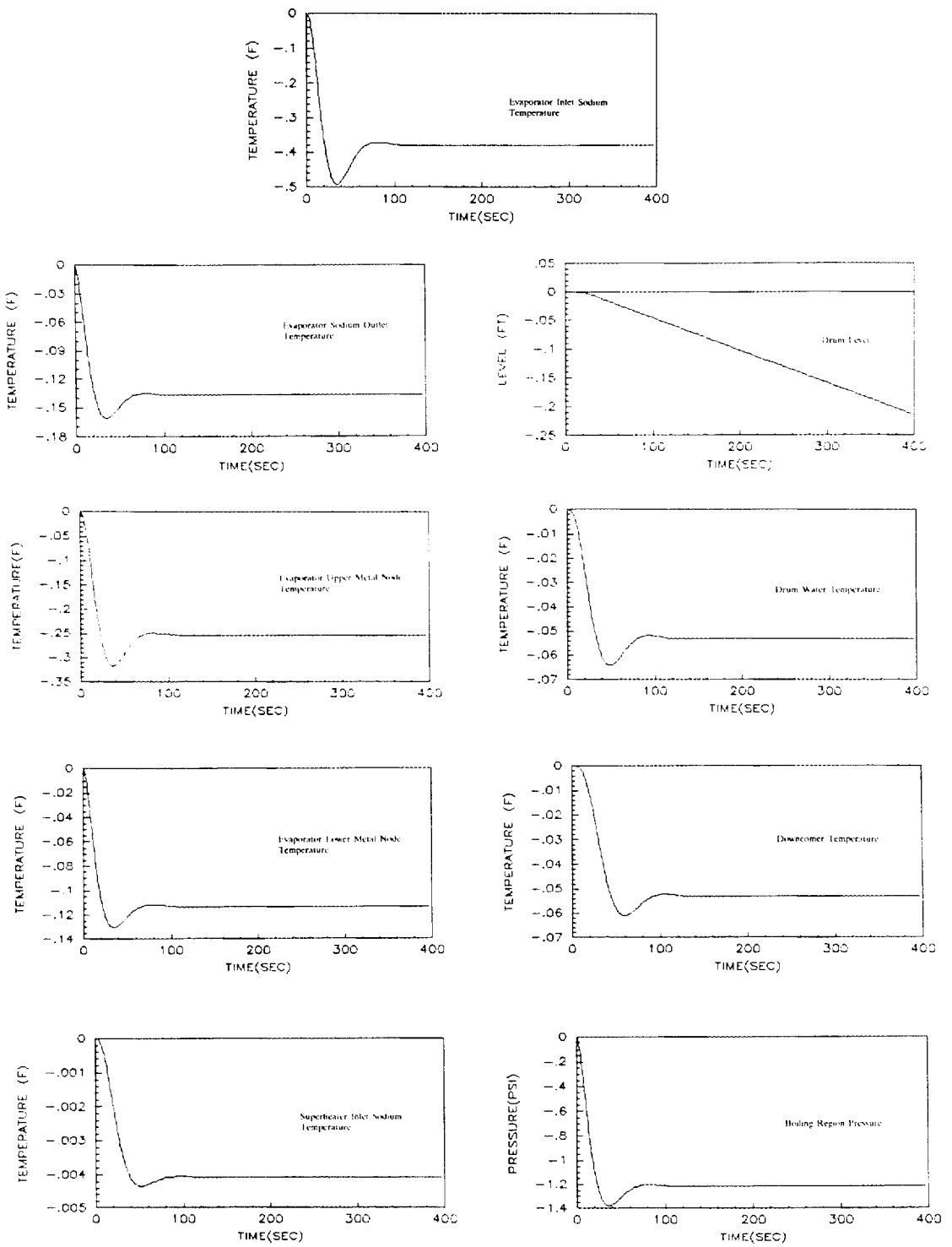

Fig. B.5. Step responses of steam generator model to a +10% steam valve opening perturbation. (Deviations from steady state.)

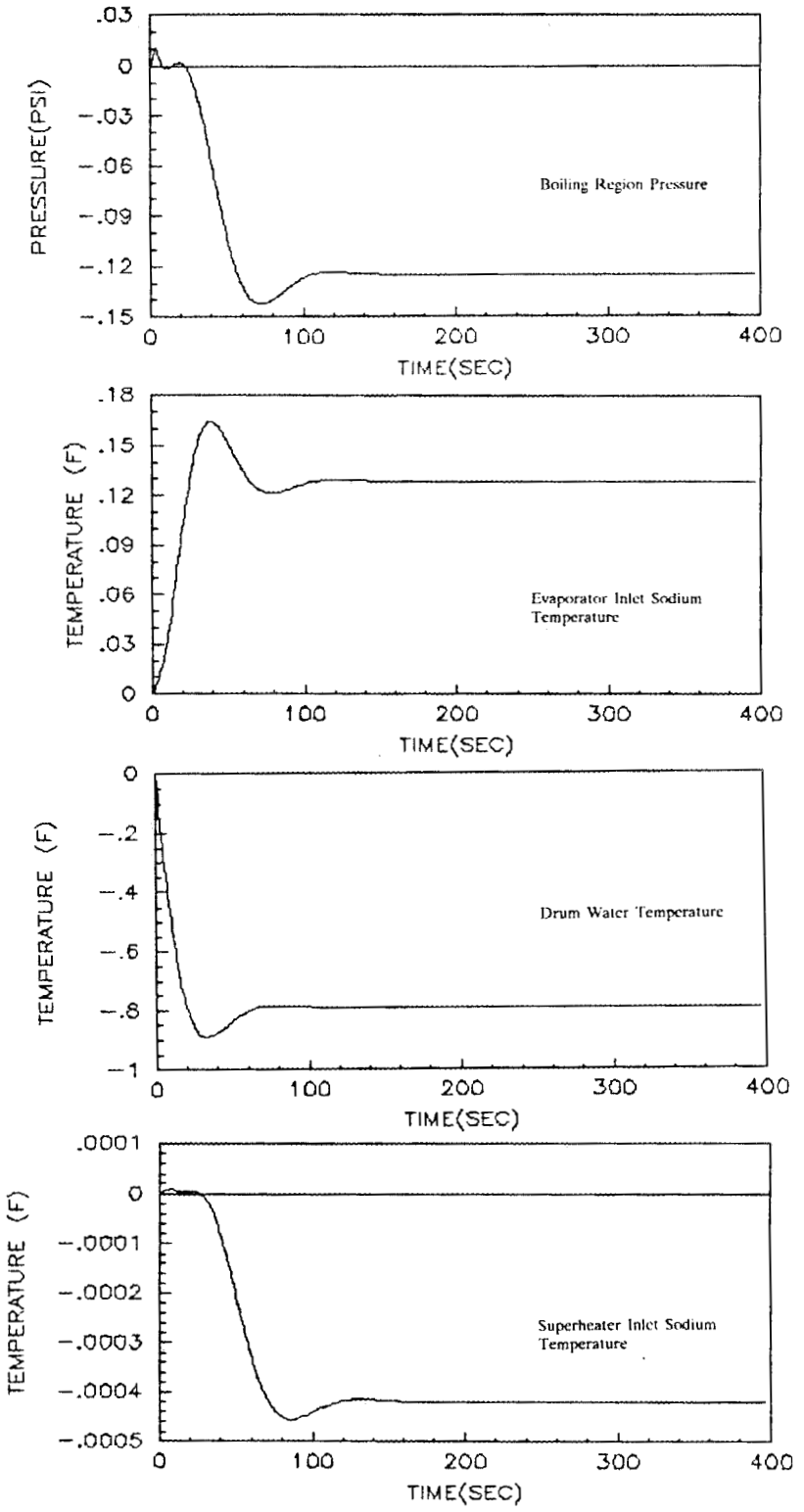

Fig. B.6. Step responses of steam generator model to a +10-lb_m/s feedwater flow perturbation. (Deviations from steady state.)

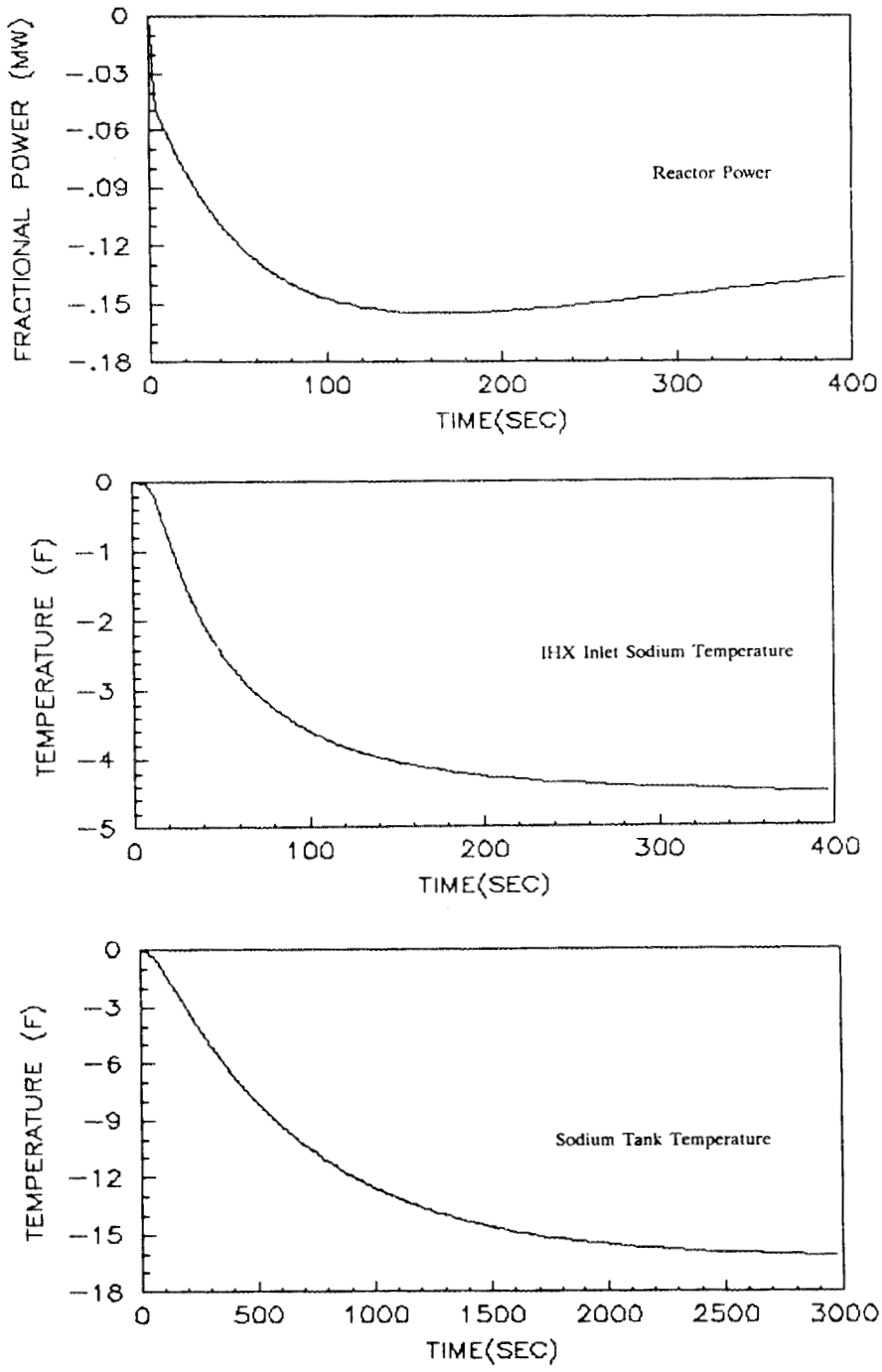

Fig. B.7. Step responses of combined model to a -5-cent reactivity perturbation. (Deviations from steady state.)

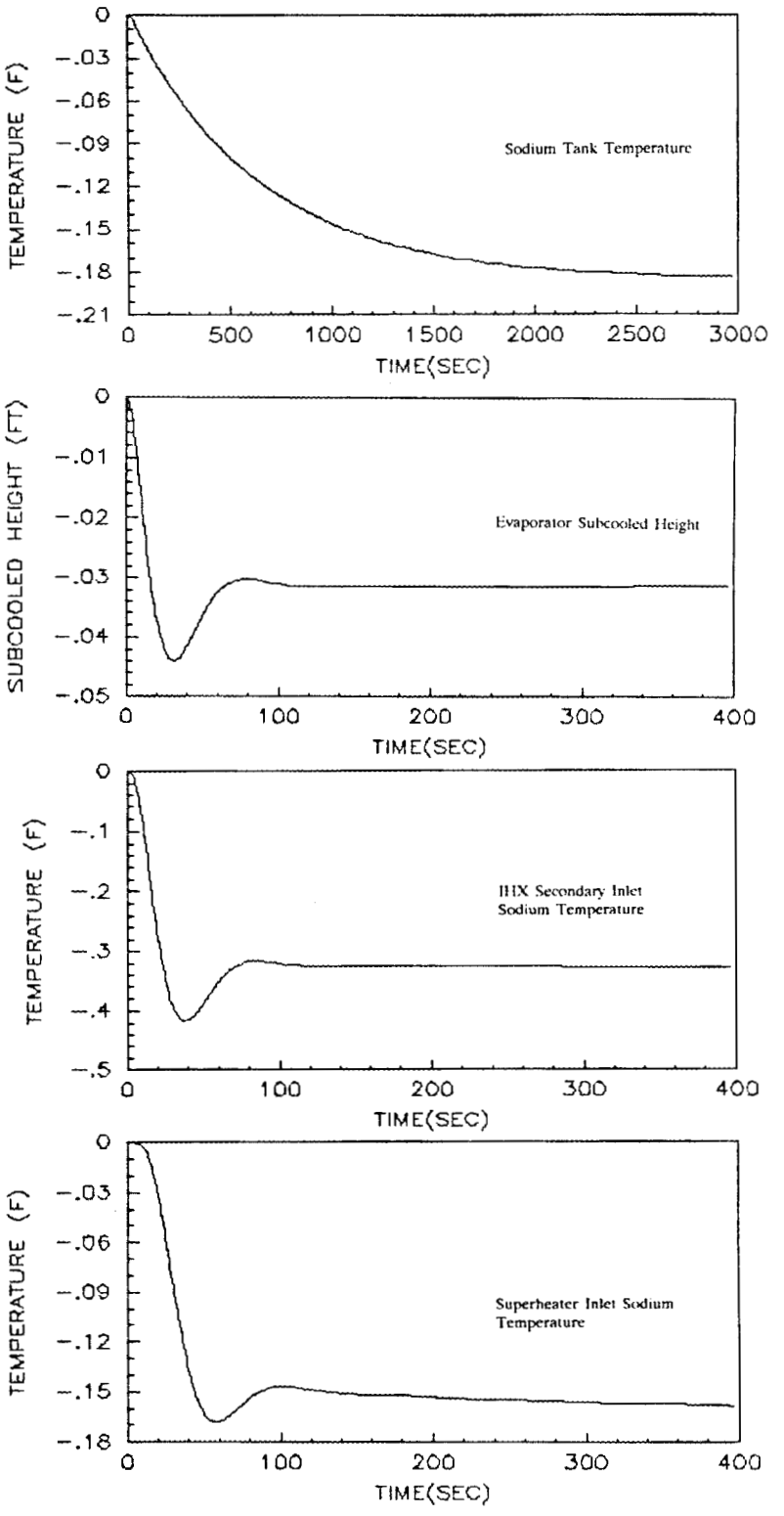

Fig. B.8. Step responses of combined model to a +10% steam valve opening perturbation. (Deviations from steady state.)

APPENDIX C

CAPABILITIES OF MATRIX_X

C.1 REPRESENTATION OF DYNAMIC SYSTEMS

Consider the following linear system,

$$\dot{\underline{X}} = A\,\underline{X} + B\,\underline{u} \quad ,$$

$$\underline{Y} = C\,\underline{X} + D\,\underline{u} \quad ,$$

where $\underline{X}$ is a vector of state variables, $\underline{Y}$ is a vector of measurements, and $\underline{u}$ is a forcing function. A, B, C, and D are the constant system matrices (see Eq. 5.1). The above state-space representation of a linear dynamic system can be loaded to the computer using the following Matrix_X syntax,

$$S = [A,B;C,D] \quad ,$$

where S is a matrix representing the overall system. The number of states should be specified by an arbitrary variable name.

The representation of systems in the transfer function domain is also possible. Consider the following transfer function.

$$G(s) = \frac{a_1\,s^2 + a_2\,s + a_3}{b_1\,s^3 + b_2\,s^2 + b_3\,s + b_4} \quad ,$$

where

a_I, i=1,..,3 = numerator coefficients,

b_I, i=1,..,4 = denominator coefficients,

$G(s)$ = transfer function in the Laplace domain.

The Matrix_X syntax for the representation of this transfer function can be made as follows.

$$\text{NUM} = [\ 0 \quad a_1\ a_2\ a_3\ ] \quad ,$$

$$\text{DEN} = [\ b_1\ b_2\ b_3\ b_4\ ] \quad ,$$

where *NUM* and *DEN* are arbitrary variable names. The order of the transfer function should be specified.

A transformation from one type of representation to another is also possible with Matrix_X (see user's manual for details, ref. 1).

C.2. SIMULATION COMMANDS

Once the linear system representation in $Matrix_X$ is completed, the transient simulations can be performed using the following commands.

```
[T,Y]=STEP(S,NS,TMAX,NPTS)
```

or

```
[T,Y]=STEP(NUM,DEN,TMAX,NPTS)  .
```

The outputs of this command are the time vector *T* and the *Y* matrix, which are the step responses of the linear system. *Y* matrix has the number of columns equal to the number of states and the number of rows equal to the number of time points.

The inputs of the simulation commands are the overall system representation, either in state-space form or in transfer function form. *TMAX* specifies the length of time and *NPTS* specifies the number of points to be calculated. The default integration algorithm is the "variable Kutta-Merson."[1] The variable Kutta-Merson integration is an explicit fourth-order one-step method. The integration step is optimized to provide the largest step while remaining within the local error tolerances. The maximum step size is equal to the time increment. The choice of *NPTS* determines the time increment, and this integration technique retains the stability of the solution regardless of any arbitrary choice of *NPTS*.

The linear system should be stable, otherwise the solution will diverge. To check the stability, the user can calculate the eigenvalues of the system matrix *A* using EIG(A).

C.3 SYSTEM-BUILD OPTION

SYSTEM-BUILD is a menu-driven interactive graphical environment for building, modifying, and editing computer simulation models. Accessing SYSTEM-BUILD can be done from the $Matrix_X$ prompt. The different dynamic models represented in $Matrix_X$ can be appended in a hierarchical structure using the SYSTEM-BUILD capabilities. In this section, an example of the construction of large-scale dynamic models using SYSTEM-BUILD is presented. Other capabilities of this software are explained in ref. 1.

The two modules of the EBR-II (the primary system model and the steam generator model) are considered. Despite the fact that these models are not too large to be coupled in the $Matrix_X$ environment, the coupling is made using the SYSTEM-BUILD methods to provide an example for future applications. The combined structure is obtained by the following steps.

Table C.1 Steps describing model buildings using SYSTEM-BUILD.

Step	Explanation	Menu	Selection
1	Edit super block	Top	2
2	Name the overall system	Name:	EBR-II
3	Continuous system	Sample Period:	0
4	First block definition	Describe Blocks Location:	1 1
5	It is a dynamic system	Type of Block	6
6	State-space representation	Dynamic Systems	3
7	Name the first block	Specifications	Primary
8	Specify the number of inputs (2)	Specifications	2
9	Specify the number of outputs (37)	Specifications	3
10	Specify the number of states (37)	Specifications	4
11	Load the system matrix S_1	Specifications System Matrix: Zero Initial states?	5 S1 Y
12	Go to the previous menu		UNDO
13	Second block definition	Describe Blocks Location:	1 3
14	It is a dynamic system	Type of Block	6
15	State space representation	Dynamic Systems	3
16	Name the second block	Specifications	Stgen
17	Specify the number of inputs (2)	Specifications	2
18	Specify the number of outputs (18)	Specifications	3
19	Specify the number of states (18)	Specifications	4
20	Load the system matrix S_2	Specifications System Matrix: Zero Initial states?	5 S2 Y
21	Go to the previous menu		UNDO
22	Necessary connections	Describe Blocks	5

Table C.1 (continued)

Step	Explanation	Menu	Selection
23	Internal and external connections	Connect Blocks	1,2,3

(The connections are made in a graphical environment, which is invoked by the connect menu.)

24	Go to the top menu	Connect Blocks Describe Blocks	UNDO TOP
25	Analyze the structure	Top Name: Sample period:	6 EBR-II 0

Upon completing these steps, the overall EBR-II system model, including the primary model in location 1 and the steam generator model in location 3, is ready for simulation studies. The superblock EBR-II is shown in Fig. C.1. The following command can be used for simulation:

$$Y = SIM(T,U) \quad ,$$

where Y is the output matrix as explained in the previous section. U is the input time vector. The dimensions of T and U must match. For a step input case, U vector contains equal entries for each time step. Note that when using this feature, any kind of input can be applied by the user-defined U vector.

The SYSTEM-BUILD option also includes different integration algorithms. The menu contains the following selections:

1. Euler integration,
2. RK2 (modified Euler),
3. Runga-Kutta fourth-order,
4. Fixed Kutta-Merson,
5. Variable Kutta-Merson (default), and
6. Stiff system solver.

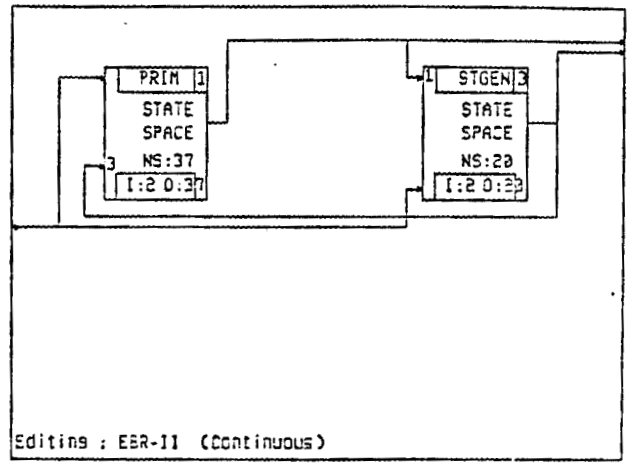

Fig. C.1. Coupling the primary and steam generator models using SYSTEM-BUILD.

APPENDIX C REFERENCE

1. *MATRIX$_X$ User's Guide*, Version 5.0, Integrated Systems, Inc., Palo Alto, Calif., October 1985.

ORNL/TM-11161
Dist. Category UC-530
Liquid Metal Fast Breeder Reactors

INTERNAL DISTRIBUTION

1. J. M. Bailey
2. S. J. Ball
3. R. E. Battle
4-8. R. C. Berkan
9. R. S. Booth
10. C. R. Brittain
11. N. E. Clapp, Jr.
12. B. G. Eads
13. C. E. Ford
14. D. N. Fry
15. F. J. Homan
16-25. R. A. Kisner
26. H. E. Knee
27. J. K. Munro
28. G. V. Murphy
29. L. C. Oakes
30. P. J. Otaduy
31. A. W. Renshaw
32. J. C. Schryver
33. R. L. Shepard
34-38. L. H. Tsoukalas
39. R. E. Uhrig
40-44. B. R. Upadhyaya
45. J. D. White
46. T. L. Wilson
47. R. T. Wood
48. A. Zucker
49. J. B. Ball, Advisor
50. P. F. McCrea, Advisor
51. T. B. Sheridan, Advisor
52-53. Central Research Library
54. Y-12 Technical Reference Section
55-56. Laboratory Records Department
57. Laboratory Records ORNL-RC
58. ORNL Patent Section
59. I&C Division Publications Office

EXTERNAL DISTRIBUTION

60. Assistant Manager for Energy Research and Development, U.S. Department of Energy, Oak Ridge Operations Office, Oak Ridge, TN 37831.
61-62. Office of Scientific and Technical Information, P.O. Box 62, Oak Ridge, TN 37831.
63. Harry A. Alter, Manager, Division of Advanced Technology Development, U.S. Department of Energy, NE-462, Washington, DC 20545
64. Sid C. Bhatt, EPRI, Project Manager, 3412 Hillview Ave., P.O. Box 10412, Palo Alto, CA 94303
65. Doug G. Carroll, Program Manager, G.E. Nuclear Energy, 6835 Via Del Oro, Box 530954, San Jose, CA 95153-5354
66. Mr. Robert L. Carroll, Department of Electrical Engineering and Computer Sciences, George Washington University, Washington, DC 20052
67. Dr. Yogi Dayal, G.E. Nuclear Energy, Advanced Nuclear Technology, Box 530954, San Jose, CA 95153-5354
68. Mohammed Jamshidi, CAD Lab Systems/Robotics, Dept. of Elec. and Comp. Engineering, Room 133A, EECE Bldg., University of New Mexico, Albuquerque, NM 87131
69. Reed Monson, P.O. Box 2528, Idaho Falls, ID 83403-2528
70. Mr. H. P. Planchon, Argonne National Laboratory, 9700 S. Cass Ave., Argonne, IL 60439

71. Dr. G. V. S. Raju, Department of Electrical and Computer Engineering, Stocker Center, Rm. 329, Ohio University, W. Green Drive, Athens, OH 45701
72. John I. Sackett, Argonne National Laboratory-West, P.O. Box 2528, Idaho Falls, ID 83402
73-128. Given distribution for Category UC-530, Liquid Metal Fast Breeder Reactors.